Analysis Of Rocket Engine Injection Combustion Processes

Final Report 31531 F-1
Contract NAS 8-31531
November 1976

Prepared For:
NASA
George C. Marshal Space Flight Center
Marshall Space Flight Center, Alabama 35812

By:
J.W. Salmon

(NASA-CR-150141) ANALYSIS OF ROCKET ENGINE INJECTION COMBUSTION PROCESSES Final Report (Aerojet Liquid Rocket Co.) 190 p HC A09/MF A01 CSCL 21H G3/20 N77-15089 Unclas 15460

Aerojet
Liquid Rocket
Company

Report 31531F-1

FINAL REPORT

ANALYSIS OF ROCKET ENGINE INJECTION COMBUSTION PROCESSES

NOVEMBER 1976

BY

J. W. SALMON

AEROJET LIQUID ROCKET COMPANY
SACRAMENTO, CALIFORNIA 95813

PREPARED FOR

NATIONAL AERONAUTICS AND SPACE ADMINISTRATION

GEORGE C. MARSHALL SPACE FLIGHT CENTER
CONTRACT NAS 8-31531
K. W. GROSS, COR

FOREWORD

This report was prepared for the NASA George C. Marshall Space Flight Center under Contract NAS 8-31531, by Aerojet Liquid Rocket Company (ALRC), Sacramento, California. The NASA Contracting Officer Representative was Mr. K. W. Gross. The study was performed during the period July 1975 to September 1976.

The ALRC Project Manager for this study was Mr. David L. Kors, Manager, Analytical Design Section, Design and Analysis Department. Mr. Larry B. Bassham was the Program Manager responsible for all fiscal and contracting functions. Mr. Jeffery W. Salmon served as Project Engineer, Principal Investigator, and the author of this program final report. The author is grateful for the valuable technical support offered by Mr. David Saltzman during the Task II development of a new mixing methodology for the LISP subprogram of the DER computer model.

TABLE OF CONTENTS

LIST OF TABLES

LIST OF FIGURES

List of Figures (cont.)

List of Figures (cont.)

I SUMMARY

The scope of this program was to include a thorough critique of the JANNAF sub-critical propellant injection/combustion process analysis computer models and application of the models to correlation of well documented hot fire engine data bases. These programs are the Distributed Energy Release (DER) model for conventional liquid propellant injectors and the Coaxial Injection Combustion Model (CICM) for gaseous annulus/liquid core coaxial injectors. The critique would identify model inconsistencies while the computer analyses would provide quantitative data on predictive accuracy. The program was comprised of three tasks; Task I - Computer Program Review and Operation, Task II - Analysis and Data Correlations, and Task III - Documentation.

There were three objectives of Task I. (1) Critique of the DER and CICM Computer Programs, (2) Correction of coding errors, updating of inadequate formulations, and addition of diagnostic printout statements, and (3) Identification of inconsistencies between the analysis computer programs and the JANNAF prediction procedures documented in CPIA 246. The results of the DER and CICM reviewsare comprehensively reported in Appendices A and B, respectively. Complete summaries of the corresponding conclusions and recommendations of the reviews are contained in Section III, Computer Program Review and Operation. There were two major conclusions resulting from the DER review. First, the intended predictive accuracy of the JANNAF rigorous performance evaluation procedure (to within 1 percent for predicted specific impulse) is, in general, currently out of the question for <u>a priori</u> performance prediction with DER. Secondly, the DER analysis originally planned to be conducted during program Task II should rather be concerned with improvement of a DER technical shortcoming. The primary conclusion of the CICM review was that the applicability and accuracy of the model is currently limited by the absence of an intra-element coaxial gas/liquid mixing model. This limitation not only makes the mixing loss calculation dependent on correct application of empirical cold flow mass distribution data, but hinders the development of general program coaxial jet atomization and drop size constants that control the program vaporization calculation.

There were originally three primary objectives of Task II. (1) Provide information on the present prediction capabilities of the JANNAF DER and CICM injection-combustion computer analysis techniques, (2) Identify conditions where reliable predictions can be obtained, and (3) Identify areas requiring further improvement and research. The CICM analysis task was completed as originally planned. The results of the CICM analysis are reported in Section IV, CICM Analysis and Data Correlations. The CICM analysis was performed by establishing the existing M-1 H_2/O_2 engine data base, executing a nominal operating point CICM analysis, correlating the CICM prediction with the test data, conducting two off-nominal test point analyses to determine the influence of velocity ratio changes on injector performance, and identifying prediction ranges and required model improvements. The CICM analysis results verified the accuracy of the CICM vaporization model for the case where injector intra-element mixing losses are negligible.

The objective of the DER Phase of Task II was altered based on the recommendations of the Task I DER computer model review. Improvement of the LISP subprogram ZOM plane mass distribution and mixing methodology was selected as the new Task II DER goal. This task was conducted in four parts. (1) An a priori ZOM plane prediction model was formulated that accounts for combustion gas acceleration effects on inter-spray fan mixing, (2) A subscale test data base was developed for analysis and the ZOM model was used to predict mixing performance for each test, (3) The model predictions were correlated with the hot fire test results, and (4) Recommendations for continuation of model development were formulated. The primary discovery of this initial ZOM model development work was that a physically mechanistic near-zone model that will predict the ZOM mixing plane location must account for both gas acceleration and reactive stream ("blowapart") forces on droplet spray fan formation and mixing.

Task III of the program resulted in eleven monthly status letters and this comprehensive final report containing explicit recommendations for improvement of the JANNAF performance prediction computer programs. The

English system of units has been exclusively employed in this report since SI units have yet to be adapted to the JANNAF system of computer programs. The program COR has concurred with and approved this choice.

II INTRODUCTION

The ICRPG (now JANNAF) Performance Standardization Working Group was formed in 1965 for the purpose of improving and recommending methodology for the analytical and experimental evaluation of the performance of liquid propellant rocket engines. In 1968, the working group published a Performance Evaluation Manual (Ref. 1) which described the procedures and computer programs recommended for the prediction, correlation, and extrapolation of the performance of liquid propellant thrust chambers. The scope of this first effort was limited to assembling, into a compatible overall system, the best relevant analytical and experimental techniques existing throughout the industry at that time. During this effort, it was concluded that the energy release phenomenon could not be adequately described or predicted by existing analytical techniques. As a result, an interim empirical procedure was adopted.

Since this first attempt at achieving a standard performance evaluation model, a semi-empirical, but mechanistic, computer model has been developed for the analysis of the liquid injector-combustion chamber energy release process. This model, termed the Distributed Energy Release (DER) model (Ref. 2) has reached the stage of development where it is being incorporated into the Improved JANNAF Performance Evaluation Methodology (Ref. 3). DER is composed of two major programs which link the atomization, vaporization and mixing processes within the combustion chamber. The first is the Liquid Injector Spray Patterns (LISP) program which calculates propellant mass and mixture ratio distributions at a specified chamber cross-sectional plane (ZOM) downstream of the injector face. The second is the Stream Tube Combustion (STC) program which calculates the propellant vaporization, reaction and acceleration from the LISP specified collection plane to the combustion chamber throat plane. Additionally, a third JANNAF recommended program has been developed for the specialized case of injector elements containing central circular orifice liquid propellant injection surrounded by annular gaseous injection. The Coaxial Injection Combustion Model (CICM) (Ref. 4) is designed to replace the DER LISP subprogram for this injector type.

While these programs provide analytical methods for evaluation of the energy release process, the program developers have identified analysis parameters which are critical to the accuracy of the resulting performance predictions. These include specification of propellant mass median droplet diameters and the LISP Spray distribution correlation coefficients, which have been established over limited ranges of element type and design conditions. Additional studies using DER have shown that the specification of the LISP-STC interface plane (ZOM) is also critical to the end performance prediction.

The objective of this program was to develop quantitative data on the present prediction capabilities of the JANNAF sub-critical propellant injection/combustion process analysis programs (LISP, STC, and CICM). The desired program end product was identification of conditions for which reliable predictions could be conducted and areas which need further improvement and research.

Future attainment of a broader overall objective was continued with conductance of the Injection Processes Program. The JANNAF Performance Standardization Working Group has the purpose of improving methodology for analytical design modeling of rocket engines. The current and future economics of rocket development do, and will certainly, make it imperative that cost saving analytical methods replace more expensive hardware development and test programs. Of course, such tools are only cost effective if they model the applicable physical processes realistically and accurately. The Injection Processes program and other related efforts have provided information on the state of JANNAF model development through application to real rocket engine systems. During this program the CICM computer program was used to correlate performance data obtained with the M-1 1 million lbf hydrogen/oxygen engine. The DER computer program has been successfully applied to design analysis of the Orbital Maneuvering System (OMS) engine for Space Shuttle, the Improved Transtage Injector Program (ITIP) currently being conducted by the USAF, and an advanced development monomethyl hydrazine/

fluorine-oxygen engine tested by the NASA. Each of these efforts has resulted in constructive criticism of the computer models that, when applied, results in further advancement of the state-of-the-art of rocket engine analytical design. The final end product of programs that support the JANNAF predictive methodology will someday be a capability to eliminate major hardware development technology programs through verified standardized analysis techniques. A superior development procedure would be constituted of initial JANNAF model analysis, fabrication and test of the full scale engine, re-analysis, full scale hardware modification, and final engine verification test. The Injection Processes Program has made this seemingly optimistic goal a bit more achievable through a comprehensive evaluation of the DER and CICM models.

III COMPUTER PROGRAM REVIEW AND OPERATION

There were three primary objectives of the first program task.

(1) Critique of the JANNAF DER and CICM programs,

(2) Correction of coding errors, updating of inadequate formulations, and addition of diagnostic printout statements, and

(3) Identification of inconsistencies between the analysis computer programs and the JANNAF prediction procedures described in CPIA 246 (Ref. 3).

The complete results of the DER and CICM reviews are contained in Appendices A and B, respectively, of this report. The computer programs are introduced and their functions in the JANNAF performance prediction procedure briefly described in the following paragraph. A complete summary of the findings and corresponding recommendations of the computer model reviews follows the program descriptions.

A flow-chart showing the DER and CICM programs and their relationship to the JANNAF Two-Dimensional Kinetic (TDK) Computer Program (Ref. 5) is illustrated in Figure 1, taken from Ref. 3. DER is composed of LISP and STC, two major programs that link atomization, vaporization, and mixing processes within the combustion chamber. The Liquid Injector Spray Patterns (LISP) program calculates propellant mass and mixture ratio distribution at a specified chamber cross-sectional plane (termed ZOM) downstream of the injector face. LISP was developed for conventional (i.e., circular orifice) liquid/liquid injection elements. The Stream Tube Combustion (STC) program calculates propellant vaporization, reaction, and acceleration from ZOM to the combustion chamber throat plane. STC can provide direct computer input data for the TDK program that continues the multiple stream tube analysis through the supersonic expansion process. CICM replaces the LISP program for the analysis of gas/liquid coaxial elements. CICM is a highly specialized program that has currently only been applied to the analysis of injection elements with a central liquid O_2 circular core surrounded by a gaseous H_2 or H_2/O_2 combustion gas mixture annulus.

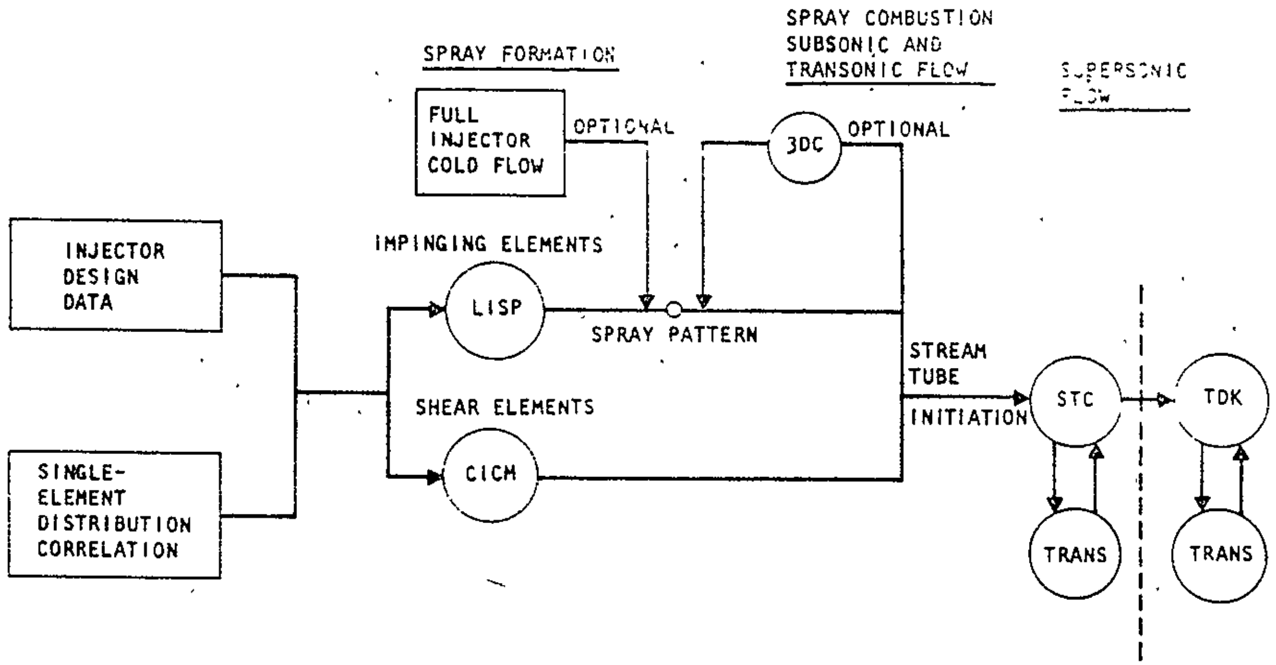

FIGURE 1. JANNAF INJECTION AND COMBUSTION ANALYSIS PROCEDURES LOGIC STRUCTURE

A. DER Computer Model Review Recommendations and Conclusions

Four subtasks were accomplished during the DER review.

(1) Identification and Correction of Coding Errors,

(2) Addition of Diagnostic Comment Cards and Print-Out Statements,

(3) Identification of Inadequate Formulations and Model Technical Formulations, and

(4) Review of the JANNAF Performance Prediction Procedures (CPIA 246) with Regard to Use of DER.

The review is applicable strictly the DER subcritical K-Prime version described in Ref. 2. The corresponding user's manual referred to in this report is Ref. 6.

The third subtask listed above was emphasized during the review for two reasons. The initial results of the review indicated that DER still requires major technical improvements and therefore subtasks (1) and (2) were considered to be of less current interest. Secondly, SDER, a new "standardized" version of DER (Contract FO 4611-75-C-0055),was developed concurrently with completion of this program. It was intended that the improved DER model be influenced by the findings summarized in this report; therefore the discovery of DER technical formulation shortcomings was considered to be of prime importance.

A major conclusion of the DER review was that the DER analysis originally planned to be conducted during program Task II should rather be concerned with improving a DER technical shortcoming. It seemed inappropriate to conduct the analysis with a computer model that possessed vaporization and mixing models containing several questionable solution formulations, as summarized in the following paragraphs concerning review recommendations. Improvement of the LISP ZOM plane mass distribution methodology was selected as the new Task II DER analysis goal. The current status of the mixing model improvement work is described in Section V of this report. Key recommendations and conclusions, resulting from the DER review results detailed in Appendix A, are listed in the following four paragraphs corresponding to the previously described review subtasks.

1. Identification and Correction of Coding Errors

a. LISP Subprogram

(1) An unsymmetrical pie section input problem was identified for the LISP program. It should be eliminated by adjusting the collected pie section mass flowrate to $\theta/360$ of the total injected flow of each propellant.

(2) Inconsistencies between published DER drop size equations and those actually existent in the DER code must be resolved.

(3) The DER code should be changed to eliminate a mass flux calculational error for triplet elements caused by an improper rotation of the ZOM collection plane around the normal x axis.

(4) The ZOM mass distributions should consider the influence of baffle height.

b. STC Subprogram

(1) The STC program limits the number of radial and circumferential mesh lines to twenty; this limitation should be noted in the DER user's manual, or preferably removed.

2. Addition of Diagnostic Comment Cards and Printout Statements

The recommended statement additions and improvements are presented in Section B of Appendix A.

3. Identification of Inadequate Formulations and Model Technical Shortcomings

a. Drop Size Prediction

(1) The inconsistencies cited, between referenced drop size correlations and those appearing in the DER code, must be resolved.

(2) It is recommended that the DER drop size equations be comprehensively reviewed with respect to available atomization correlations and their impact on DER performance prediction accuracy. A task performed during the SDER development program was to be concerned with such a review, although the results have not been published.

(3) Interim to release of SDER, all DER drop sizes should be user input and justified.

b. ZOM Plane Selection

(1) The ZOM point source flow assumption should be tested empirically. That is, it should be determined if the LISP spray distribution coefficients are a function of the cold flow collection plane distance.

(2) The ZOM mass distribution methodology should account for combustion effects such as gas acceleration and reactive stream separation forces. A proposed model approach is detailed in Section V of this report.

(3) The LISP spray coefficient matrix should be expanded if the ZOM technique is retained in DER.

c. DER Vaporization Sensitivity Study

(1) The implications of the work of Bracco (Ref. 7) with respect to DER vaporization modeling should be evaluated.

(2) The DER K-Prime vaporization model insensitivity to chamber pressure should be investigated. The argument suggested in Appendix A to be the source of this error should be evaluated.

(3) The DER integration technique droplet downstream station velocity error should be eliminated. Additionally, the Euler predictor-corrector technique should be evaluated through a study using different calculational step sizes and number of corrective iterations. The possibility of developing a more efficient integration technique should be investigated.

(4) The results of this study and the work of Bracco both indicate the importance of the droplet drag coefficient (C_D) assumption. The drag coefficient literature should be reviewed and the selected DER drag coefficient formulation justified.

(5) The DER vaporization model should account for droplet heatup.

(6) The DER user manual and CPIA 246 should include an expanded section on droplet size distribution input selection.

d. Near-Zone Combustion and Monopropellant Flame Considerations

(1) It is recommended that DER incorporate a monopropellant flame model for reasons cited in Section C.4. of Appendix A.

e. Combustion Gas Acceleration and Reactive Stream Separation (RSS) Effects on Cold Flow Mass Distribution

(1) It is recommended that a RSS model be considered for DER.

(2) The initial development of an a priori ZOM plane selection methodology (See Section V) should be brought to fruition.

f. Turbulent Mixing Model

(1) The characterization of turbulent mixing effects in DER would comprise a large step toward providing DER with the desired a priori prediction capability. It is recommended that such a model be considered for DER.

g. Development of an A Priori DER Mixing Model

(1) It is recommended that the current LISP ZOM model be improved by incorporating the influences of combustion gas acceleration, reactive stream separation, and turbulent mixing. As previously mentioned, an a priori ZOM calculational technique is also required. This topic is expanded in Section C.7. of Appendix A.

4. Inconsistencies Between JANNAF Procedures and DER Computer Program Operations

The primary conclusion is that the intended predictive accuracy of the JANNAF (DER) rigorous procedure (to within 1 percent for predicted specific impulse) is currently out of the question for a priori performance prediction. This directly relates to the program decision to forego the originally planned Task II DER analysis and concentrate, instead, on improvement of the ZOM plane mass distribution methodology.

B. CICM Computer Model Review Recommendations and Conclusions

The CICM review was accomplished in three subtasks.

(1) Identification of Operational Problems Including a Code Review and Inclusion of Diagnostic Print-Out Statements,

(2) Identification of Inadequate Formulations and Model Technical Shortcomings, and

(3) Review of the JANNAF Performance Prediction Procedure (CPIA 246) with Regard to the Use of CICM and Identification of Inconsistencies.

The review is applicable to the CICM version described in Ref. 4, which also contains the user's manual referenced continually in this report.

The review was initiated by executing the program documented sample case and attempting to interface the program output with the STC subprogram of DER, as recommended in CPIA 246 for gas/liquid coaxial injector rigorous performance analysis. It was determined that the current CICM interface routine, DERINI, was incomplete and punched several improperly formated cards for input to the STC subcritical K-Prime version. First priority, during the review, was given to development of a new CICM/STC interface procedure because of the need for an accurate and cost-effective method of interfacing CICM and STC during the program Task II CICM analysis. The resulting new procedure is detailed in Section C.3. of Appendix B. The key recommendations and conclusions resulting from the CICM review results detailed in Appendix B are listed in the following three paragraphs corresponding to the previously described review subtasks.

1. Coding Errors and Diagnostic Statements

It is recommended that the CICM calculational problem that results in periodic "dropping" of drop size groups from the calculation be investigated.

2. Identification of Inadequate Formulations and Model Technical Shortcomings

The identification of inadequate CICM formulations and technical shortcomings was considered to be the next most important review task after improvement of the CICM interface procedure. CICM is a relatively new JANNAF program that has not been used extensively, except by the developers of the model. Therefore, it was considered important that basic model assumptions and analysis techniques be critically evaluated. The recommendations and conclusions resulting from the CICM technical formulations review are summarized below.

a. A review of the CICM stripping rate correlation should be conducted. The derivation of the current, or any proposed alternate correlation, should be substantiated and be made open to critical review.

b. A review of the CICM drop size correlation should be conducted. Such a study could also investigate the sensitivity of coaxial injector performance to the predicted jet mass median drop size. This would allow determination of the performance prediction uncertainty due to the availability of many different drop size correlation equations.

c. The drop size distribution tabulated at the end of a CICM run is only the summation of several constant mass median diameter groups; each group being calculated over a particular axial step. This resultant distribution is quite different than a drop size group calculated with distributions typically used to model rocket combustor sprays (e.g., Nukiyama-Tanasawa, Logarithmic-Normal, etc.). It is recommended that the significance of this CICM model simplification be evaluated.

d. It is strongly recommended that the CICM technique for accounting for intra-element mixing be improved. If the use of single element cold flow data to specify the intra-element mass distribution is continued, a standard measurement technique should be developed. A standard methodology for interpreting and inputting the data to CICM is also required. Preferably, an intra-element mixing model should be developed for CICM. Applicable models have been derived from experiment for gas/gas coaxial element mixing. The first step in adapting such models would be to determine the feasibility of applying a gas/gas mixing model to the solution of gas/liquid mixing.

e. All JANNAF engine analyses should record estimated manifold maldistribution performance losses, to build up a reference data base.

3. Inconsistencies Between JANNAF Procedures and Program Operations

The new CICM/STC interface procedure was written during this review subtask. The recommendations and conclusions resulting from the review of CICM's role in the JANNAF performance procedures are listed below.

a. The original provision of the CICM/STC interface was for the supercritical DER program version. The new CICM/STC interface procedure described in Section C.3. of Appendix B should be used for subcritical propellant analysis. This procedure should also be adopted for use in the new "standardized" DER program currently being developed.

b. The CICM and STC programs should be interfaced at a chamber axial plane where all the calculated oxidizer drop size groups have been heated to the chamber "wet bulb" temperature.

c. A standard JANNAF procedure or technique should be developed to predict single coaxial element intra-element mass distribution.

d. A procedure should be developed for allowing for the effect of diffusion mixing on face plane measured manifold mass distributions.

e. An accurate CICM mass distribution analytical model or empirical approach is required to allow JANNAF standard atomization coefficients (C_A and B_A) to be backed out from coaxial injector hot fire data.

IV CICM ANALYSIS AND DATA CORRELATIONS

The original objectives of Task II were: (1) Provide information on the present prediction capabilities of the JANNAF DER and CICM injection-combustion computer programs; (2) Identify conditions where reliable predictions can be obtained; and (3) Identify areas requiring further improvement and research. The CICM phase was completed as originally planned, while the DER phase of the task was rescoped (see Section V). The CICM model was applied to correlation of characteristic exhaust velocity efficiency (η_{C*}) for three tests conducted with the M-1 pressure fed 600,000 lbf (at 550 psia chamber pressure) hydrogen/oxygen engine. The CICM analysis was limited to tests with subcritical liquid oxygen inlet conditions. Excellent agreement was obtained between $\eta_{C*_{TEST}}$ and $\eta_{C*_{PRED}}$ from the JANNAF simplified prediction methodology for two of the three tests analyzed. The results of the analysis have verified the accuracy of the CICM model for the case where injector intra-element mixing losses are negligible.

A. M-1 Engine Experimental Data Base

The data base selected for the analysis and correlation of the CICM computer program was that of the M-1 thrust chamber developed by ALRC under NASA Contracts NAS 3-2555 (Ref. 8) and NAS 3-11214 (Ref. 9). The M-1 engine was designed to utilize liquid oxygen/liquid hydrogen propellants and deliver 1,500,000 of thrust when operating at its nominal design conditions of 1000 psia chamber pressure and 5.49 mixture ratio. During development, the thrust chamber was tested with LO_2/GH_2 propellants with a low area ratio ablative combustion chamber over a range of chamber pressure (550-1050 psia), mixture ratio (4-6), and hydrogen inlet temperature (80-130°R). The CICM data base met all the pre-defined program requirements for the following eight reasons:

1. Conventional injector element applicable to CICM (gas/liquid coaxial);
2. Capable of direct modeling with CICM/DER;
3. Subcritical propellant conditions (P_c = 550 psia);
4. Propellants of future interest (O_2/H_2);

5. Low area ratio test configuration (ε = 2:1);
6. Simple wall boundary conditions (no mass addition, minimal fuel film cooling of 1/2 percent of the total flow rate);
7. Test data at nominal and off-nominal operating conditions (O/F, hydrogen density variations);
8. Element to element mass distribution cold flow data.

Detailed descriptions of all the M-1 test hardware, facilities, and data measurement techniques are contained within the JANNAF-Simplified Performance Prediction narrative of Appendix C. The S/N 012 injector analyzed during the study is pictured in Figure 2. The injector contained 3,248 elements with gaseous hydrogen being injected annularly around the oxidizer. A row of 360 orifices drilled through the porous rigimesh face were located around the injector periphery and provided the chamber wall film cooling. Approximately 3.7 percent of the total fuel flow rate was used for chamber wall film cooling. Total fuel element flow rate was 89.8 percent of the thrust chamber fuel flowrate with a baffle fuel film cooling flow percentage of 3.9 percent. The remaining 2.6 percent of the fuel flowed through the rigimesh injector face. The coaxial element consisted of two basic components which were threaded together. An oxidizer tube was recessed within the fuel sleeve producing a fuel annulus between the two parts. The oxidizer tube was flared at a fifteen degree half angle and was recessed 0.231 inches from the injector face. Elements were arrayed in 33 concentric rows. The low area ratio combustion chamber used for testing with the M-1 injector was comprised of an outer steel shell and an inner ablative liner (tape wrapped silica-reinforced phenolic). The assembled combustion chamber (See Figure C-4 of Appendix C) consists of an upper fuel torous and a lower conical combustion chamber.

The test data that was reduced during the task data evaluation effort is tabulated in Table I. Nomenclature for Table I is shown in Figure C-1 of Appendix C. The three tests that were selected for CICM analysis are detailed in Table II. Test 009 was at the nominal operating point. Test 010 was analyzed to investigate the influence of mixture ratio on performance. Test 016 was analyzed to correlate the effect of injection velocity ratio change due to

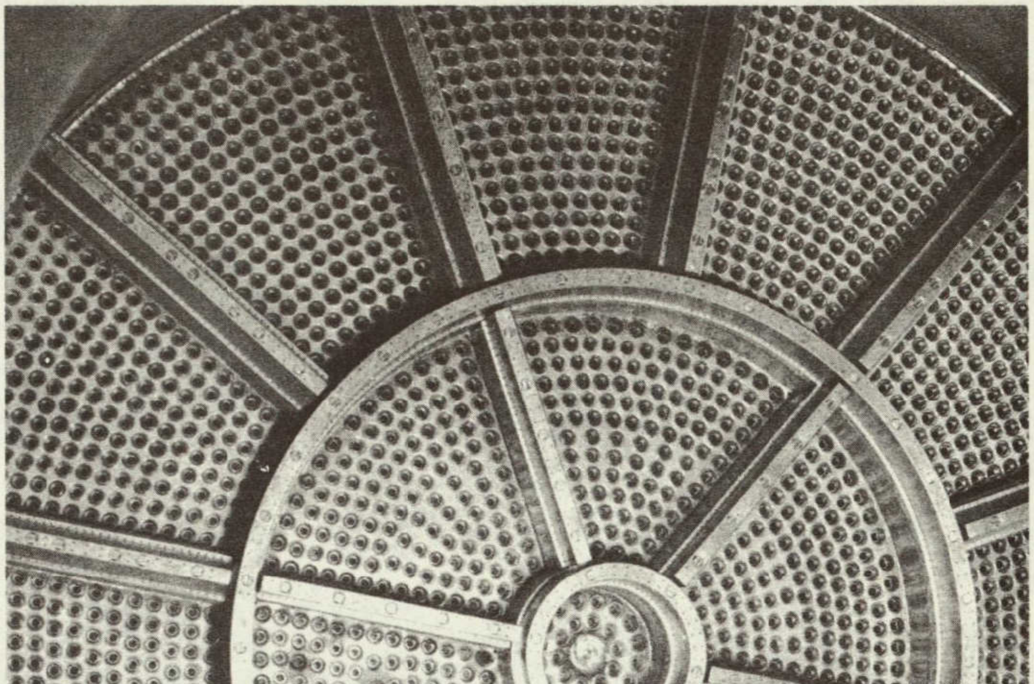

FIGURE 2. INJECTOR S/N 012 SHOWING FACE AND BAFFLE PATTERN

TABLE I. SEA LEVEL SUB-CRITICAL TEST DATA

Test No.	Summary Time Start (sec)	Summary Time Stop (sec)	Duration (sec)	Throat Area Pre (in^2)	Throat Area Post (in^2)	Chamber Pressure (psia)	O/F	Thrust Meas. (lbs)	Isp Meas. (sec)	W_o (#/sec)	W_F (#/sec)	$W_{F(GH_2)}$ (#/sec)	W_{FT} (#/sec)	W_T (#/sec)
007	44.2	44.7	44.72	707.370	711.860	582.8	4.87	492840	305.0	1340.7	249.4	26.0	275.3	1616.0
009	44.3	44.8	44.81	728.269	735.994	556.6	5.46	495409	300.5	1393.4	220.2	35.0	255.2	1648.6
010	46.8	47.3	47.33	735.994	736.308	572.0	4.04	510096	310.4	1317.6	296.4	29.6	325.9	1643.6
014	46.8	47.3	47.38	706.495	722.048	541.1	5.30	481765	303.5	1335.4	213.4	38.6	251.9	1587.3
016	45.0	45.5	45.56	722.048	727.902	567.9	5.53	501304	301.7	1407.1	209.0	45.6	254.6	1661.7
017	46.3	46.8	46.89	727.902	728.368	571.0	4.76	506116	307.5	1360.1	245.7	40.1	285.7	1645.8
019	44.3	44.8	44.89	733.644	736.391	576.0	5.15	516590	304.4	1421.3	236.1	39.9	276.1	1697.3
020	46.5	46.5	46.5	736.391	748.222	569.4	5.07	510642	298.7	1428.1	240.0	41.6	281.5	1710.0

Test	PFT (psia)	PFFM-2 (psia)	PF_{MIX}-2 (psia)	PFTCV-1 (psia)	PFTCV-2 (psia)	PFJ-3A (psia)	TFFM (°R)	TFTCV-2 (°R)	TFJ (°R)	POT (psia)	POFM (psia)	POTCV-1 (psia)	POTCV-2 (psia)	POJ-2A (psia)	TOFM (°R)	TOTCA-2 (°R)	TOJ (°R)	PC4B-1 (psia)	PC4B-2 (psia)
007	805	731	722	719	703	624	44	102	84	749	729	729	724	680	171	186	173	482.4	482.6
009	808	748	740	741	720	619	44	117	97	750	732	729	737	674	168	181	169	464.4	463.8
010	878	773	761	763	742	638	45	89	82	749	737	734	737	685	173	177	174	477.5	476.9
014	832	778	758	763	746	523	45	116	110	730	720	717	705	662	173	180	174	451.5	450.1
016	872	823	805	808	788	646	44	127	122	769	750	746	734	686	173	181	174	474.0	472.3
017	897	831	804	812	787	652	45	108	106	759	686	742	732	686	170	181	171	476.7	475.4
019	899	830	811	816	792	658	45	117	110	788	769	762	740	700	171	179	172	480.4	478.3
020	900	832	814	816	793	656	44	115	107	787	769	762	753	706	169	180	170	475.3	473.7

TABLE II

M-1 TESTS SELECTED FOR CICM ANALYSIS

TEST	W_o (lbm/sec)	W_F (lbm/sec)	T_o (°R)	T_f (°R)	O/F	P_c (psia)	V_F/V_o	ΔV (ft/sec)	ρ_F (lbm/ft^3)	η_{C*}
009	1393	255.2	169	97	5.46	524	18.2	310	1.45	.959
010	1318	325.9	174	82	4.04	538	16.2	264	2.16	.964
016	1407	254.6	174	122	5.53	534	25.8	456	1.0	.980

009 Nominal Conditions

010 Effect of Fuel Gas Density at Constant ΔV

016 Effect of ΔV

hydrogen density variation.

B. M-1 Coaxial Injector Analysis with JANNAF Simplified Prediction Procedure

The procedures and results of the CICM analysis of the M-1 engine tests are summarized in the following three subsections, that describe in turn: (1) calculation of test characteristic exhaust velocity efficiency; (2) prediction of C* efficiency with the JANNAF simplified performance evaluation methodology; and (3) determination of test measured C* uncertainties. The JANNAF simplified prediction procedures described in CPIA 246 were utilized to economize and speed the analysis.

Examination of the DER and CICM review results previously presented in Section III can, admittedly, lead to the conclusion that the M-1 performance analysis described below has been conducted with inadequate models. An important consideration was the fact that the M-1 thrust chamber design is very similar to the J2-S design used to calibrate key CICM jet stripping rate and drop size constants. (See Ref. 6 and J2-S sample case in CPIA 246). Also, both the M-1 and J2-S engines posses extremely long chambers that eliminate significant intra-element mixing losses. Therefore, the M-1 predictions were not invalidated by assuming uniform intra-element mass distribution, as described in a following paragraph. Additionally, using the STC subprogram of DER downstream of CICM was not considered an analysis weakness because STC utilizes similar key vaporization model analytical techniques to those of CICM (e.g., both models use the same droplet drag coefficient model). It should be remembered that a primary objective of the analysis was to verify that an independent user of the CICM/STC JANNAF analysis methodology could obtain an accurate performance prediction for a gas/liquid coaxial injector.

1. Calculation of Test C* Efficiency

Test C* was calculated from the equation shown below, taken from Section 2.1.2 of CPIA 245.

$$C^*_{TEST} = \frac{Pc_{eff}\, A_{T_{TEST}}}{\dot{M}_{T_{TEST}}} \tag{1}$$

Pc_{eff} is the effective throat stagnation pressure, calculated from available chamber static pressure measurements. Two static pressure measurements were taken; at the Pc_5 and Pc_4 locations shown in Figure C-2 of Appendix C. The chamber combustion total pressure loss resulted from the CICM/STC computer run executed during the C* prediction analysis described in the next section. The CICM/STC calculated chamber static pressure profile correlated extremely well with the measured static pressures, as explained in Section IV.C.1. This correlation verified the CICM/STC calculated combustion (Rayleigh Line) total pressure loss. The test summary periods for analysis were selected to occur just prior to test FS2 so that the post-test ablative chamber throat diameter measurement would result in an accurate test throat area value.

Test C* efficiency is simply the ratio of the test C* to the theoretical ODE C* value at the test propellant inlet, mixture ratio, and chamber pressure conditions.

$$\eta_{C^*_{TEST}} = \frac{C^*_{TEST}}{C^*_{ODE}} \qquad (2)$$

C* ODE was calculated with JANNAF TDK computer program (Ref. 5) at the test conditions indicated in Table III. The resulting test C* efficiencies are also shown in Table III.

2. JANNAF Test C* Prediction

The JANNAF simplified performance prediction methodology described in Section 3 of CPIA 246 was utilized. Appendix C of this report contains a narrative of the application of the procedure to analysis of the selected M-1 tests and sample input for all the JANNAF computer programs executed. The predictive equation for C* is expressed in terms of efficiencies for the significant chamber loss processes.

$$\eta_{C^*_{Pred}} = \eta_{C^*_{HL}} \times \eta_{C^*_{TD}} \times \eta_{C^*_{KIN}} \times \eta_{C^*_{BL}} \times \eta_{C^*_{MIX}} \times \eta_{C^*_{VAP}} \qquad (3)$$

TABLE III

TEST CONDITIONS FOR $\eta_{C^*_{TEST}}$ CALCULATION

TEST	O/F	PC_{eff} (psia)	T_o (^oR)	T_f (^oR)	H_{f_o} (cal/g-mole)	H_{f_f} (cal/g-mole)	C^*_{ODE} (ft/sec)	C^*_{TEST} (ft/sec)	$\eta_{C^*_{TEST}}$
009	5.46	514	169	97	-3027	-1827	7694	7376	.959
010	4.04	532	174	82	-2991	-1918	7960	7674	.964
016	5.53	534	174	122	-2991	-1733	7685	7529	.980

The purpose of the M-1 test data analysis was to verify the capability of the CICM model to calculate the $\eta_{C^*_{MIX}}$ (mixing) and $\eta_{C^*_{VAP}}$ (vaporization) efficiencies for a GH_2/LO_2 coaxial injector. The meaning of and the technique used to evaluate each of the efficiency terms are explained in the following six paragraphs.

a. Heat Loss Efficiency ($\eta_{C^*_{HL}}$)

The chamber heat loss efficiency was assumed to be 1.0 for each test. This assumption was made for two reasons. (1) The thrust chamber wall was composed of an ablative silica-reinforced (tape-wrapped) phenolic that resulted in an effective adiabatic wall condition; and (2) Chamber heat loss to the injector face would be directly transferred to the propellants because of the plenum manifolds on the injector face backside.

b. Two-Dimensional Flow Efficiency ($\eta_{C^*_{TD}}$)

The two-dimensional C* flow efficiency accounts for the reduction of the throat potential flow area due to inlet effects. The equation used is simply the inverse of the inviscid flow discharge coefficient.

$$\eta_{C^*_{TD}} = \frac{\dot{M}_{ODE}}{\dot{M}_{TDE}} = \frac{1}{C_{D_{INV}}} \qquad (4)$$

The JANNAF ODE and TDE programs contained in TDK calculated the M-1 chamber $\eta_{C^*_{TD}}$ value of 1.002 (C_d = 0.998). This high throat C_d value occurs because of the large M-1 chamber throat inlet radius ratio value of 2.132.

c. Reaction Kinetic Efficiency ($\eta_{C^*_{KIN}}$)

The reaction kinetic C* efficiency was calculated with the ODK option of the TDK program. For all mixture ratios from 1.0 to 12.0 $\eta_{C^*_{KIN}}$ was calculated to be 1.0 for the M-1 engine. This occurs because of the high operating chamber pressure and thrust level of the engine (550 psia and 500,000 lbf, respectively).

d. Boundary Layer Efficiency ($\eta_{C^*_{BL}}$)

The C* boundary layer efficiency accounts for the displacement boundary layer effect on the throat potential flow area.

$$\eta_{C^*_{BL}} = \frac{A_T}{A_T - 2\pi \; R_T \; \delta^*_T} \tag{5}$$

The TDK program was run at the Test 009 nominal O/F to establish edge conditions for a boundary analysis with the JANNAF BLIMP computer program (Ref.10). Wall temperature and calculated ablative chamber regression rates documented in Ref. 9 were used to establish input for BLIMP. BLIMP was executed by using the assigned wall temperature and assigned blowing rate input options, and edge gas properties for a mixture ratio of 2.5:1. This mixture ratio is the nominal Test 009 wall mixture ratio, based on M-1 injector manifold mass distribution results described in the next paragraph. The BLIMP calculated throat displacement thickness was -5. x 10^6 ft which resulted in $\eta_{C^*_{BL}}$ of 1.000. Since the boundary layer effect on C* was found to be small, this value was assumed to be correct for all three tests analyzed.

e. Mixing Efficiency ($\eta_{C^*_{MIX}}$)

The purpose of the M-1 data analysis is to verify the capability of the JANNAF CICM computer program to predict energy release efficiencies for GH_2/LO_2 coaxial injectors. The C* energy release efficiency is composed of a mixing and vaporization term.

$$\eta_{C^*_{ERL}} = \eta_{C^*_{MIX}} \times \eta_{C^*_{VAP}}$$

The C* simplified mixing efficiency definition is shown below.

$$\eta_{C^*_{MIX}} = C^*_{\substack{ODE \\ INJ\ MR \\ MULTIZONE}} \Big/ C^*_{\substack{ODE \\ AVG\ INJ\ MR}} \qquad (7)$$

CICM does not calculate intra-element (shear) or inter-element (diffusion) mixing, however, the program has the capability to accept multiple zones of varying mixture ratio and to calculate the corresponding effect on the LO_2 atomization and vaporization rates. Since CICM simply solves the equation shown above for $\eta_{C^*_{MIX}}$, this calculation was evaluated externally from the CICM program to allow inexpensive parametric evaluation of the M-1 injector mass distribution data.

The M-1 injector manifold radial mixture ratio distribution is shown in Figure 3. The three levels of mixture ratio are due to a segmenting of the fuel manifold at the location of two injector baffle rings. Because of symmetric inlet conditions, circumferential distributions were calculated to be within $\pm$ 2 percent of nominal, and thus were ignored for purposes of the $\eta_{C^*_{MIX}}$ calculation.

Intra-element maldistribution data was not available for the M-1 design configuration, therefore no intra-element mixing loss was calculated for the injector. The mixing efficiency term accounts only for manifold induced element-to-element mass maldistribution. The H_2/O_2 gas/gas empirically based mixing model developed in Ref. 11 was used to estimate the intra-element mixing efficiency for the M-1 injector. The model indicated that intra-element mixing losses would be insignificant because of the long (29.75 inch) M-1 chamber design.

A simple computer program was written to sum streamtube performance and to evaluate the injector manifold induced mixing loss; by solving the following equation.

$$C^*_{\substack{ODE \\ INJ\ MR \\ MULTIZONE}} = \sum_{i=1}^{i=n} \frac{\dot{W}_i}{\dot{W}_T} \times C^*_{\substack{ODE \\ ZONE\ MR}} \qquad (8)$$

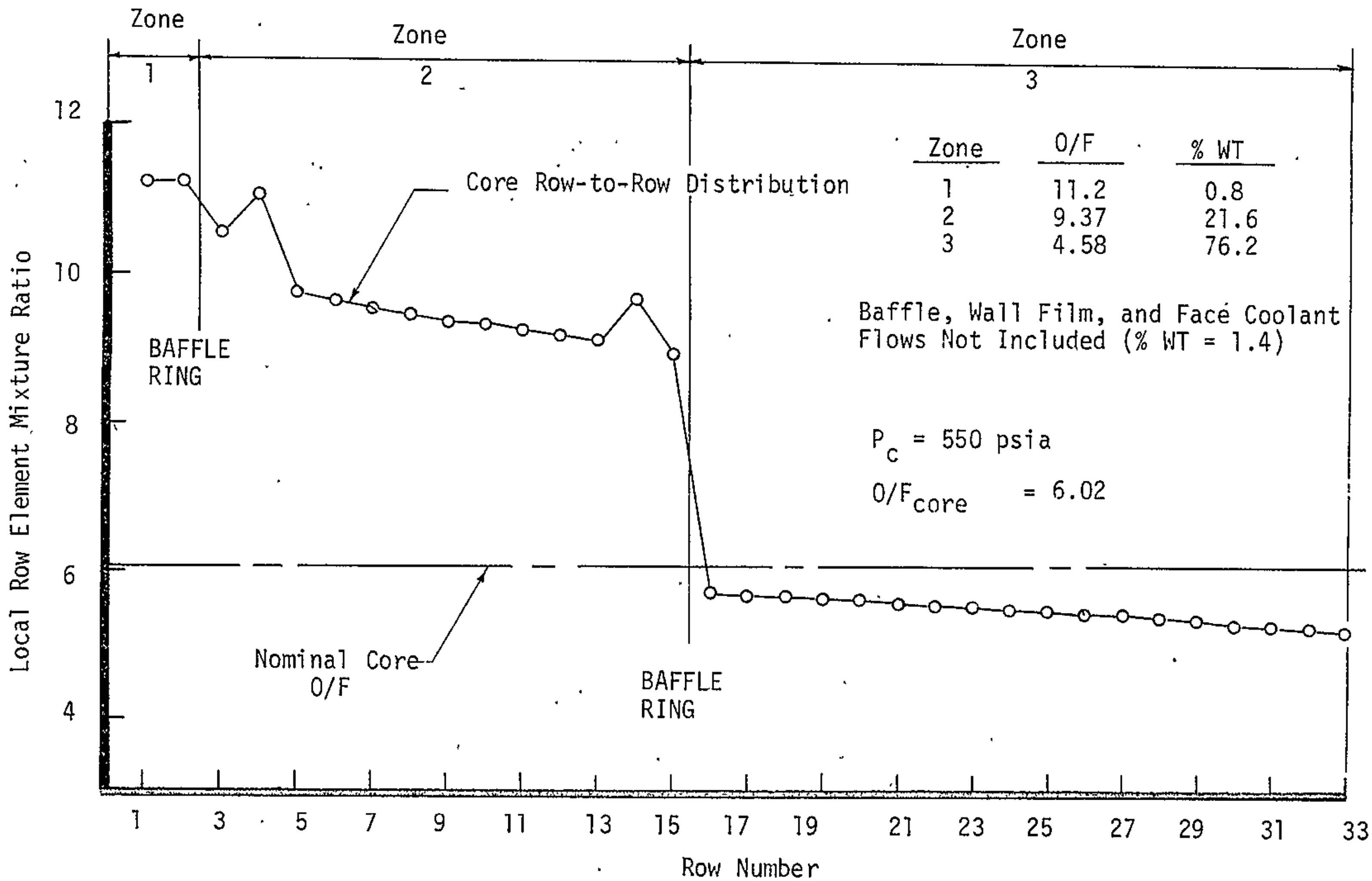

FIGURE 3. M-1 INJECTOR CORE RADIAL MIXTURE RATIO DISTRIBUTION

Figure 4 indicates the results of the $\eta_{C*_{MIX}}$ evaluation. Calculations were made ranging from 1 to 36 streamtubes (33 injector rows plus two baffle ring and one outer film cooling row) to determine the influence of stream tube mass assignment on the $\eta_{C*_{MIX}}$ calculation. The calculated efficiency is seen to be extremely sensitive to the selected number of streamtubes for flow division. The $\eta_{C*_{MIX}}$ value decreases as the number of streamtubes is increased as would be expected. This sensitivity points out a general weakness of the JANNAF performance prediction methodology, that is, there are no standardized techniques for streamtube mass assignment in any of the JANNAF performance programs (i.e., CICM and DER). Since, as shown in Figure 3, the M-1 manifold design resulted in three distinct chamber flow field mixture ratio zones, a three zone $\eta_{C*_{MIX}}$ calculation was performed. This result is indicated by the dashed line in Figure 4. The calculated value was equal to the case where a streamtube was assigned to each injector row. This $\eta_{C*_{MIX}}$ calculation technique was selected for analysis because it was consistent with the physical injection zones created by the injector baffle design. The calculated $\eta_{C*_{MIX}}$ ranged from 0.976 for tests 009 and 016 to 0.980 for the low mixture ratio test number 010.

f. Vaporization Efficiency ($\eta_{C*_{VAP}}$)

The JANNAF CICM and STC computer programs were utilized to calculate the injector LO_2 vaporization efficiency. As explained in Appendix B, the recommended program interface technique,which was utilized during the analysis, is to run CICM until all LO_2 droplets have approached the chamber wet-bulb temperature. The CICM analysis was conducted by inputing required M-1 injector/chamber geometry and selecting the program user's manual recommended atomization rate (C_A) and vaporization rate (B_A) constants shown in Table IV. The test vaporization calculations are summarized in Table IV. CICM was run to a chamber axial location of 4.10 inches (wet bulb plane determined through one trial CICM run) from the injector face plane for all three tests. STC completed the calculation to the chamber throat plane axial location of 29.75 inches. One zone analyses (at the test mixture ratio) were executed

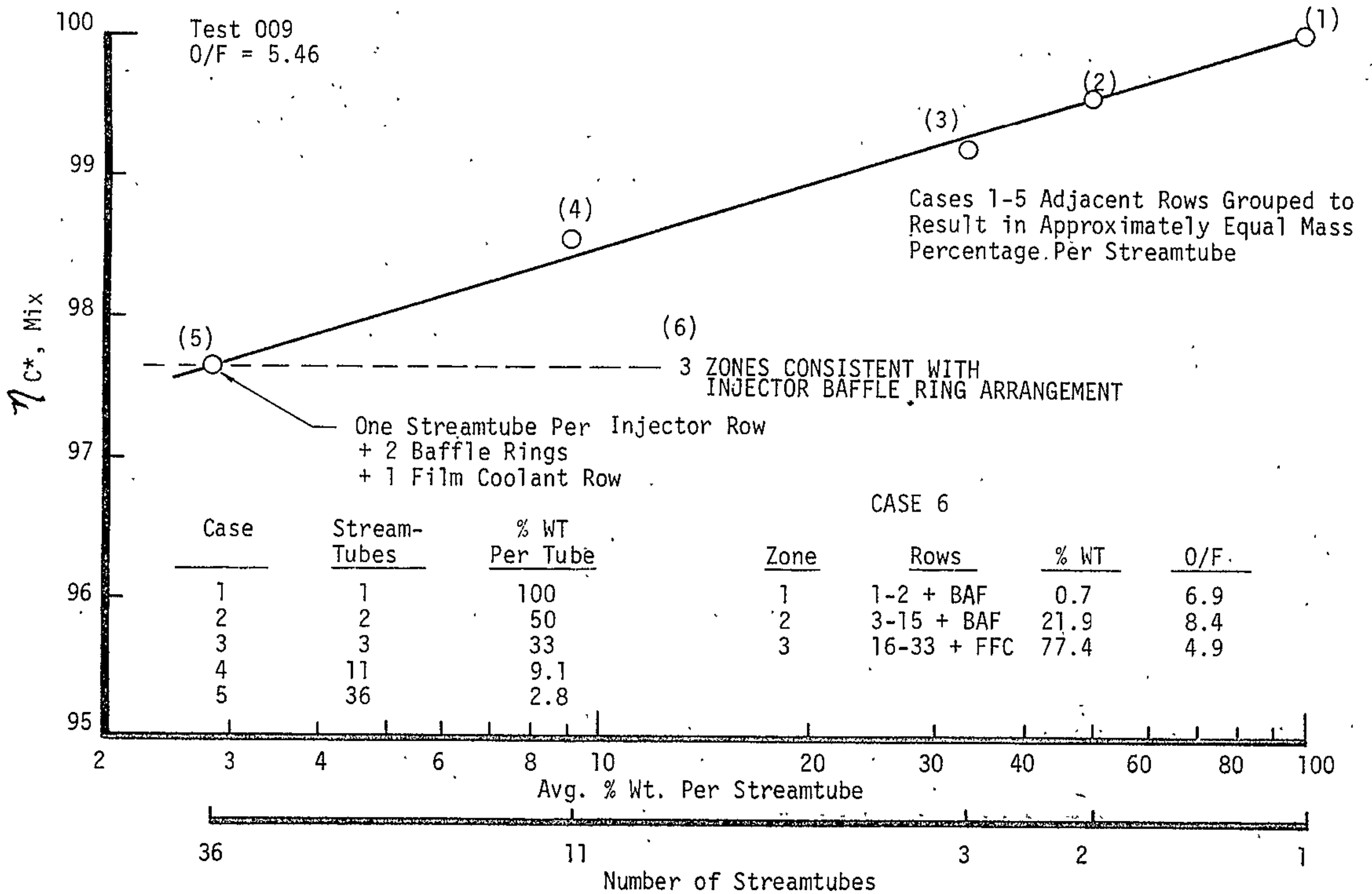

FIGURE 4. MIXING LOSS SENSITIVITY TO STREAMTUBE MASS DISTRIBUTION

TABLE IV

CICM/STC VAPORIZATION CALCULATION SUMMARY

RUN	TEST	PROGRAM	ZONES	O/F	CA	BA	$\%VAP_{OX}$	ηc^*_{VAP}
1	009	CICM/STC	1	5.46	0.08	120	.973	.982
2	010	CICM/STC	1	4.04	0.08	120	.992	.994
3	016	CICM/STC	1	5.53	0.08	120	.997	.997
4	009	CICM only	1	5.46	0.08	120	~.98	~.99

for all three tests to calculate $\eta_{C^*_{VAP}}$. Multiple zone analyses were not conducted for two reasons. First, initial correlation of the test 009 C* prediction with the test value showed excellent agreement utilizing a one zone $\eta_{C^*_{VAP}}$ value. Secondly, approximately 75 percent of the injector mass flow is contained in the outer zone (rows 16-33, See Figure 3). All of these rows have mixture ratio values only slightly lower than the nominal injector core mixture ratio.

In addition to the three CICM/STC runs for each test, a CICM only run was conducted for test 009 to note any difference between a CICM/STC calculation and a complete CICM chamber calculation. The CICM run stopped at an axial station of 24 inches in the 29.75 inch M-1 chamber because of a continuity check error caused by improper input of the chamber throat area. For this reason, the corresponding efficiency values shown in Table IV were deduced through extrapolation. A complete discussion of the CICM and STC vaporization calculation results is included in the section on data correlation and analysis to follow. The CICM/STC $\eta_{C^*_{VAP}}$ calculations were utilized in the C* efficiency predictions summarized in the next subsection.

g. C* Efficiency Prediction ($\eta_{C^*_{PRED}}$)

The calculated test C* efficiencies are tabularized below in Table V. A discussion on correlation of the predicted and test values follows the next section on test measurement uncertainties.

TABLE V

TEST η_{C^*} PREDICTION SUMMARY

TEST	$\eta_{C^*_{HL}}$	$\eta_{C^*_{TD}}$	$\eta_{C^*_{KIN}}$	$\eta_{C^*_{BL}}$	$\eta_{C^*_{MIX}}$	$\eta_{C^*_{VAP}}$	$\eta_{C^*_{PRED}}$	$\eta_{C^*_{TEST}}$
009	1.000	1.002	1.000	1.000	0.976	0.982	0.960	0.959
010	1.000	1.002	1.000	1.000	0.980	0.994	0.977	0.964
016	1.000	1.002	1.000	1.000	0.976	0.997	0.976	0.980

3. Test Measurement C* Uncertainties

The correlation of the test and predicted η_{C*} depend on the uncertainty of both values. The net correlation uncertainty is defined by CPIA 245 (Ref. 12) as:

$$U = \sqrt{S_{TEST}^2 + S_{PRED}^2} + B_{TEST} + B_{PRED} \qquad (9)$$

The precision (S) and bias values (B) depend on a knowledge of measurement and prediction calibrations and trends. To correlate the M-1 prediction and test values the following simplifications were made, because of lack of data.

$$S_{PRED} = 0, \; B_{TEST} = 0, \; B_{PRED} = 0.$$

These assumptions indicate that the only uncertainty that can be accurately evaluated for the M-1 analysis is the precision of the test data C* measurement. The following C* measurement 2σ data uncertainties were known.

Total Weight Flow	$\pm$ 0.8%
Chamber Pressure	$\pm$ 0.4%
Ablative Throat Area	$\pm$ 0.7%

The resultant uncertainty in test measured C* is $\pm$ 1.1%. Therefore, even by assuming zero uncertainty in the C* prediction and no measurement or prediction bias the agreement between measured and predicted C* (See Table V) is well within the accuracy of the test data, except for test 010. This result is discussed in the next section.

C. Data Correlation and Analysis

The results of the M-1 test data correlation will be discussed in two parts: (1) a discussion on the results of the CICM/STC and CICM computer model combustion chamber energy release predictions; and (2) results of the correlation of the JANNAF simplified prediction procedure C* efficiencies with the test values.

1. Vaporization Model Results

The CICM/STC calculated chamber pressure profiles for the three tests analyzed are shown in Figure 5. The analytically calculated profiles pass closely to the test measured static pressure values, indicating that the chamber energy release characteristic is being realistically modeled with CICM. These good correlations verified the use of the CICM/STC calculated chamber total pressure loss for the determination of the $P_{c_{eff}}$ value for each test, as previously described in Section IV.B.1.

As previously mentioned, a CICM only run was executed for test 009 to determine if the use of the simpler STC vaporization model of DER was compromising the accuracy of the vaporization calculation. The LO_2 vaporization profiles for each calculational method is shown in Figure 6. The two calculations agreed within one to two percent over the entire chamber length. The CICM only calculation was extrapolated beyond the 24-inch axial station because of an input throat area error described in the next paragraph.

The test 009 chamber pressure profiles calculated by CICM/STC and CICM only are compared in Figure 7. As displayed, the pressure profile agreement is excellent. The slight differences are attributable to the incorrect throat area input to CICM for the CICM only calculation. This input error resulted in a continuity check error as the throat plane was approached.

2. Correlation of Predicted and Test C* Efficiencies

The predicted and test C* efficiencies summarized in Table V are graphically compared in Figure 8. Agreement was excellent for tests 009 and 016, while there was a 1.4 percent difference (compared to a test measurement uncertainty of $\pm$ 1.1 percent) between prediction and test for test 010.

The test conditions are compared in Table II. The primary operating difference between test 016 and the nominal test 009 is an increase

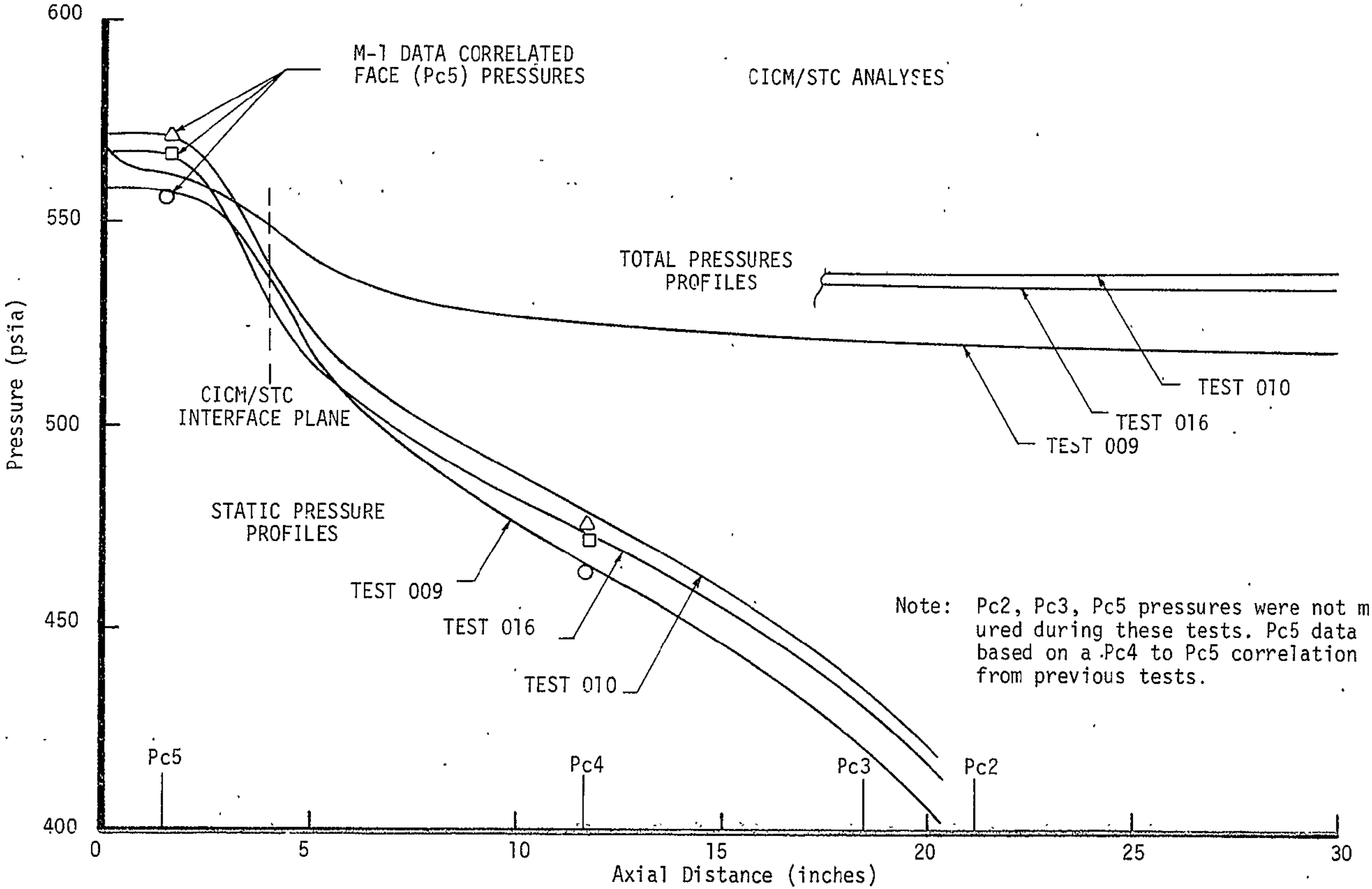

FIGURE 5. MEASURED AND CALCULATED CHAMBER PRESSURE PROFILES

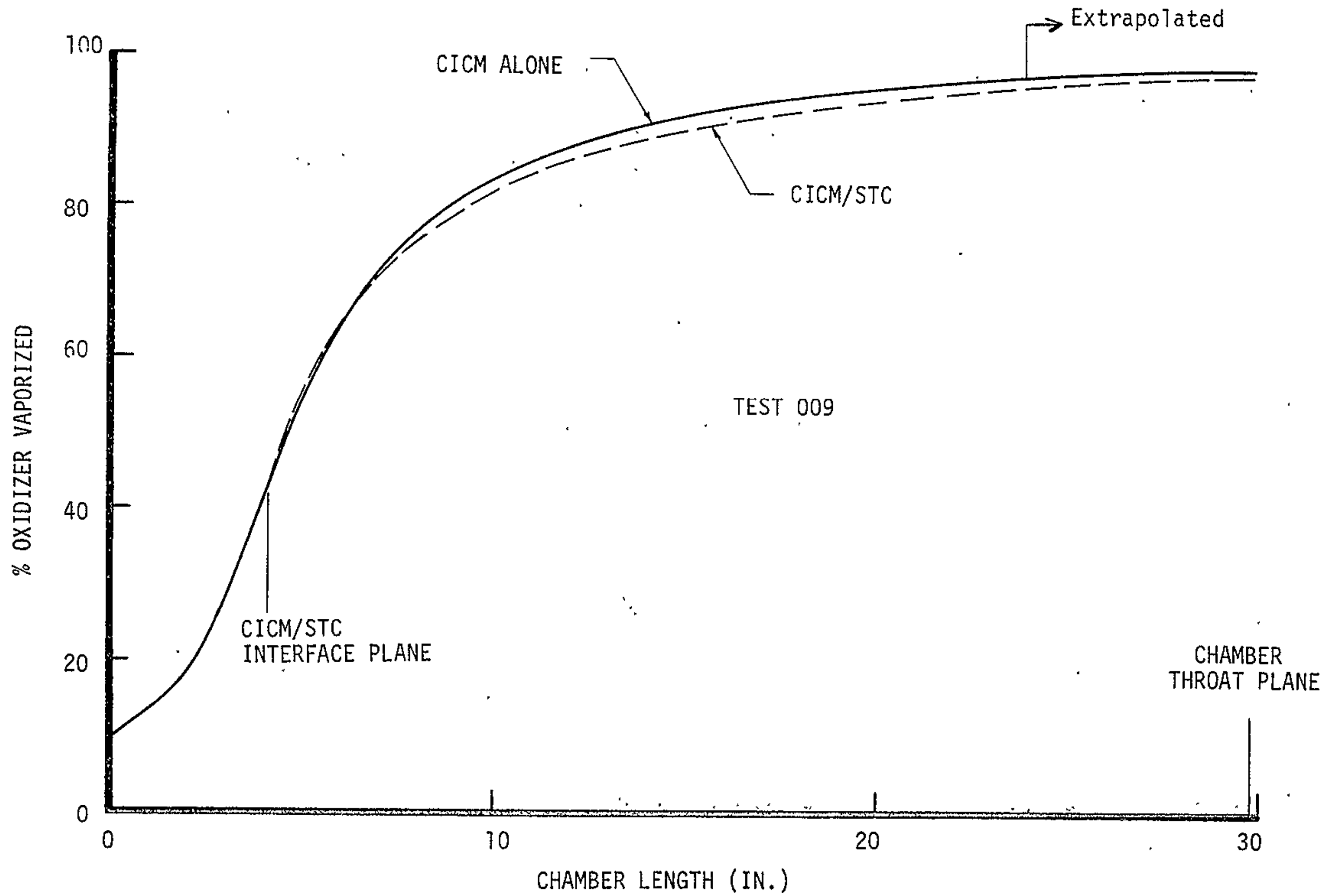

FIGURE 6. COMPARISON OF CICM AND STC OXIDIZER VAPORIZATION PROFILES

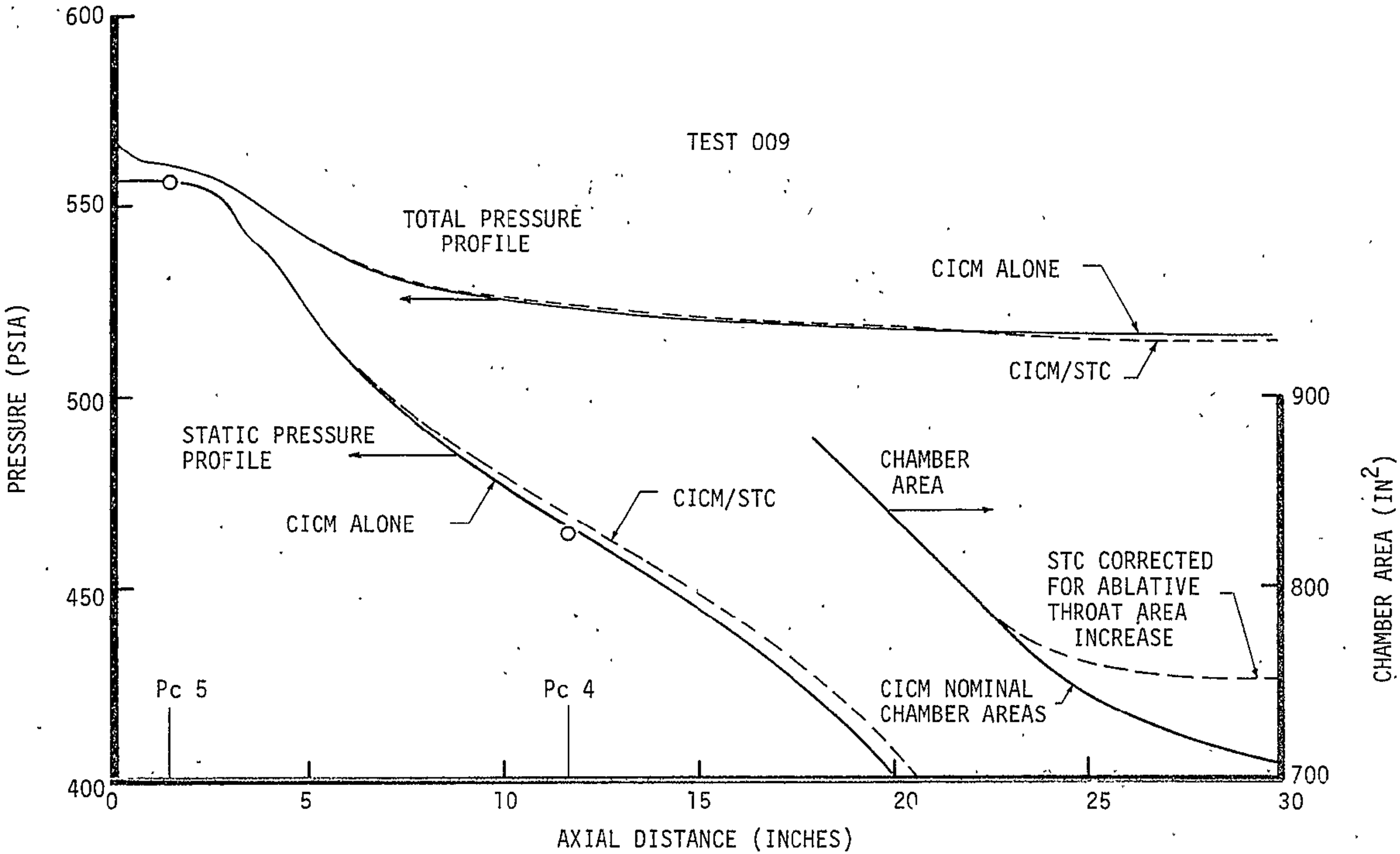

FIGURE 7. COMPARISON OF CICM AND STC PRESSURE PROFILES

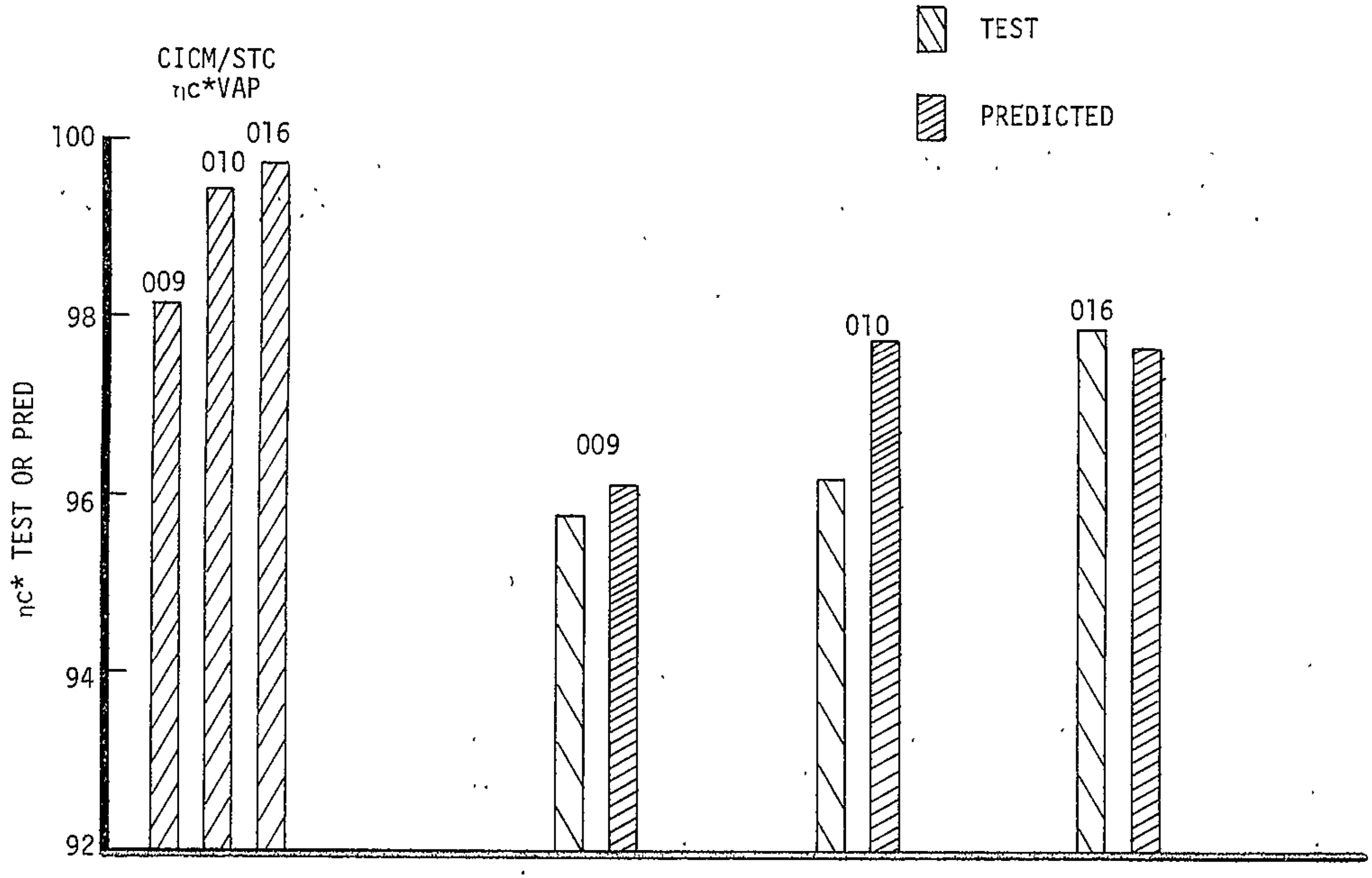

FIGURE 8. CORRELATION OF PREDICTED AND TEST ηc*'s

in the injection velocity difference of from 310 to 456 ft/sec. The increase occurs because of the fuel density decrease associated with increasing the fuel inlet temperature from 97°R to 122°R. The CICM equations accurately predict the performance increase due to the smaller drop sizes produced by a higher velocity difference between the gaseous H_2 annulus and the liquid O_2 core. This inverse relationship is evident from the CICM mass median drop size correlation equation shown below.

$$D_j = B_A \left[\frac{\mu_j \quad (\sigma_j/\rho_j)^{1/2}}{\rho_g \; U_r^{\,2}} \right]^{2/3} \tag{10}$$

The JANNAF/CICM η_{C*} prediction for test 010 was 1.4 percent higher than the test value. As protrayed in Figure 8, the test performance for test 010 is only slightly higher than the nominal test 009 value. Referring again to Table II, it can be seen that a test 010 increase in fuel flowrate is offset by a higher fuel density that results in a net decrease in the gas to liquid jet relative gas velocity. This effect should lower predicted performance. However, the higher H_2 inlet density increases predicted performance as can be seen from equation (10). The mass median drop size is inversely proportional to the fuel gas density (ρ_g) raised to the 2/3 power. As described in Section B.2 of Appendix B, this CICM correlation dependency on the gaseous annulus density is much more severe than predicted by the other empirically based circular jet drop size models that has correlated a gas density influence. The model of Ingebo (Ref. 13) shows drop size to be inversely proportional to gas density raised to the 3/10 power. It is therefore suggested that CICM overpredicts the performance of test 010 because the gas density term is too significant in the equation (10) drop size relationship.

The following two observations, that resulted from the CICM analysis, are reiterated here to help clarify the results of the M-1 data correlation work. (1) The M-1 thrust chamber design is very similar to the J2-S design used to calibrate key CICM jet stripping rate and drop size constants.

(See Ref. 4 and J2-S sample case in CPIA 246). This is a definite reason for the success of the M-1 performance predictions. (2) Both the M-1 and J2-S engines possess extremely long chambers that eliminate large intra-element mixing losses. Therefore, the M-1 predictions were not invalidated by assuming uniform intra-element mass distribution.

D. Conclusions and Recommendations

1. Conclusions

The following conclusions have resulted from the JANNAF/ CICM analysis of the M-1 thrust chamber.

a. The CICM model has been verified for high performing thrust chambers with negligible intra-element mixing losses.

b. The CICM mass median drop size dependency on the gaseous annulus density is overly significant. It must be noted that changing the equation would most likely result in the requirement of recorrelating the key drop size constant, B_A.

c. The primary weakness of the CICM model is the simplified methodology for calculation of intra-element and inter-element (manifold induced) mixing losses.

2. Recommendations

The following recommendations are made based on the above conclusions regarding the M-1 analysis.

a. An intra-element mixing model should be developed for CICM.

b. CICM should be applied to correlation of test data obtained with a short chamber coaxial injector thrust chamber with a finite intra-element mixing loss.

c. Reformulation and verification of the CICM mass median drop size correlation equation should be considered.

V DER MASS DISTRIBUTION MODEL IMPROVEMENT

The original objective of Task II was to provide information on the present prediction capabilities of the JANNAF DER and CICM computer programs through correlation of well documented hot fire data bases. DER was to be used to analyze a 6000 lbf like doublet pair injector developed on the OMS engine program while CICM was to be applied to the 500,000 lbf M-1 engine gas/liquid coaxial injector. The CICM analysis was completed as originally planned and is documented in Section IV of this report.

After a careful evaluation of the Task I DER Computer Program Review, it was concluded that the DER subcritical K-Prime program contains inadequacies in the analytical formulations that could produce invalid data when applied to the OMS thrust chamber analysis. It was decided that the originally considered funds for this task should rather be used to remove detected shortcomings in the model.

Improvement of the LISP ZOM plane mass distribution methodology was selected as the new Task II analysis goal for three reasons. First, the "standardized" DER (SDER) development program (Contract FO 4611-75-C-0055), conducted concurrently with this program, has concentrated on improvement of the DER vaporization modeling, but not on mass distribution and mixing modeling. Secondly, as discussed in Appendix A, the ZOM plane location is known to be a key DER input parameter which significantly influences the calculated chamber mixing performance efficiency. Lastly, recent empirical investigations have led to formulation of a model for calculation of the ZOM plane location on an *a priori* basis.

The current development status of the new ZOM mass distribution model is summarized in the following four paragraphs that concern, respectively, (1) an explanation of the hypothesized model, (2) presentation of the subscale like doublet pair injector data base used to correlate the predictions of the formulated model, (3) results of data analysis and model correlation effort, and (4) conclusions and recommendations of this initial model development work.

A. Model Approach

During a recent development effort on the Space Shuttle OMS engine program subscale injectors were tested to model combustion stability response (Ref. 14). The test combustion chamber was densely instrumented with static pressure transducers to allow calculation of the local combustion gas flowrate and velocity through the use of isentropic flow relationships. Bracco (Ref. 15) has also utilized this technique and developed a method for accurately interpreting such measurements. The availability of the OMS test data has resulted in empirically based mass vaporization profiles that eliminate the uncertainty associated with calculating chamber gas profiles with DER or other available vaporization models. The uniquely accurate OMS data allowed calculations of the influence of near-zone combustion gas formation and acceleration on liquid spray fan profiles. The results of initial calculations indicated that these effects are significant, and that further investigation and formulation of an analytical model was warranted.

That the initial model development effort described in the following paragraphs of this section utilized empirical energy release rate data as the primary model input does not imply that such data will always be required. The test data was used instead of analytical predictions made with DER because accurate vaporization profiles near the injector face were required. DER does not account for monopropellant burning of hydrazine based fuels (the OMS subscale test propellant combination was NTO/MMH) that is known to significantly effect near zone energy release rates. (Monopropellant flame effects are discussed in Section C.4 of Appendix A). If the proposed model is ever adopted as a standard analytical procedure in DER it is probable that the DER vaporization models would have to account for monopropellant burning to result in accurate mixing loss predictions.

The originally proposed calculational technique is graphically portrayed in Figure **9**. The top plot in Figure 9 displays an empirically determined near zone (0-2 inches from the injector face plane) mass vaporization profile. Static pressure measurements included the five axial locations

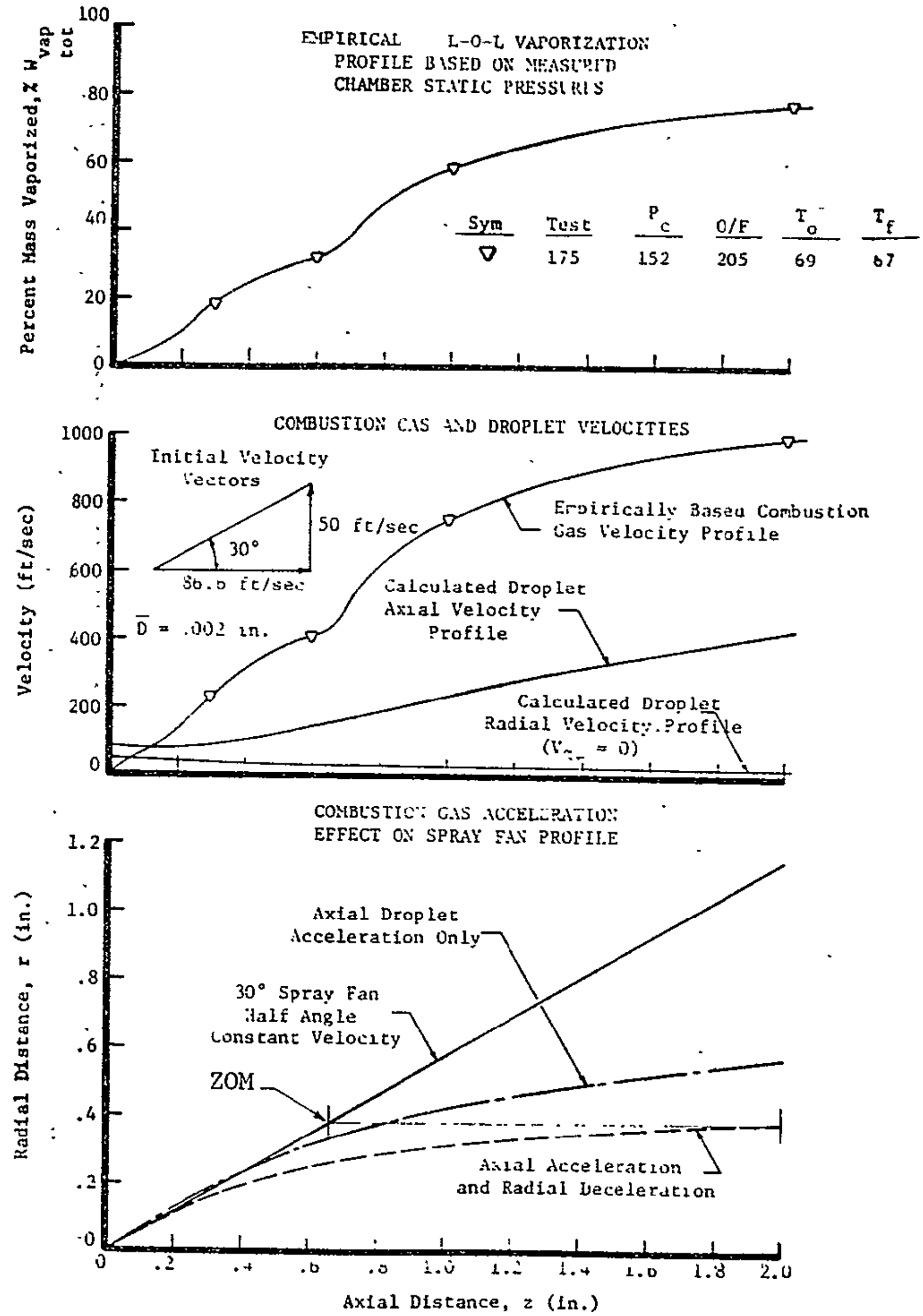

FIGURE 9. PROPOSED METHODOLOGY FOR ZOM GAS ACCELERATION EFFECTS MODEL

shown; 0.0, 0.3, 0.6, 1.0 and 2.0 inches from the face. Isentropic flow relationships were used to determine the local gas flowrate, resulting in the plot of percent mass vaporized versus axial distance. The equations used to develop gas flowrate (i.e., mass vaporization) profiles from chamber static pressure measurements are detailed in Appendix D , taken from Ref. (15).

The local gas flowrates were then used to calculate a chamber combustion gas axial velocity profile. Knowing the gas velocity profile allowed calculation of droplet velocity profiles through use of the standard drag equation and an assumed droplet drag coefficient model. These results are shown in the middle plot of the figure. A mass median droplet with a constant diameter of .002 inches was assumed to have an initial velocity vector as shown. The droplet axial velocity increases as the combustion gas axial velocity increases, because of axial aerodynamic drag. The droplet radial velocity decreases because the combustion gas was assumed to have a radial velocity component of zero.

The bottom plot on the figure shows the effect of combustion gas acceleration on the trajectory of a propellant droplet assumed to be on the outer spray fan streamline. Cold flow correlation techniques (e.g. the DER ZOM mass distribution method) assume a constant droplet velocity resulting, for the given initial droplet conditions, in the 30° spray fan half angle shown. If gas acceleration effects are accounted for the droplet trajectory, or spray fan profile, changes significantly. One of the corrected trajectories shown in the figure assumes the droplet is accelerated in the axial direction only. The other includes the effect of radial deceleration.

The results shown in the figure indicate that, for the case considered, spray fan radial spreading becomes insignificant at distances beyond 1.8 inches of the injector face. This result implies that little interelement mixing would occur downstream, thus pinpointing the area for selection of the correct value of the DER cold flow mixing plane, ZOM. The initially proposed ZOM determination technique, indicated in the figure, was to project the corrected spray fan radial dimension back to the cold flow case. The hot fire spray fan mass distribution was assumed to be correctly characterized by the cold flow mass distribution at the calculated ZOM plane location.

A four part task was conducted to develop the proposed ZOM calculation technique.

(1) Model Formulation

The purpose of this task was to formulate the proposed model for calculation of a predicted hot fire ZOM plane location. The model was coded for the digital computer to allow rapid reduction of the test data to be correlated in the data analysis subtask.

(2) Data Analysis

A test data reduction program was written to calculate test C* efficiencies and chamber axial gas velocity profiles. The ZOM prediction model used the gas velocity profile for each test to calculate the combustion corrected spray fan radial dimension and project back to the corresponding cold flow radial location to calculate the ZOM plane location.

(3) Performance Data Correlation

The DER LISP subprogram was used to predict C* mixing efficiency ($\eta_{C^*_{mix}}$) as a function of the ZOM plane location. An empirically determined $\eta_{C^*_{mix}}$ value was backed out for each test knowing the measured C* efficiency and analytically calculating the test vaporization efficiency. An empirical ZOM value was calculated for each test from the $\eta_{C^*_{mix}}$ versus ZOM relationship calculated by LISP. Test determined ZOM values and trends were compared to those calculated by the analytical model.

(4) Results and Recommendations

The results of the initial model development effort were evaluated and conclusions reached. Recommendations for continuation of model development were formulated.

B. OMS Subscale Injector Experimental Data Base

The OMS subscale injector test program documented in Ref. 14 provides a uniquely accurate and comprehensive data base for correlation of predictions of the new ZOM model. Sixty-eight multi-element combustion tests with intensive chamber pressure profile instrumentation were used to infer axially distributed combustion profiles for the various injector designs. The OMS engine utilizes NTO/MMH propellants at a nominal chamber pressure of 125 psia. Mixture ratio, chamber pressure, and propellant temperature variations were tested to gain quantitative data on the combustion response influences of these engine operating variables.

The combustion chamber design utilized during the testing is sketched in Figure 10. Pressure measurements were made at planes located 0., 0.3, 0.6, 1.0, 2.0, 3.5 and 5.4 inches from the injector face plane. The chamber was 8.0 inches in length, resulting in measured test C* efficiencies of 80 to 90 percent of theoretical. The relatively low test C* efficiency for the coarse subscale injectors resulted in data that provided excellent insight into the effect of test variables on injector/chamber performance.

Two conventional circular orifice like doublet pair (quadlet) and four platelet injectors were tested. A quadlet injector design was selected for analysis because the DER LISP subroutine contains empirical spray distribution coefficients for only conventional circular orifice element types. The six element, 135 lbf thrust, quadlet injector is pictured in Figure 11. The fuel doublet is positioned nearest the wall and the oxidizer doublet is located inboard. A sketch of the quadlet element design is detailed in Figure 12. The quadlet tests selected for the ZOM model development effort are summarized in Table VI.

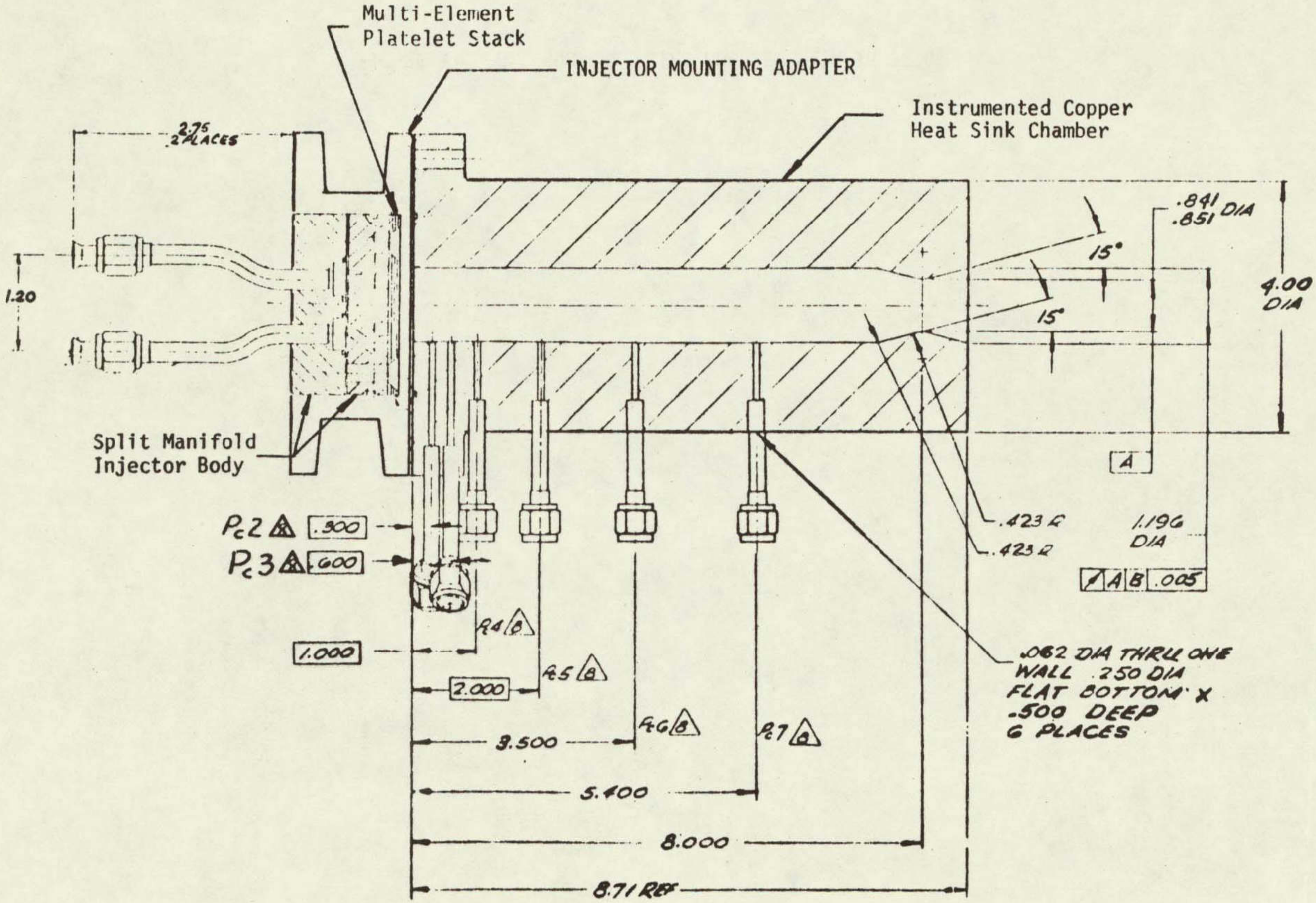

FIGURE 10. OMS MULTI-ELEMENT INJECTOR TEST COMBUSTION CHAMBER

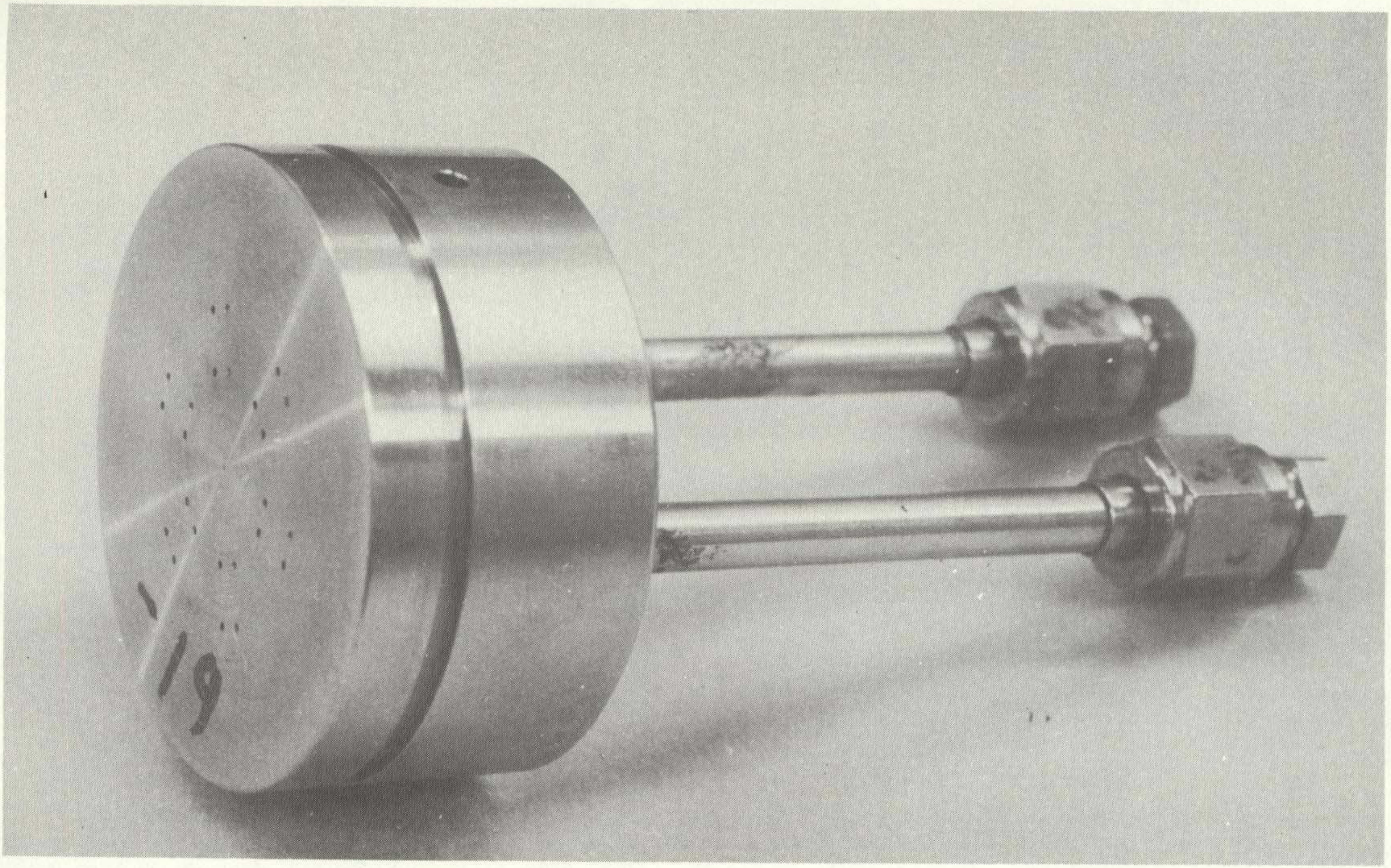

FIGURE 11. OMS SUBSCALE LIKE DOUBLET PAIR INJECTOR

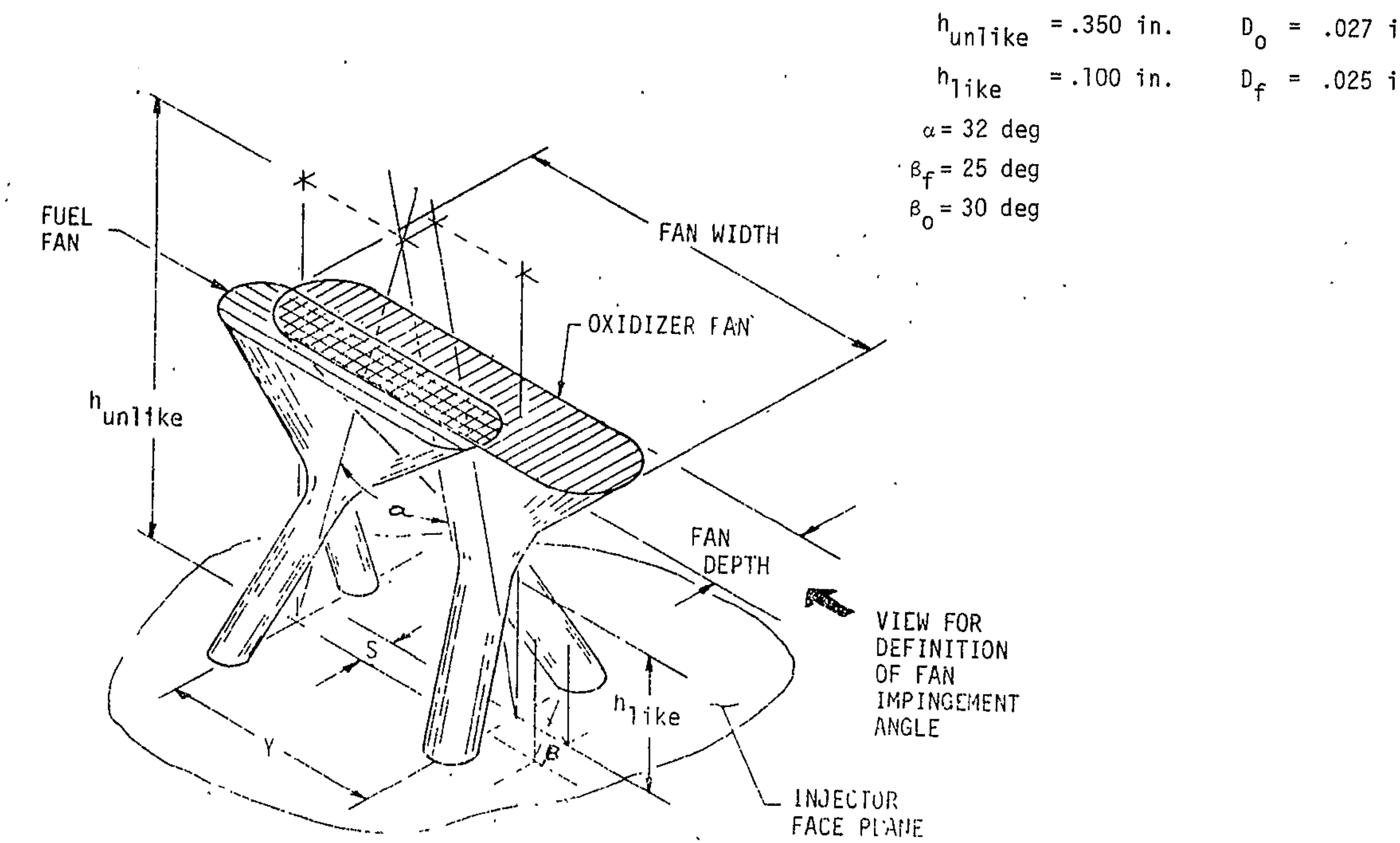

FIGURE 12. QUADLET (LOL PAIR) ELEMENT DESIGN

TABLE VI

SUBSCALE QUADLET TEST SUMMARY

Test	O/F	P_c (psia)	T_o (°F)	T_f (°F)	η_{C*} (%)
175	2.05	152.5	69	77	89.3
176	1.87	120.7	69	77	88.9
177	1.60	120.8	69	75	87.4
178	1.59	97.6	71	75	88.9
179	1.69	99.3	72	75	88.8
180	1.71	79.9	73	75	90.2
181	1.66	141.0	74	76	87.0
182	1.70	142.1	75	75	86.4
183	1.64	121.5	73	190	86.5
184	1.67	123.9	69	184	87.2
185	1.72	124.2	69	217	86.6
186	1.72	123.1	141	215	85.1
187	1.68	141.1	137	283	86.3
188	1.73	146.3	130	271	84.3

Statistical characterization of C* efficiency and calculation of empirically determined combustion gas velocity profiles for these tests is detailed within the following section concerning model data analysis and correlation.

C. Model Data Analysis and Correlation

1. Quadlet Injector Test Data Reduction

A computer program was coded to reduce the quadlet injector tests selected for analysis and summarized in Table VI. The primary test variables input to the program are injector flow areas, chamber throat area, propellant flowrates, temperatures, and manifold pressures and the measured chamber static pressures.

A subroutine was included in the program that contained parametric NTO/MMH combustion gas properties as a function of chamber pressure, mixture ratio, and propellant temperatures. The one dimensional equilibrium (ODE) properties calculated with the routine included characteristic exhaust velocity (C*), molecular weight, stagnation temperature, dynamic viscosity, and the ratio of specific heats (γ). The ODE C* value was used to define test C* efficiency through comparison to the test calculated value. The remaining gas properties were used to compute throat effective chamber pressure and the test combustion gas velocity profile from the chamber axial static pressure measurements.

A sample output case of the test data reduction program is displayed in Figure 13. The gas velocity profile printed as a function of 0.1 inch axial chamber increments was generated by applying a 2nd order curve fit to the measured static pressure data. The primary program outputs used as input to the ZOM calculational model described in the next paragraph are the gas velocity profile and the calculated propellant injection velocities.

2. ZOM Prediction Model Formulation

The ZOM prediction model approach introduced previously was coded for the computer to allow rapid reduction and correlation of the sub-scale quadlet injector tests. The function of the computer model is to integrate the basic equation for droplet acceleration based on input droplet size, injection velocity, spray fan half angle (i.e., the initial droplet trajectory) and the computed chamber gas velocity profile. The droplet acceleration equation is shown below.

$$\frac{dV}{dt} = -\frac{3}{4} \; C_D \; \frac{\rho_g}{\rho_l} \; \frac{(V_g - V_D)^2}{\overline{D}} \qquad (11)$$

The equation was converted to allow integration with respect to the axial chamber distance, x.

****** MULTIELEMENT LOL CORE ******

MEASURED VALUES

TEST	TIME	PC1	PC2	PC3	PC4	PC5	PC6	PC7	POJ	PFJ	TOJ	TFJ
180	2.72	84.30	84.10	83.68	82.49	77.88	76.49	75.21	112.31	104.41	73.	75.

CALCULATED PERFORMANCE

PCU	DPOJ	DPFJ	KWO	KWF	WO	WF	WT	MR	C*	%C*
79.92	28.01	20.11	.0278	.0247	.1767	.1035	.2801	1.71	5142.	90.24

CALCULATED VELOCITIES

VOX	VFL	VBAR
41.26	46.53	43.21

CALCULATED LOCAL PRESSURE,PERFORMANCE & GAS VELOCITY DATA

X	PCS (PSIA)	PERE	PVAP	VGAS (FT/SEC)
.00	84.30	.00	.00	.0
.10	84.26	4.69	4.23	58.7
.20	84.19	10.82	9.76	135.2
.30	84.10	16.74	15.10	209.2
.40	84.00	19.94	18.00	249.3
.50	83.86	21.08	19.03	263.5
.60	83.68	25.54	23.04	319.1
.70	83.42	29.88	26.97	373.4
.80	83.13	34.56	31.18	431.7
.90	82.82	38.81	35.02	484.8
1.00	82.49	42.98	38.78	536.8
1.10	81.90	49.65	44.80	619.8
1.20	81.33	55.41	50.00	691.5
1.30	80.80	60.32	54.43	752.6
1.40	80.29	64.77	58.45	807.8
1.50	79.82	68.69	61.98	856.5
1.60	79.37	72.22	65.17	900.3
1.70	78.96	75.43	68.06	940.0
1.80	78.57	78.29	70.65	975.4
1.90	78.21	80.87	72.97	1007.3
2.00	77.88	83.20	75.06	1036.2
2.20	77.68	84.63	76.37	1053.8
2.40	77.48	86.00	77.61	1070.7
2.60	77.29	87.31	78.79	1086.9
2.80	77.10	88.57	79.92	1102.4
3.00	76.92	89.76	81.00	1117.2
3.20	76.75	90.93	82.05	1131.5
3.40	76.58	92.04	83.05	1145.2
3.60	76.41	93.11	84.02	1158.4
3.80	76.26	94.13	84.94	1171.0
4.00	76.11	95.11	85.82	1183.0
4.20	75.96	96.04	86.66	1194.4
4.40	75.82	96.92	87.46	1205.3
4.60	75.69	97.76	88.22	1215.7
4.80	75.56	98.56	88.94	1225.5
5.00	75.44	99.32	89.62	1234.8

FIGURE 13. TEST REDUCTION PROGRAM SAMPLE OUTPUT

$$\frac{dV}{dx} = -\frac{3}{4} \quad C_D \quad \frac{\rho_g}{\rho_l} \quad \frac{(V_g - V_D)^2}{\overline{D} \quad V_D} \qquad (12)$$

The computer program utilized a special subroutine formulation of the Adams-Bashforth integration method. The Adams-Bashforth method is a extremely efficient predictor-corrector variable step size integration technique.

The Ingebo (Ref. 16) drag coefficient correlation was built into the computer model coding.

$$C_D = 27 \quad Re_D^{-0.84} \qquad (13)$$

The influence of the drag coefficient assumption on the predictions of the ZOM model was not investigated during this initial development effort.

The model begins execution at a designated axial plane. A spray droplet of mass median diameter $\overline{D}$ is introduced at the initial plane with an input radial and axial velocity component. The droplet acceleration equation is integrated and the droplet trajectory calculated versus chamber axial distance. The calculation is terminated at the axial plane at which the droplet axial velocity vector is within 0.1 percent of the total droplet velocity vector. That is,

$$\frac{V_{axial}}{V_{Resultant}} \geq 0.999.$$

At this point droplet radial velocity forces that would induce inter-spray fan mixing are negligible. The final droplet trajectory point radial dimension is used to calculate the predicted ZOM value assuming a cold flow linear spray fan half angle consistent with the droplet initial radial and axial velocity components. This calculational process is explained in equation form below.

$$\theta = \tan^{-1} \frac{V_{ri}}{V_{ai}} \qquad (14)$$

$$ZOM = \tan \theta \times r_f \qquad (15)$$

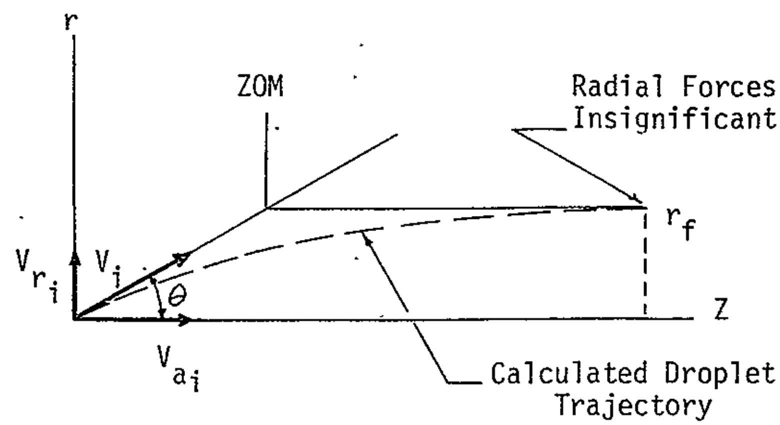

where:

V_{ri} = initial drop radial velocity vector

V_{ai} = initial drop axial velocity vector

r_f = final droplet radial location corresponding to point where axial droplet velocity forces are predominant

A sample case output of the ZOM prediction model is shown in Figure 14. The droplet location can be traced through the calculated axial and radial locations, X (1) and X (2), respectively. The calculated local axial and radial velocity components at these locations are V (1) and V (2) respectively. The ZOM value tabulated at the final calculational point is the model predicted cold flow spray fan ZOM value for mixing efficiency prediction with the LISP sub-program of DER.

3. Model Analysis and Data Correlation Results

a. Statistical Evaluation of Quadlet Injector Test Data

The tests selected for analysis were subjected to a statistical evaluation to allow characterization of injector performance as a function of engine operating variables. A computer model was utilized that combines least squares curve fits with standard multiple regression and co-variance techniques. The primary test variables that were evaluated during the test program were chamber pressure and propellant temperature.

CASE	FUEL TEMP (F)	OXID TEMP (F)	PC (PSIA)	MR	INITIAL VEL (FT/SEC)	THETA (DEG)
180	75.	73.	84.	1.71	43.2	90.0

CSTARE (FT/SEC)	TGAS(R)	MOLECULAR WT	GAMMA	VISCOSITY (LB/FT-SEC)
5698.	5455.	20.66	1.23	.0000605

X1	GAS VELOCITY VG (FT/SEC)
.000	.0
.100	58.7
.200	135.2
.300	209.2
.400	249.3
.500	263.5
.600	319.1
.700	373.4
.800	431.7
.900	484.8
1.000	536.8
1.100	619.8
1.200	691.5
1.300	752.6
1.400	807.8
1.500	856.5
1.600	900.3
1.700	940.0
1.800	975.4
1.900	1007.3
2.000	1036.2
2.200	1053.2
2.400	1070.7
2.600	1086.9
2.800	1102.4
3.000	1117.2
4.000	1183.0
5.000	1234.8

X(1)	X(2)	V(1)	V(2)	RE(1)	RE(2)	V(1)/V(RESULT)	ZOM(INCHES)	CD(1)	CD(2)
.313-05	.262-05	.331+02	.278+02	.407+01	.342+01	.766+00	.313-05	.830+01	.962+01
.560-01	.465-01	.320+02	.261+02	.158+00	.319+01	.774+00	.554-01	.127+03	.102+02
.101+00	.817-01	.326+02	.246+02	.328+01	.302+01	.798+00	.973-01	.996+01	.107+02
.152+00	.118+00	.353+02	.232+02	.764+01	.285+01	.836+00	.140+00	.489+01	.112+02
.203+00	.148+00	.402+02	.220+02	.119+02	.270+01	.877+00	.177+00	.336+01	.117+02
.254+00	.174+00	.466+02	.211+02	.161+02	.259+01	.911+00	.207+00	.262+01	.122+02
.306+00	.194+00	.539+02	.203+02	.194+02	.249+01	.936+00	.232+00	.224+01	.126+02
.350+00	.210+00	.614+02	.197+02	.211+02	.242+01	.952+00	.250+00	.208+01	.129+02
.402+00	.225+00	.687+02	.191+02	.222+02	.235+01	.963+00	.268+00	.199+01	.132+02
.453+00	.238+00	.754+02	.186+02	.221+02	.229+01	.971+00	.284+00	.200+01	.135+02
.504+00	.250+00	.816+02	.182+02	.225+02	.223+01	.976+00	.298+00	.197+01	.138+02
.555+00	.261+00	.876+02	.178+02	.251+02	.218+01	.980+00	.311+00	.180+01	.140+02
.606+00	.271+00	.941+02	.174+02	.280+02	.214+01	.983+00	.323+00	.164+01	.143+02
.651+00	.279+00	.101+03	.171+02	.302+02	.210+01	.986+00	.332+00	.154+01	.145+02
.702+00	.287+00	.108+03	.168+02	.328+02	.206+01	.988+00	.342+00	.144+01	.147+02
.754+00	.295+00	.115+03	.165+02	.356+02	.203+01	.990+00	.351+00	.134+01	.149+02
.805+00	.302+00	.122+03	.163+02	.383+02	.200+01	.991+00	.359+00	.126+01	.151+02
.856+00	.308+00	.130+03	.160+02	.407+02	.197+01	.992+00	.367+00	.120+01	.153+02
.901+00	.313+00	.137+03	.158+02	.428+02	.194+01	.993+00	.374+00	.115+01	.154+02
.952+00	.319+00	.145+03	.156+02	.449+02	.192+01	.994+00	.380+00	.111+01	.156+02
.100+01	.325+00	.152+03	.154+02	.475+02	.190+01	.995+00	.387+00	.105+01	.158+02
.105+01	.330+00	.160+03	.152+02	.517+02	.187+01	.995+00	.393+00	.982+00	.159+02
.111+01	.334+00	.168+03	.151+02	.559+02	.185+01	.996+00	.398+00	.919+00	.161+02
.115+01	.338+00	.177+03	.149+02	.591+02	.184+01	.996+00	.403+00	.877+00	.162+02
.120+01	.342+00	.185+03	.148+02	.624+02	.182+01	.997+00	.408+00	.839+00	.164+02
.125+01	.346+00	.194+03	.146+02	.652+02	.180+01	.997+00	.413+00	.808+00	.165+02
.130+01	.350+00	.203+03	.145+02	.678+02	.178+01	.997+00	.417+00	.782+00	.166+02
.136+01	.354+00	.211+03	.144+02	.703+02	.177+01	.998+00	.421+00	.758+00	.167+02
.141+01	.357+00	.220+03	.143+02	.726+02	.175+01	.998+00	.425+00	.739+00	.169+02
.145+01	.360+00	.229+03	.141+02	.744+02	.174+01	.998+00	.429+00	.724+00	.170+02
.150+01	.363+00	.237+03	.140+02	.763+02	.173+01	.998+00	.432+00	.708+00	.171+02
.155+01	.366+00	.246+03	.139+02	.780+02	.171+01	.998+00	.436+00	.695+00	.172+02
.160+01	.369+00	.254+03	.138+02	.796+02	.170+01	.999+00	.439+00	.683+00	.173+02
.166+01	.371+00	.262+03	.137+02	.811+02	.169+01	.999+00	.443+00	.672+00	.174+02
.170+01	.374+00	.271+03	.137+02	.823+02	.168+01	.999+00	.445+00	.664+00	.175+02
.175+01	.376+00	.279+03	.136+02	.836+02	.167+01	.999+00	.448+00	.656+00	.176+02
.180+01	.379+00	.287+03	.135+02	.848+02	.166+01	.999+00	.451+00	.648+00	.177+02
.185+01	.381+00	.295+03	.134+02	.858+02	.165+01	.999+00	.454+00	.641+00	.178+02
.191+01	.383+00	.303+03	.133+02	.868+02	.164+01	.999+00	.457+00	.635+00	.178+02

FIGURE 14. ZOM MODEL SAMPLE OUTPUT

The results of the statistical analysis are plotted in Figure 15. The analysis indicated that chamber pressure and fuel temperature variances significantly influence injector C* efficiency. The statistical analysis resulted in the curve fit equation written below.

$$\eta_{C^*_{TEST}} = 95.36 - .05279\ P_c - .009468\ T_f \qquad (16)$$

As shown in the figure, the equation results in decreasing C* efficiency as chamber pressure and fuel temperature increase.

The statistical analysis results indicated real injector operating variable influences on performance that could, hopefully, be modeled with the ZOM prediction model. Also, the analysis indicated that the quadlet injector tests comprise a high quality, repeatable data base void of significant measurement error or bias influences.

b. Model Analysis

The initial model analysis work concentrated on the influence of chamber pressure on test performance and evaluation of the model's capability to calculate the correct absolute magnitude of the ZOM plane location.

The data statistical analysis indicated a significant test performance efficiency sensitivity to chamber pressure. Examination of the test combustion gas velocity profiles calculated with the test data reduction program gave the initial indication that the model would accurately predict the chamber pressure influence trend. Figure 16 shows the empirically based gas velocity profile for a low Pc test (# 180) and a high Pc test (# 182). Both tests were conducted with ambient temperature propellants. As shown, the low Pc test resulted in a C* efficiency nearly 4 percent higher than the high Pc test. Interestingly, as displayed in the figure, the lower performing high Pc test actually possessed a significantly faster rate of near injector zone energy release, as reflected by the higher calculated combustion gas velocity. In other words, the test that exhibited high performance near the

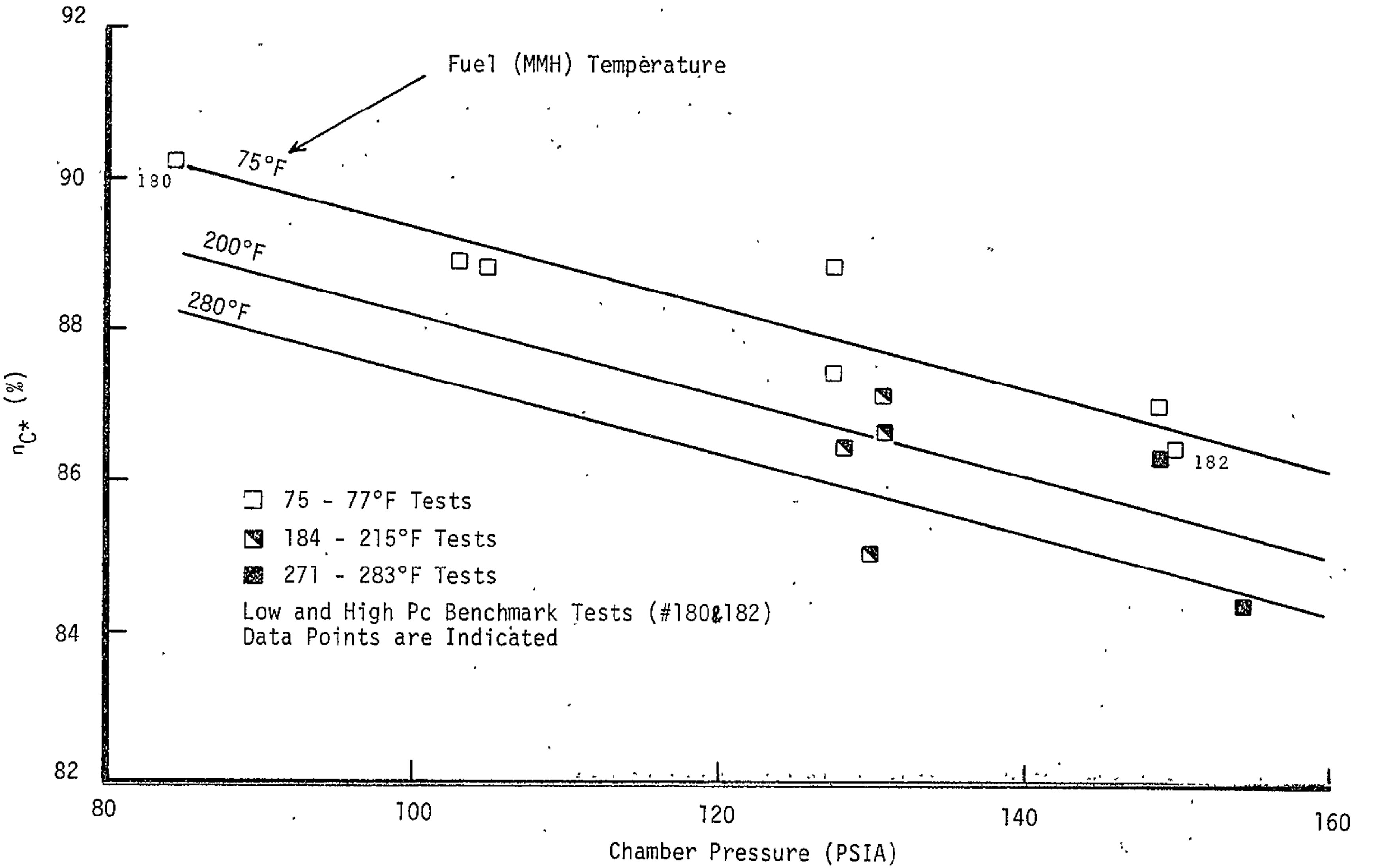

FIGURE 15. PERFORMANCE CHARACTERIZATION FOR SUBSCALE QUADLET INJECTOR

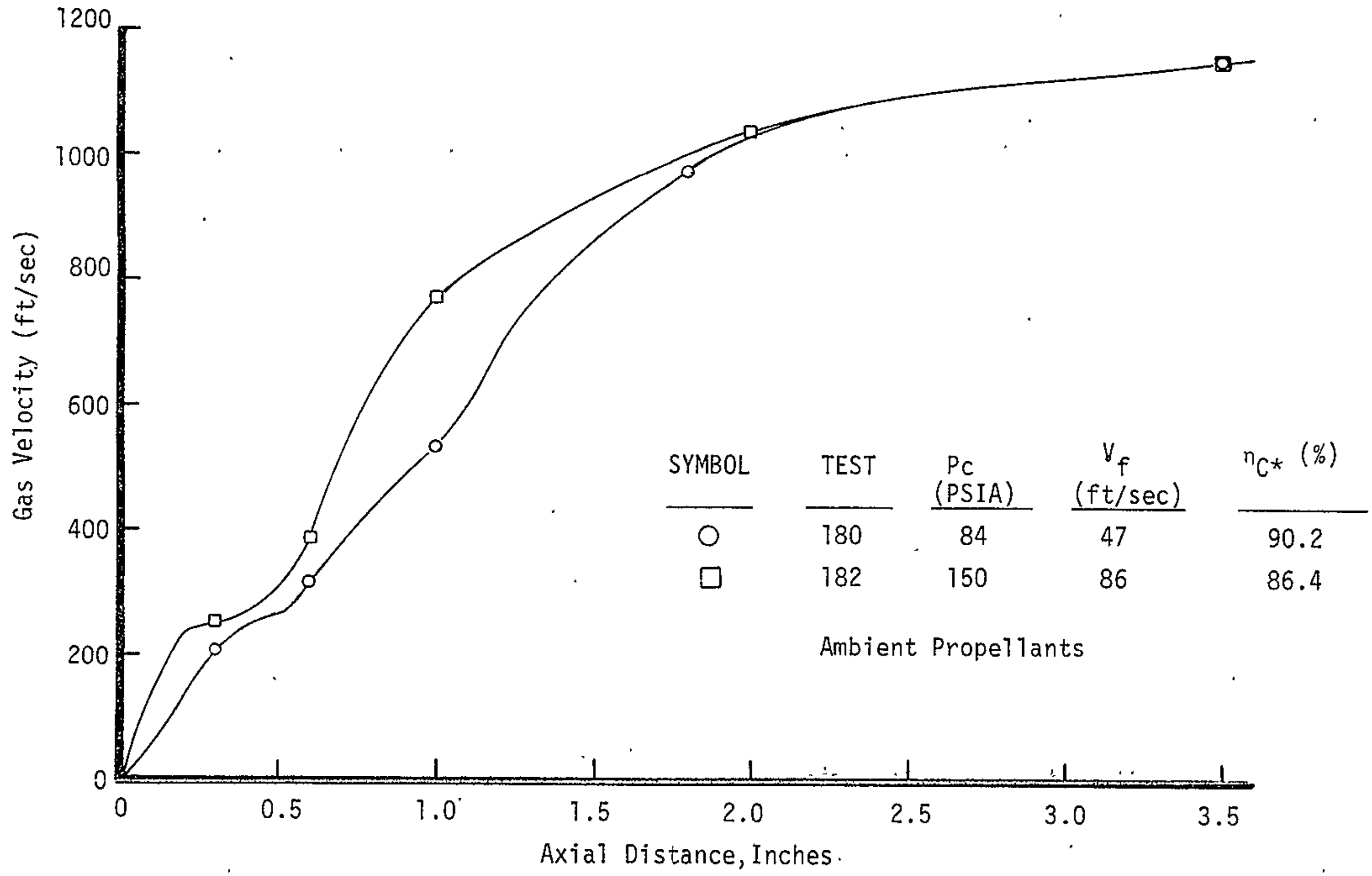

FIGURE 16. CHAMBER PRESSURE INFLUENCE ON GAS VELOCITY PROFILE

injector face (the area of spray fan formation and mixing) possessed lower overall performance. This result appears to mechanistically agree with the formulated ZOM prediction model for the following reason. The higher axial combustion gas velocity near the face results in more rapid axial acceleration of spray fan droplets, thus flattening the droplets trajectory. The more rapid attainment of an axially directed spray fan results in a lower calculated value of ZOM. A lower ZOM value results in a reduction in predicted mixing C* efficiency with the LISP computer model.

The initial ZOM model prediction results, for the calculational technique that will be termed the baseline model, are shown in Figure 17. In the baseline case radial velocity deceleration is calculated by assuming a combustion gas velocity component of zero in the radial direction, thus the droplet radial velocity component is reduced as the calculation proceeds axially down the chamber. The initial quadlet spray half angle was selected to be 40 degrees based on cold flow spray fan photographs and mass distribution measurements. The calculated ZOM value for each test is plotted versus test chamber pressure. To allow clear interpretation of the model predictive trend only the ambient propellant temperature test point predictions are plotted. The calculated trend is opposite from that expected; that is, the lower performing high pressure tests have high calculated ZOM values.

Model predictions were repeated for the same tests with varying calculational assumptions to ascertain the reason for the incorrectly calculated trend of ZOM versus chamber pressure. The results are displayed in Figure 18. The test data points were eliminated for clarity. The first calculational change (Case 2 in the figure) eliminated radial deceleration by assuming a constant droplet radial velocity equal to the injection radial component. The predicted trend of ZOM versus chamber pressure is the same but the absolute ZOM value is increased. ZOM increases because the constant radial velocity assumption results in a greater time to flatten the droplet trajectory because velocity is only changing in the axial direction. The second calculational change (Case 3 in the figure) was to initiate the calculation at an axial distance of 0.4 inches from the injector face plane (using the empirically calculated gas velocity consistent with this location). It was

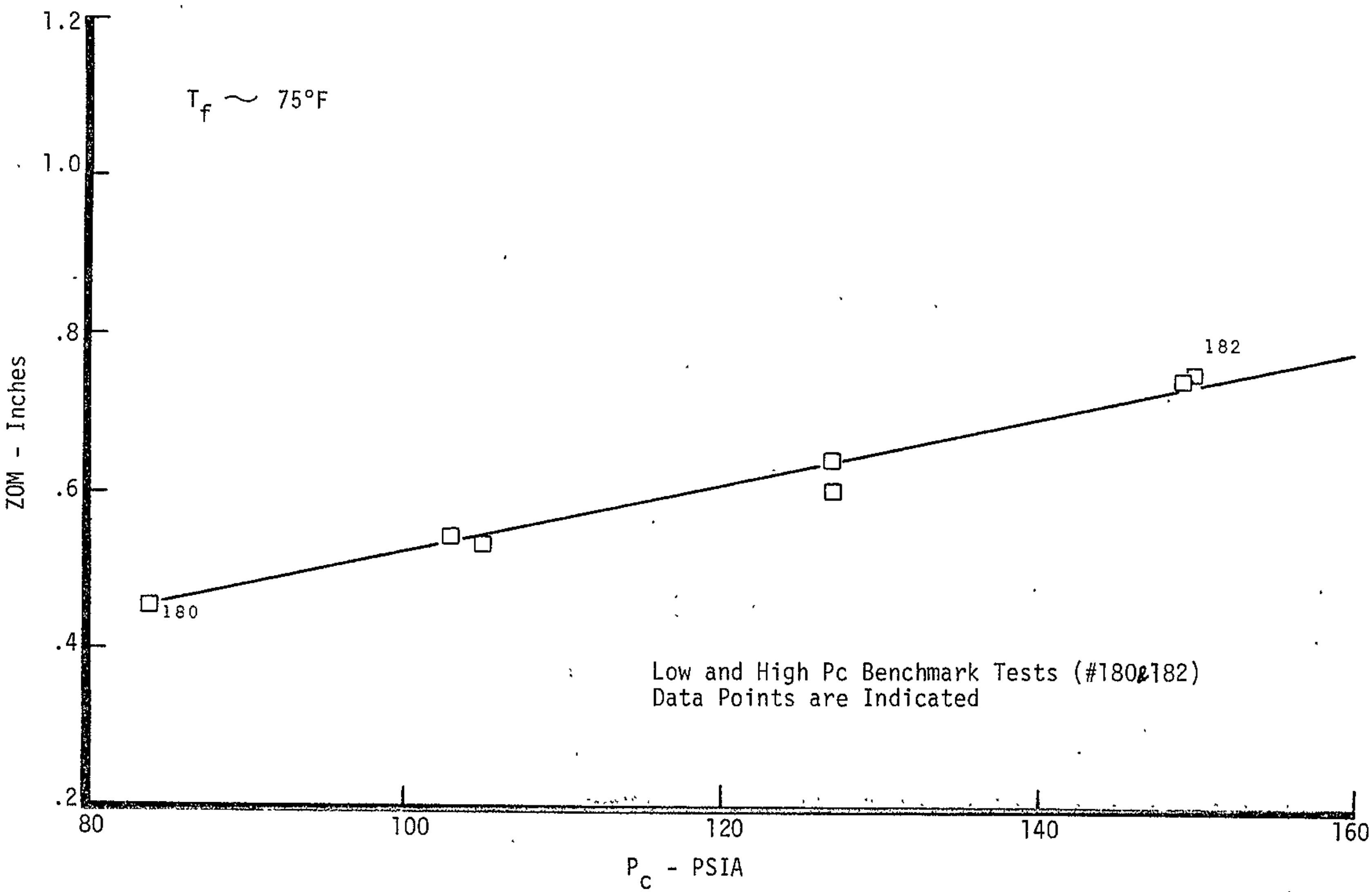

FIGURE 17 . CHAMBER PRESSURE INFLUENCE ON ZOM BASELINE MODEL

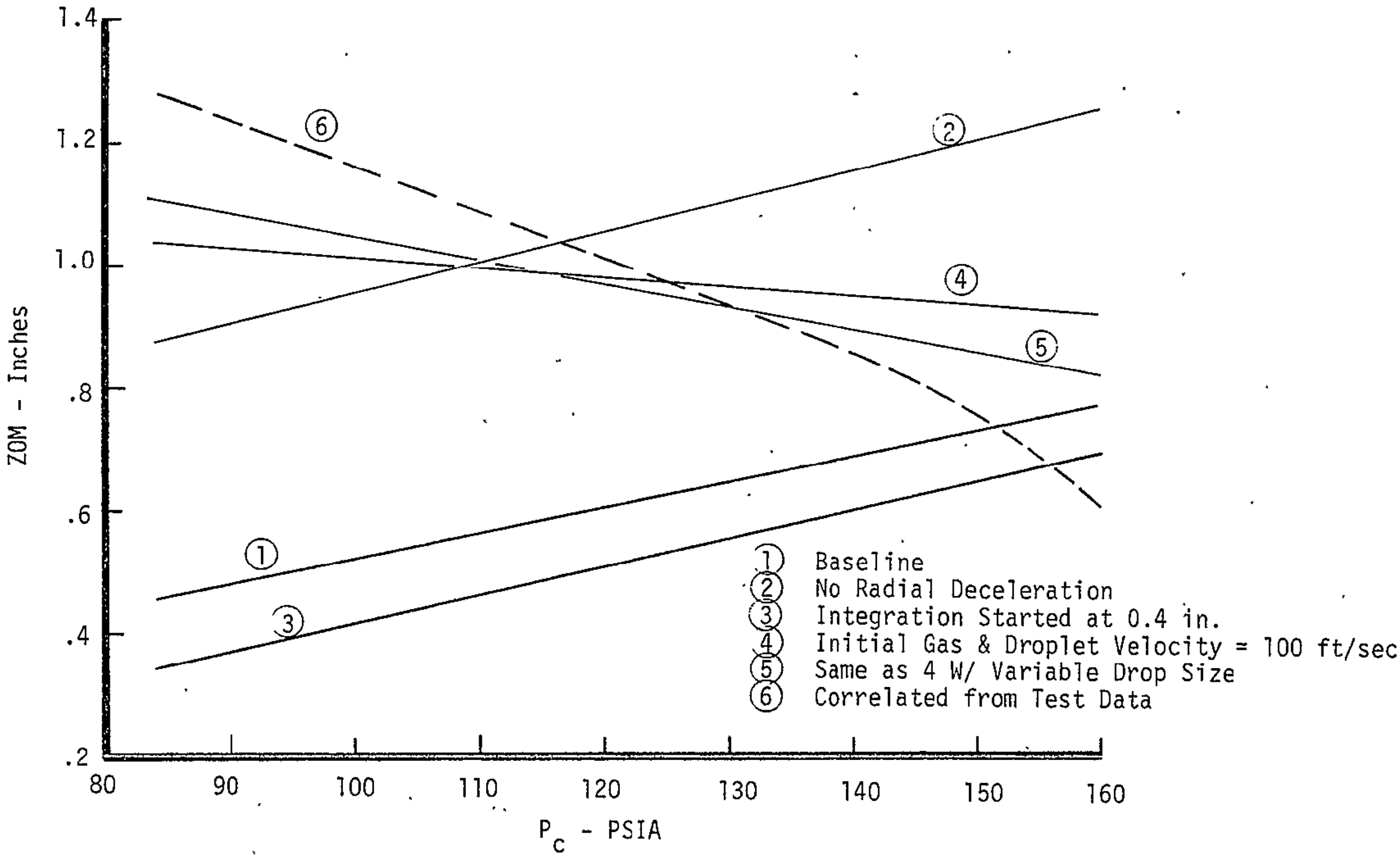

FIGURE 18. ZOM SENSITIVITY FOR DIFFERENT MODEL CALCULATIONAL ASSUMPTIONS

reasoned that since jet impingement and breakup require a finite time to occur the droplet acceleration calculation should begin at an axial plane consistent with initial development of atomized droplets. This calculational method did not significantly affect the trend or absolute magnitude of the predicted ZOM value. The third calculational change was based on the following observation. Although the tests at higher chamber pressure possessed higher near zone gas velocities that should flatten the droplet trajectory more rapidly they also result in higher initial injection velocities. The high initial radial velocity component is decelerated at a much slower rate than the axial component is accelerated. This results in the initial radial component predominating the calculation of the local droplet velocity vector as the droplet is marched downstream. Therefore, to verify this observation the third calculational change (Case 4 in the figure) was to assume an initial gas and droplet velocity for each test of 100 ft/sec. The droplet acceleration calculation was initiated when the empirically calculated gas velocity exceeded 100 ft/sec. The resultant ZOM trend is opposite to the previous cases because the influence of droplet injection velocity has been eliminated. This ZOM trend is consistent with the test data trend of decreasing C* efficiency with increasing chamber pressure. This method was varied only slightly in the final case 5 calculation by accounting for an influence of jet injection velocity on the atomized mass median drop diameter.

These initial model ZOM predictions were evaluated by "backing out" test ZOM values based on actual measured test C* efficiency. The test correlated ZOM trend is shown as curve 6 in Figure 18. This curve was developed through use of Figures 19 and 20. Figure 19 displays calculated test vaporization efficiency versus chamber pressure. The calculation was made with a "two-flame" modified version of the Priem L-General model (Ref. 17). Figure 20 shows the DER LISP subprogram predicted relationship between the ZOM plane location and mixing efficiency. This sensitivity curve of $\eta_{C^*_{mix}}$ versus ZOM was based on quadlet mass distribution coefficients developed in-house at ALRC. The test "backed out" ZOM value was calculated knowing the measured test C* efficiency and the predicted test vaporization efficiency.

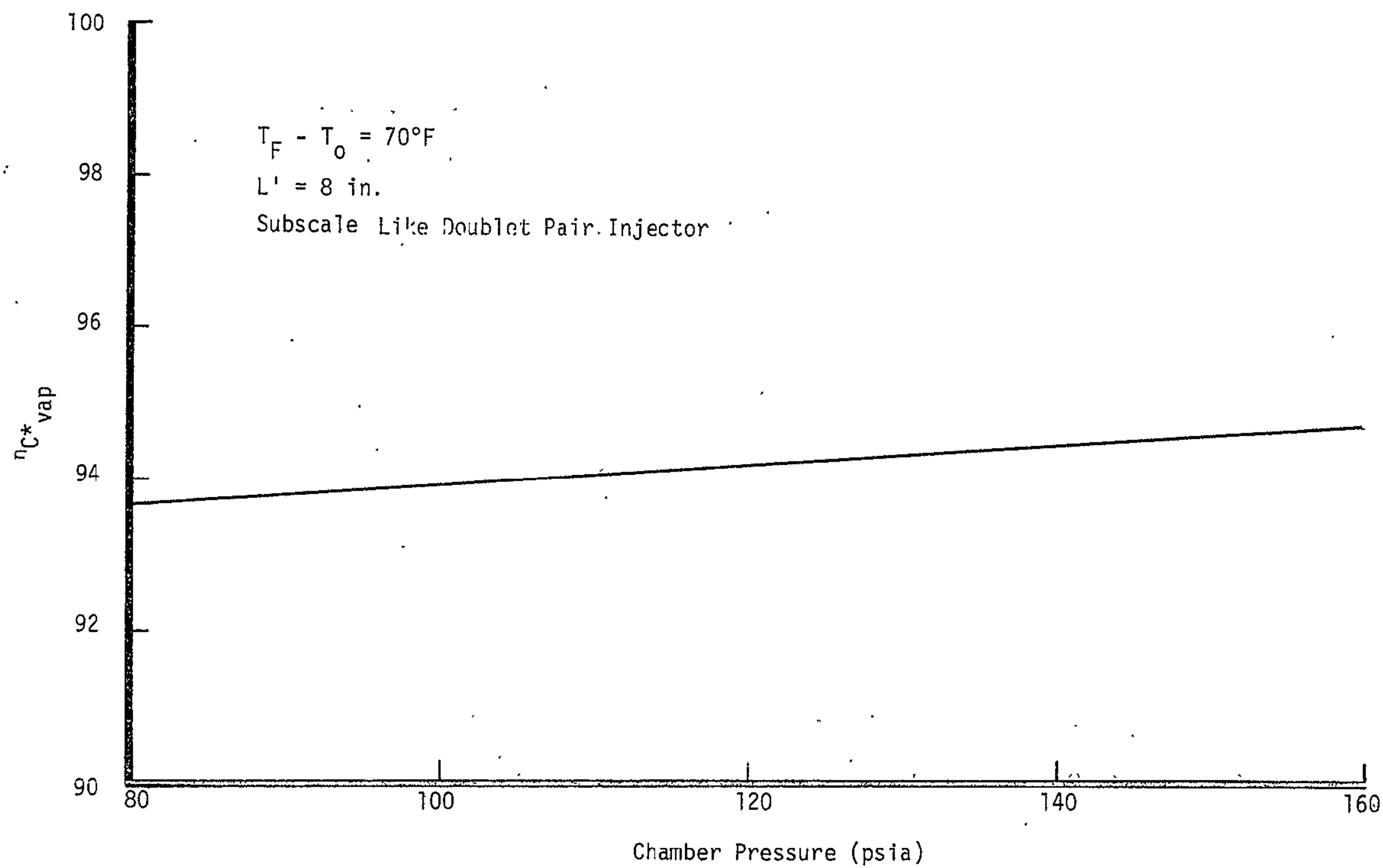

FIGURE 19. VAPORIZATION EFFICIENCY SENSITIVITY TO CHAMBER PRESSURE

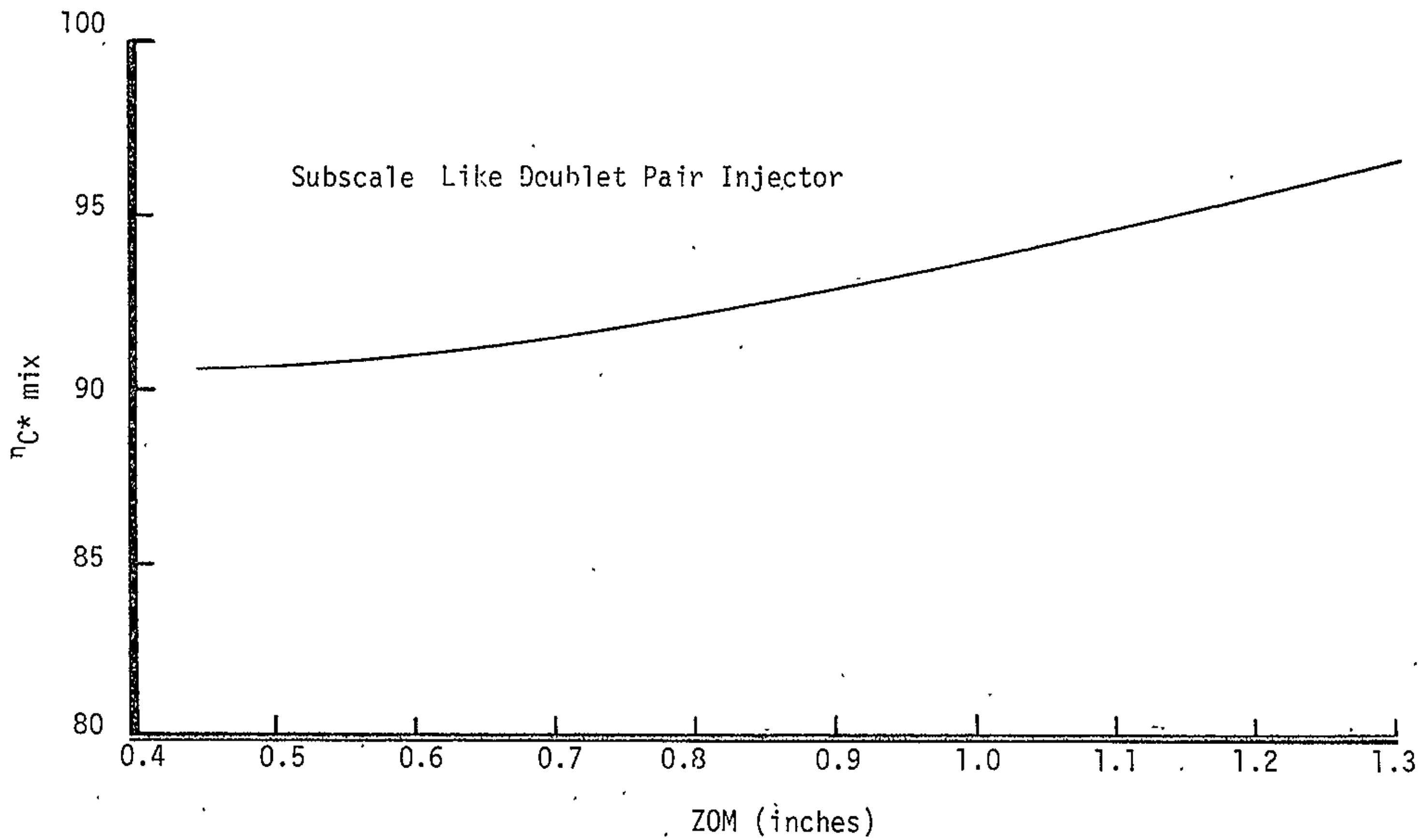

FIGURE 20. C* MIXING EFFICIENCY SENSITIVITY TO ZOM PLANE

$$\eta_{C^*_{mix}} = \eta_{C^*_{test}} / \eta_{C^*_{vap}} \tag{17}$$

$$ZOM = f\,(\eta_{C^*_{mix}}),\ \text{from Figure 20} \tag{18}$$

The absolute magnitude of the test ZOM value can be affected by error influences of the vaporization calculation, the LISP calculation, and the test C* efficiency measurement. However, the trend of test ZOM versus chamber pressure accurately reflects the actual test results of increasing performance with increasing test chamber pressure. Returning to Figure 18, it is encouraging that the model predicts ZOM values that have absolute values near those determined from the test data. However, it is apparent that only the case 4 and 5 ZOM calculational methods produce a trend approaching that deduced through "backing out" ZOM from the test data.

The correlations shown in Figure 18 resulted in the observation that droplet injection momentum forces dominate the ZOM calculation in a way that overshadows the influence of higher combustion gas velocity forces on droplet trajectories. Opposingly, the test data trend clearly reflects a test variable influence that affects measured performance to a greater degree than injection velocity. For this reason, the possibility that Reactive Stream Separation (RSS or "blowapart) forces affected quadlet injector performance was investigated. A discussion on RSS is included in Section C.5 of Appendix A. A recently completed subscale injector test investigation (Ref. 18) indicates that RSS can be accurately modeled and predicted in terms of injector/chamber design and operating variables. The application of the Ref. 18 quadlet RSS model to the task test data base is shown in Figure 21. The model predicts that the majority of the quadlet test data is in the separated operating mode. The previously presented ZOM model prediction results indicate that strong reactive forces, such as produced by RSS, are required to result in the measured quadlet test data trends. Encouragingly, for modeling purposes, the test data indicates that RSS is a continuous process (note the linear test η_{C^*} trend versus chamber pressure in Figure 15) that does not result in step function changes in injector performance. The same conclusion was reached in Ref. 18, after reduction and correlation of several hundred tests conducted with many different injector

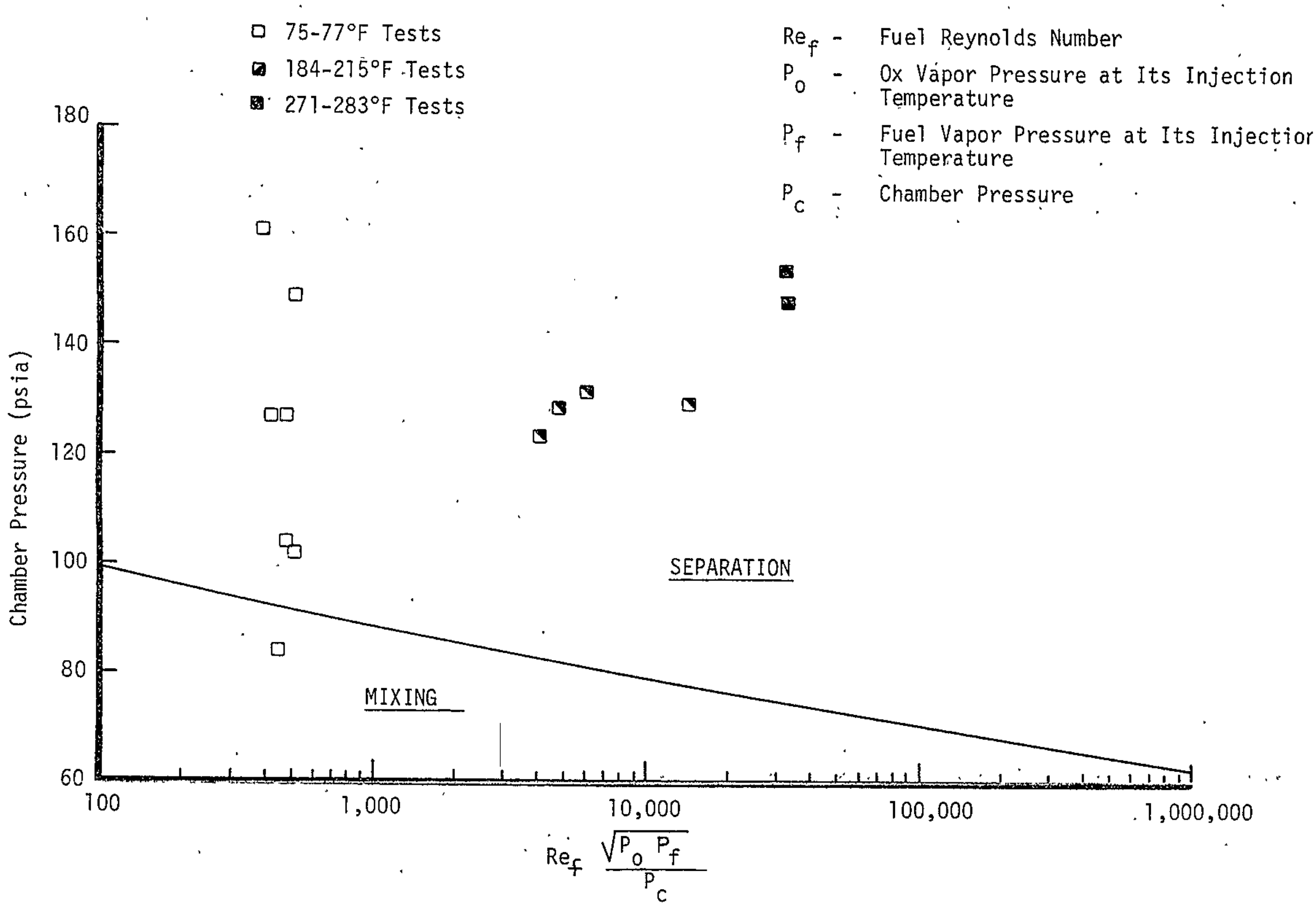

FIGURE 21. LIKE DOUBLET PAIR INJECTOR RSS CHARACTERIZATION

types and designs. Additionally, work has already been initiated towards the analytical modeling of the RSS phenomenon (Ref. 19).

The influence of fuel temperature on the ZOM prediction trends was also investigated to gain further data in support of the conclusions reached from the chamber pressure correlation effort. Figure 22 displays the influence of fuel temperature on test C* efficiency for six tests conducted at a chamber pressure of 130 psia. Test C* shows a significant decreasing trend as the fuel temperature is increased. The relationship between the empirically based combustion gas velocity profile for a low and high fuel temperature test is shown in Figure 23. Again, the higher performing test (Test #176) has a lower rate of energy release in the injector near zone. The ZOM model predictions for the six tests are presented in Figure 24. As before, an incorrect ZOM trend was produced with the baseline model. As fuel temperature increases the fuel density decreases resulting in increased injection velocity that again dominates the influence of increased axial acceleration forces. The fuel temperature correlations supports the previous results of the chamber pressure correlation effort.

D. Conclusions and Recommendations

1. <u>Conclusions</u>

The following conclusions have been reached from the initial <u>a priori</u> ZOM prediction model development effort.

a. The OMS subscale test program (Ref. 14) has resulted in an excellent data base for the investigation of near-zone combustion and mixing phenomenon.

b. The formulated ZOM prediction model should be tested with a data set that is void of significant "blowapart" forces.

c. The gas acceleration effects ZOM model calculates ZOM values on the level of those required to accurately predict injector mixing performance. Therefore, the model most probably accurately accounts for near zone injection and gas acceleration momentum forces.

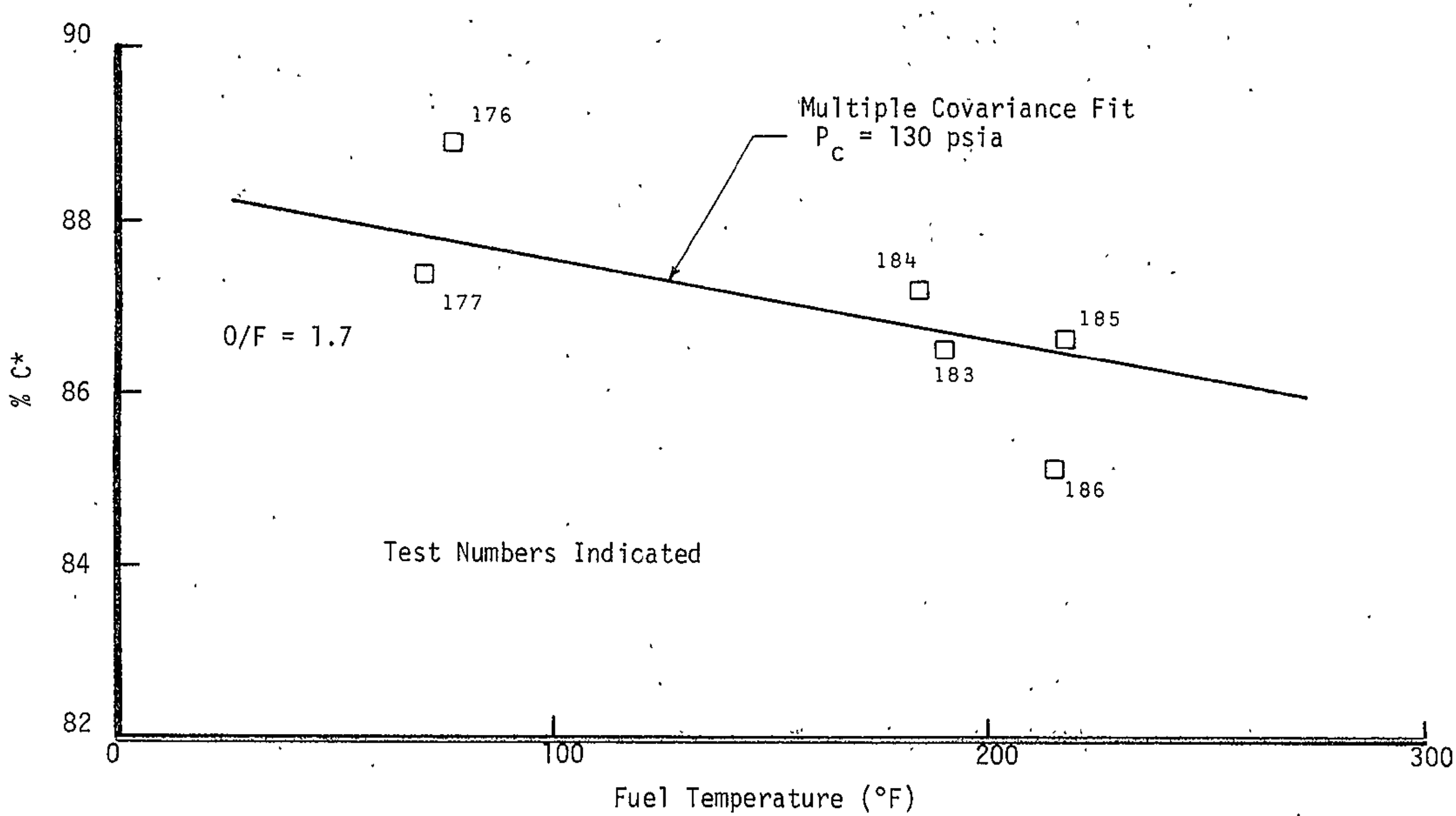

FIGURE 22. FUEL TEMPERATURE INFLUENCE ON INJECTOR PERFORMANCE

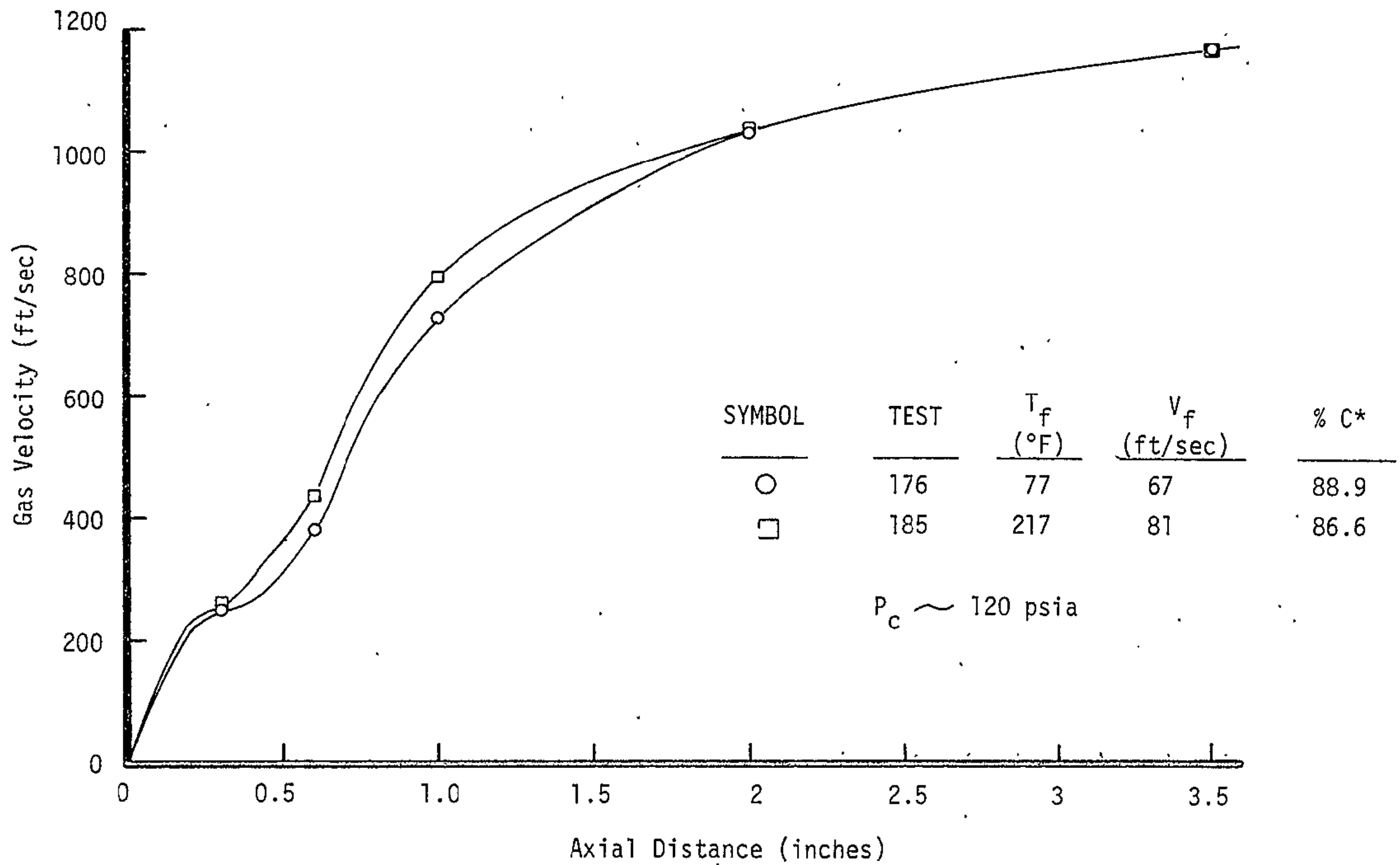

FIGURE 23. FUEL TEMPERATURE INFLUENCE ON CHAMBER GAS VELOCITY PROFILE

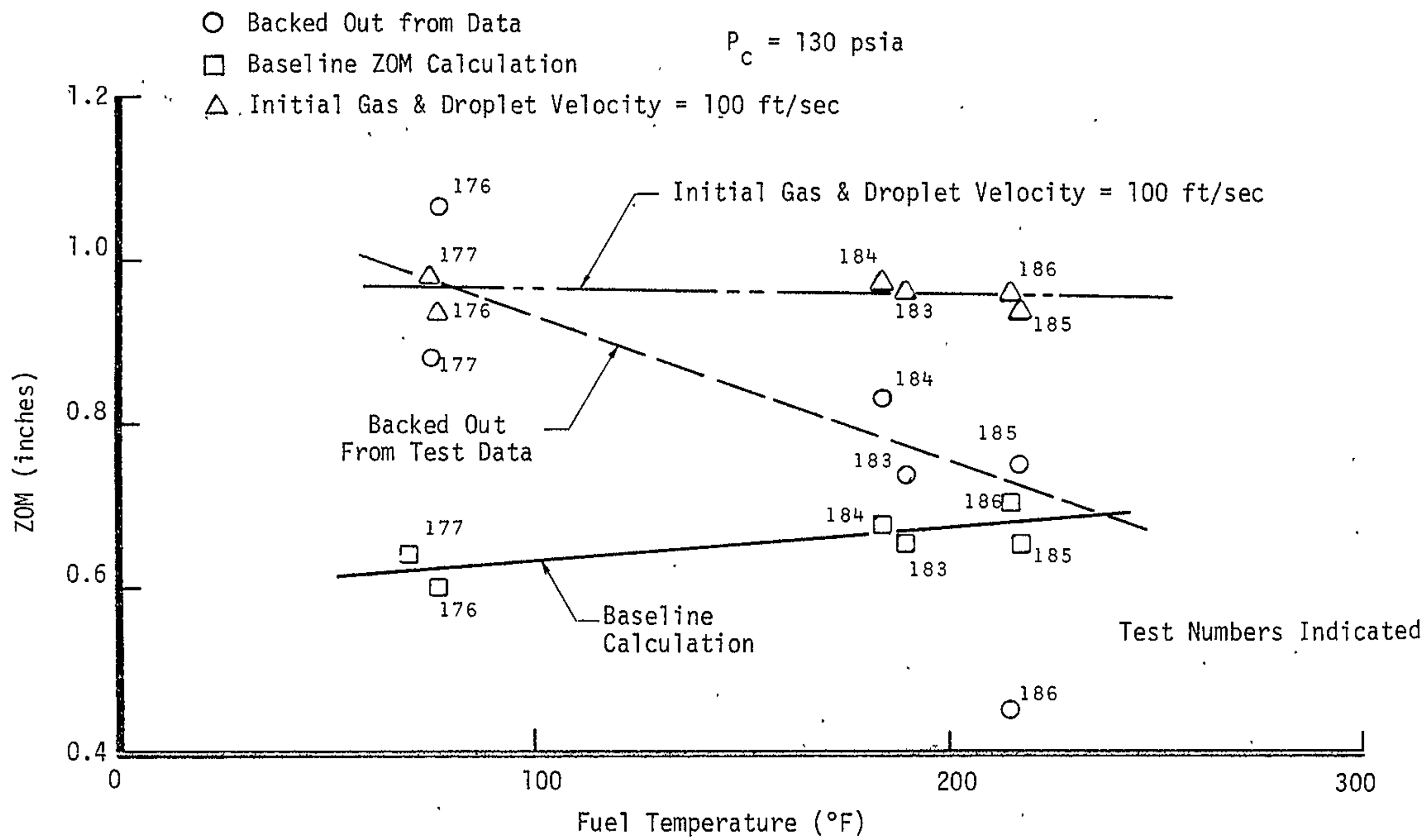

FIGURE 24. FUEL TEMPERATURE INFLUENCE ON ZOM

d. Combustion reactive forces due to the mechanism termed "blowapart" strongly alter droplet inertial forces.

e. A physically mechanistic near-zone model that will predict the ZOM location must account for both gas acceleration and reactive stream forces on droplet spray fan formation and mixing.

2. Recommendations

The following recommendations are made based on the above conclusions reached from the ZOM prediction model correlation task.

a. The gas acceleration effects model should be further tested through application to a data base void of significant "blowapart" forces. Subscale (1K lbf) quadlet injector data, similar to the OMS data, was developed on the current Improved Transtage Injector Program. This data is at low chamber pressure and injection velocities and therefore is well suited for such an evaluation.

b. The ZOM prediction model development effort should be continued with emphasis on the analytical modeling of reactive stream forces. The work initiated in Ref. 19 should be evaluated for application to the ZOM model.

VI CONCLUSIONS

The major conclusions from this program were:

1. The JANNAF Performance Evaluation Methodology is being advanced with regard to accuracy and applicability through conductance on this and other related technology programs. Such programs must continue based on resultant recommendations to end in valuable, standardized analytical prediction procedures.

2. The intended predictive accuracy of the JANNAF rigorous prediction procedure(to within 1 percent for predicted specific impulse) is, in general, out of the question for a *priori* performance prediction.

3. The generality of the CICM program is limited due to absence of an intra-element mixing model. If the use of single element cold flow data to specify the intra-element mass distribution is continued, a standard measurement technique should be developed. A standard methodology for interpreting and inputing the data to CICM is also required. Preferably, an intra-element mixing model should be developed for CICM.

4. The CICM analysis results verified the CICM vaporization model for the case where injector intra-element mixing losses are negligible.

5. The new ZOM mixing model development initiated during the program should be continued with the emphasis on the analytical modeling of reactive stream forces. A physically mechanistic near-zone model that will predict the ZOM location must account for both gas acceleration and reactive stream forces on droplet spray fan formation and mixing.

APPENDIX A

DER COMPUTER MODEL REVIEW RESULTS

APPENDIX A

DER COMPUTER MODEL REVIEW RESULTS

TABLE OF CONTENTS

This appendix details the results of the DER computer program review. The review was accomplished in four subtasks. (1) Identification and Correction of Coding Errors, (2) Addition of Diagnostic Comment Cards and Print-Out Statements, (3) Identification of Inadequate Formulations and Model Technical Shortcomings, and (4) Review of the JANNAF Performance Prediction Procedures (CPIA 246) with regard to use of DER. A complete summary of the recommendations resulting from the review are included in Section III.A. of this report.

A. Identification and Correction of Coding Errors

A new "standardized" DER program is currently undergoing final development. General release is planned for the fall of 1976. This effort will result in a code considerably changed from the subcritical K-Prime version reviewed during Task I of the Injection Processes (IP) Program. For this reason no attempt was made to verify every formulation in the DER code. The results of the coding review are presented below. The majority of the comments do not concern errors, as such, but points that should be brought to the attention of the DER user to generate increased understanding of program limitations.

1. LISP Unsymmetrical Pie Section Input Problem

The following must be true to result in an accurate total propellant flowrate integration calculation at the LISP collection plane (ZOM).

(a) For an injector slice of θ degrees the slice must contain exactly (θ/360 x 100) percent of the total number of injector elements. This requirement is sometimes difficult to achieve for fine patterns. If the above stipulation is met LISP will execute properly. However, the total flowrates used in STC will be in error unless the following is also true:

(b) θ must be a integer divisor of 360 degrees. That is, a θ value of 40 degrees will work, but a θ value of 39 degrees will cause an error in the STC total flowrate.

In the case of an unsymmetrical injector it is sometimes impossible to satisfy both points (a) and (b). An improved technique would be to adjust the collected pie section mass flowrate to θ/360 of the total injected flow of each propellant.

2. STC Mesh Point Dimensional Limits

LISP will execute properly if the total number of mesh points (NRML, constant radius lines x NTHML, constant θ lines) is equal to 400 or less. Any combination of NRML and NTHML will work. However, dimensional arrays in STC require that NTHML < 20 and NRWALL $\leq$ 20 (number of NRML to wall). Otherwise, the STAPE and SCRMBL routines will compute inaccurate streamtube flowrates. This STC limitation is not noted in the DER user's manual. It should be noted in the user's manual, or preferably removed to allow any NTHML-NRWALL combination in STC.

3. Drop Size Equation Inconsistencies

Examination of the drop size routine DSIZE indicated that two drop size equations differ from the equations given in DER documentation. The equations were inconsistent for (1) the center orifice of a Triplet or Pentad (4-on-1) element, and (2) the contraction ratio adjustment factor for secondary atomization of like doublet elements. The differences should be resolved, but basic questions concerning the validity of DER drop size prediction equations are a more important issue. The drop size equations are thoroughly evaluated in Section C.1. of this appendix.

4. Triplet and Pentad Collection Plane Rotation Error

An error exists in the LISP calculation of the ZOM mesh point mass fluxes for triplet and pentad elements. Inline triplet and pentad elements are symmetrical about both the face plane X and Y axis. The LISP subroutine SCOEF calculates a rotation of the ZOM collection plane around the normal X axis based on the relative fuel and oxidizer element momentum. For a regular symmetrical triplet or pentad the resultant spray fan will always be normal to the chamber longitudinal (Z) axis. The skewing of the collection plane calculated by LISP results in incorrectly computed ZOM nodal point mass fluxes. This error can be eliminated by setting the variable ALFMOM equal to 0 in the triplet section of the SCOEF code.

5. LISP Infinite Baffle Height Assumption

When calculating mass distributions for injectors with baffles, the LISP subroutine BNDY assumes infinite baffle height. This technique results in large accumulation of mass at the baffle boundary. The ZOM mass distribution should be a function of baffle height. This limitation should be noted in the DER user's manual.

B. Addition of Diagnostic Comment Cards and Printout Statements

Error message requirements identified from Section A of this appendix and previous DER analyses are listed below. They are confined to the main LISP and STC routines.

1. LISP Error Messages

The main inconvenience for the user of LISP is that input errors that are detected do not have accompanying error messages that specifically pinpoint the problem.

(a) An error message is required to explain inconsistency between the program NTHML, NTHL, and NTHR inputs.

(b) An error message is required to identify input that assigns excessively high values to the NMESH, NEL, and NLSPEC program variables. NMESH is the total number of LISP nodal points, i.e., the product of the inputs NRML and NTHML. NEL is the total number of injector elements and NLSPEC the number of different element specifications input.

(c) An error message is required to specifically state the program failure associated with improper input of the Type 8 injector spray coefficients.

2. STC Error Messages

(a) The limitation on the STC radial and angular mesh lines has been alluded to (NTHML and NRWALL ≤ 20). If this limitation is not removed an error message should be included in STC to identify the problem.

C. Identification of Inadequate Formulations and Model Technical Shortcomings

Several inadequate formulations and shortcomings have been identified which limit the current predictive capability of DER. The purpose of this subtask of the DER review was to identify model problem areas and, if possible, to propose alternate approaches for improvement. Incorporation of the improvements is, for the most part, beyond the scope of this program, but their identification will provide a basis for future DER work. The model critique is summarized in the following six separate sub-sections concerned with, respectively; drop size predictions, ZOM plane selection, a DER vaporization model sensitivity study, near-zone combustion and monopropellant flame considerations, combustion gas acceleration and reactive stream separation effects on cold flow mass distributions, and the need for a turbulent mixing model in the STC subprogram. A seventh and final section contains a proposed approach for combining ZOM plane, combustion gas acceleration, reactive stream separation, and turbulent mixing considerations inot a physically realistic mass distribution and mixing model for DER.

1. Drop Size Prediction

The inaccuracy of the LISP drop size predictions has been a major DER shortcoming identified by two studies that used DER to analyze engine performance data (Refs. 20 and 21). The DER drop size correlations were examined for coding accuracy and for reference DER equation predictions were compared to those made with the empirically based drop size model of Priem (Ref. 17). The drop size prediction equations for LISP element types 1-5 (unlike doublet, like doublet, like-doublet pair, triplet, pentad (4-on-1), respectively) were included in the study. Several DER publications indicate that Ref. 22 includes a section showing all current DER drop size equations, but examination of this report uncovered no such write-up.

a. Unlike Doublet Drop Size Equations

The DER unlike drop size equations are presented in Ref. 23. They are shown below.

Unlike Doublet (larger Diameter Orifice)

$$\overline{D}_{HW} = 1.27 \left(\frac{D_{opp}}{D}\right)^{.38} \frac{1}{U_{D,opp}^{1.19} \; U_D^{.86}} \qquad \text{(A-1)}$$

Unlike Doublet (Smaller Diameter Orifice)

$$\overline{D}_{HW} = 2.29 \; \frac{D^{.27} \; D_{opp}^{.023}}{U_D^{.74} \; U_{D,opp}^{.33}} \qquad \text{(A-2)}$$

$\overline{D}_{HW}$ is the mass median drop diameter (inches) determined from molten wax atomization experiments (Ref. 24). $\overline{D}_{HW}$ is corrected in the DER code to account for secondary (aerodynamic) break-up with the following general equation (developed in Ref. 25).

$$\overline{D} = \frac{1}{\frac{J_A}{\overline{D}_{HW}} + B} \qquad \text{(A-3)}$$

For unlike doublets DER uses values of .8 and 250 for J_A and B, respectively.

In Figure A-1 drop size predictions made with the DER like doublet equations are shown. The predictions shown were made for equal orifice diameters ($D_{large} = D_{small}$) for orifices from .01 inch to .1 inch in diameter (a typical orifice design range). There are four apparent anomalies with the equations. The first peculiarity is that for the same jet size and velocity the large orifice and small orifice $\overline{D}_{HW}$ equations predict drop sizes one order magnitude different. Secondly, whereas the secondary break-up correction reduces the predicted small orifice drop size significantly, the correction actually increases the large orifice drop size prediction. The

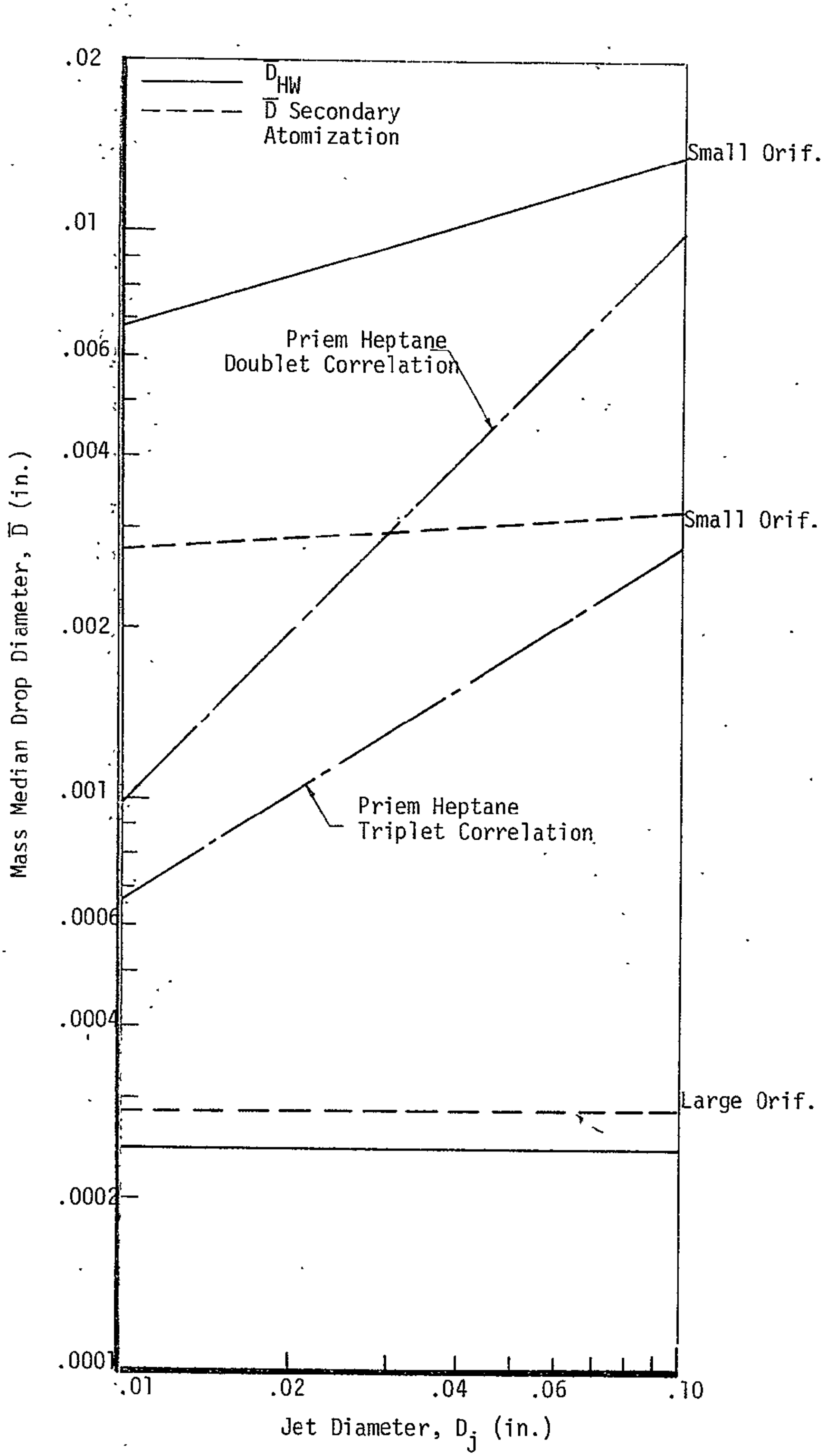

FIGURE A-1. UNLIKE DOUBLET DROP SIZES

third anomaly is that the large orifice equation correlated from the hot wax experiments shows that jet diameter has no influence on the mass median drop size. Included in the figure, for reference, are predicted drop size trends made with the Priem model for liquid heptane drops. The Priem data shows a significant effect of jet diameter on drop size. Last, the unlike doublet equations do not allow for propellant property effects on the predicted drop size. Priem's model results in drop size being proportional to the propellant properties grouping shown.

$$\bar{D} \sim \left(\frac{\sigma_L \quad \mu_L}{\rho_L} \right)^{1/4} \qquad \text{(A-4)}$$

Typical atomization models found in the literature, such as those of Weiss and Worsham (Ref. 26), Ingebo and Foster (Ref. 27), and Nukiyama and Tanasawa (Ref. 28) also allow for the influence of liquid properties on the atomized drop diameter.

b. Triplet and Pentad Drop Size Equations

The drop size equations for triplets and pentads, taken from Ref. 23, are shown below.

Triplet and 4-on-1 (Center Orifice) (Ref. 23)

$$\bar{D}_{HW} = 0.85 \frac{D^{.1} D_{opp}^{.12}}{U_D^{.74} U_{D,opp}^{.33}} \qquad \text{(A-5)}$$

Triplet and 4-on-1 (Outer Impinging Streams)

$$\bar{D}_{HW} = 3.82 \frac{D^{.68}}{D_{opp}^{.35} U_D^{.56} U_{D,opp}^{.57}} \qquad \text{(A-6)}$$

Examination of the DER code revealed a different equation for the center orifice.

Triplet and 4-on-1 (Center Orifice) (DER Code)

$$\overline{D}_{HW} = 0.85 \quad \frac{D^{.1} \quad D_{opp}^{\;.12}}{U_D^{\;.086} \; U_{D,opp}^{\;.89}} \qquad \text{(A-7)}$$

For triplets and pentads DER uses J_A and B values of 0.03 and 310, respectively, in the secondary breakup equation (Eq. A-3). The variation in J_A and B constants for unlike doublets and triplets imply that equal drop sizes produced with different injector element types result in different secondary breakup characteristics. There would appear to be no physical basis for such an effect.

Predictions made with the DER triplet equations, for a range in orifice diameter from .01 to .1 inches, are shown in Figure A-2. The $\overline{D}_{HW}$ (hot wax) equations show realistic trends, but these results are obliterated by the secondary breakup correction. As an example, the outer orifice $\overline{D}_{HW}$ predictions range from about .006 to .013 inches. When inserted in Eq. A-3 the predicted drop size range is from .00317 inches to .00320 inches. It is apparent from this result that the DER triplet equation is effectively a constant (1/310), since the first term in the Eq. A-3 denominator will always be small compared to the constant second term. Additionally, as was the case for the unlike doublet, the triplet equations do not allow for the effect of propellant properties on the predicted mass median drop size.

c. Like Doublet (single or pair) Drop Size Equations

Ref. 2 shows the following equation to account for the combined effects of hydraulic and secondary breakup for like doublet elements.

$$\overline{D} = 1.524 \quad \left\{ 2.64 \left(\frac{U_D}{D} \right)^{1/2} + \frac{0.0978}{C_{pr}} \; f\,(\varepsilon_c) \left| \frac{480}{\varepsilon_c} - U_D \right| \right\}^{-1} \qquad \text{(A-8)}$$

The formula for the contraction ratio function (ε_c) varies between Ref. 2 and the DER code.

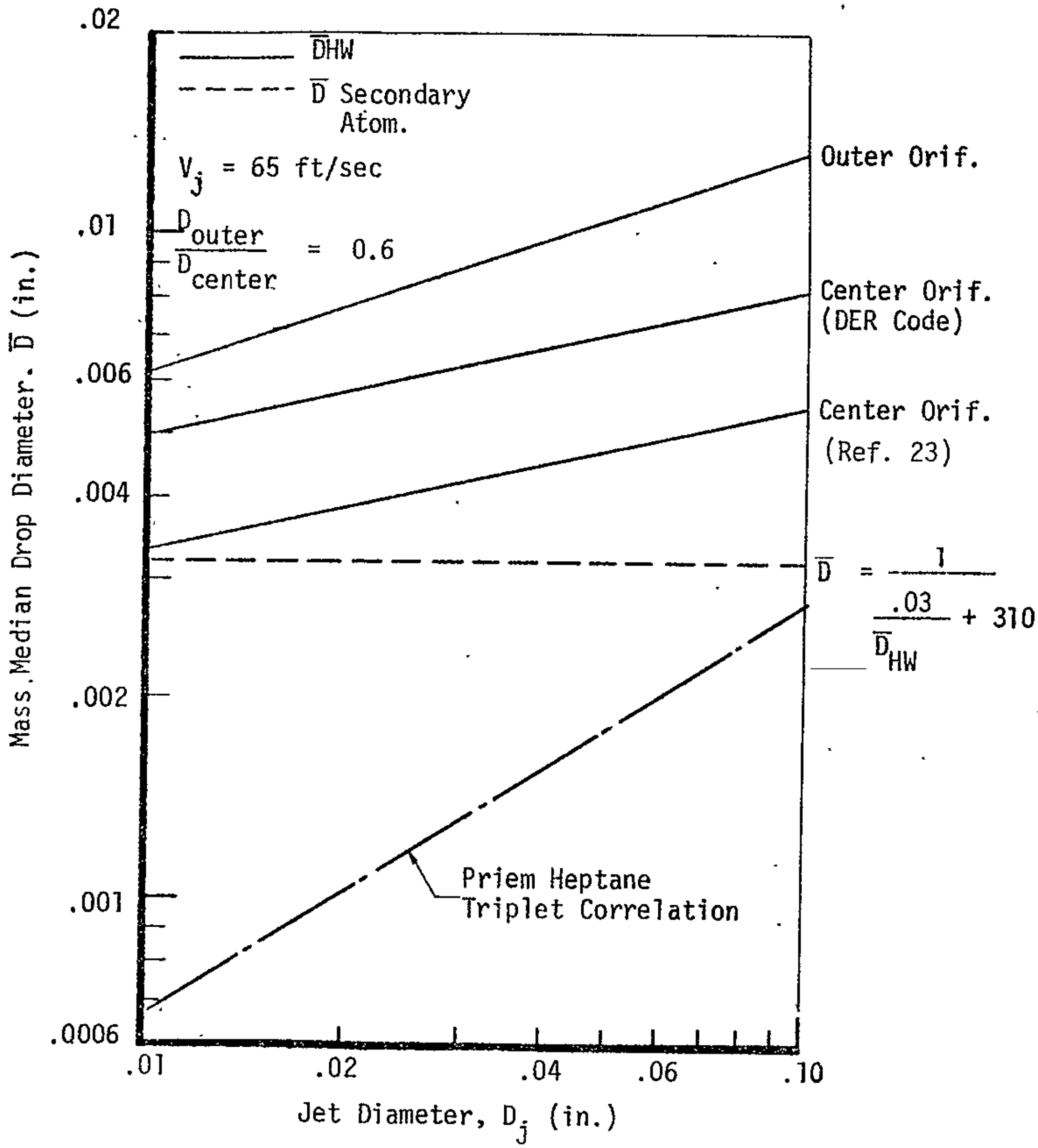

FIGURE A-2. TRIPLET AND PENTAD (4-on-1) DROP SIZES

$$f(\varepsilon_c) = \frac{5(\varepsilon_c - 1)}{\varepsilon_c + 3} \qquad \text{(Ref. 2)} \qquad \text{(A-9)}$$

$$f(\varepsilon_c) = \frac{(\varepsilon_c - 1)}{\varepsilon_c + 3} \qquad \text{(DER Code)} \qquad \text{(A-10)}$$

Predicted drop sizes for these equations are shown in Figure A-3. As shown, the Priem like doublet correlation shows considerably more sensitivity to jet orifice diameter than the DER correlations. The variable C_{pr} is a propellant properties term, that is only included for the secondary breakup part of the drop size equation.

2. ZOM Plane Selection

ZOM is the interface plane (measured from the injector face plane) between the LISP and STC subprograms that comprise DER. ZOM is the plane at which the LISP mass distribution is calculated. The mixing limited performance loss is directly dependent on the ZOM plane calculated mass distribution because STC does not account for turbulent mixing or combustion effects. Two analytical studies (Ref. 20 and 21) have determined that DER predictions are quite sensitive to selection of a value for ZOM. Ref. 2 provides only the following two guidelines to selection of ZOM: (1) the collection plane should be far enough downstream to account for substantial spray spreading and wall impingement, and (2) because LISP does not account for inter-element spray interaction, spray mixing and impingement effects can be overpredicted if ZOM is too far downstream. It is apparent that an a priori method for selection of ZOM does not currently exist.

LISP calculates the mass distribution from an injector element with the following general equation.

$$w_i(x,y,z) = \frac{w_{001}}{z^2} \left\{ \left[1 + C_1\left(\frac{y}{z}\right) + C_2\left(\frac{y}{z}\right)^2 \right] + \left[C_3\left(\frac{x}{z}\right) + C_4\left(\frac{x}{z}\right)^2 \right] \left[1 + C_5\left(\frac{y}{z}\right) + C_6\left(\frac{y}{z}\right)^2 \right] \right\} e^{-a\left(\frac{x}{z}\right)^2 - b\left(\frac{y}{z}\right)^2} \qquad \text{(A-11)}$$

Z is the distance from the element impingement point (H), thus ZOM is the sum

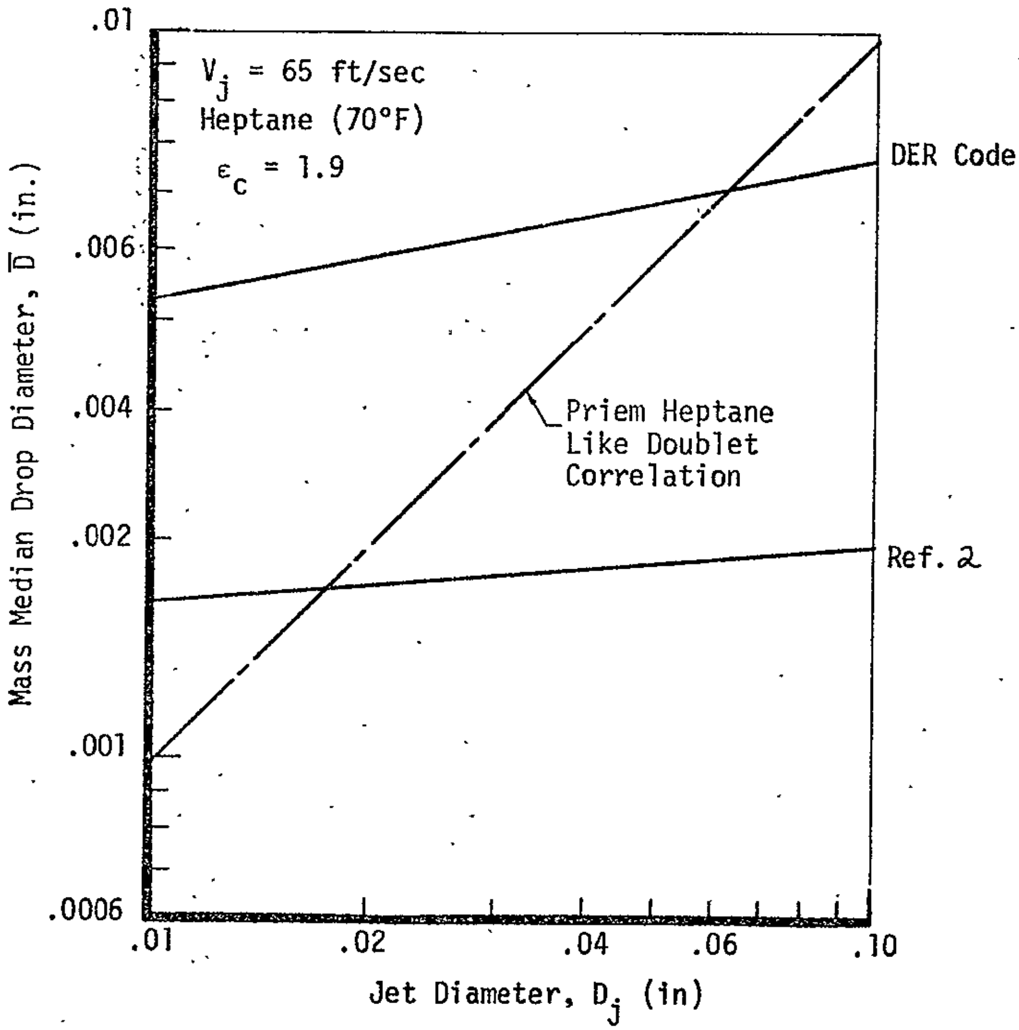

FIGURE A-3. LIKE DOUBLET DROP SIZES

of Z and H. The mass distribution coefficients (C_1, C_2, C_3, C_4, C_5, C_6, a,b) are evaluated empirically from single element cold flow data generated with propellant simulants. The equation assumes that the element spray can be characterized as point source flow and that the spray coefficients for the equation are constant, independent of the Z distance. This assumption has not been verified experimentally.

The LISP mass distribution equation results in a linear half angle spray fan spreading characterization as shown in Figure A-4. Inter-spray mixing increases as ZOM is increased because of spray fan overlap. LISP does not account for any spray fan interaction thus adjacent spray fan mass distributions are simply superimposed on one another. Since no consistently accurate a priori method for selection of the ZOM value exists, attainment of an accurate value usually depends on an iterative process utilizing available hot fire performance data.

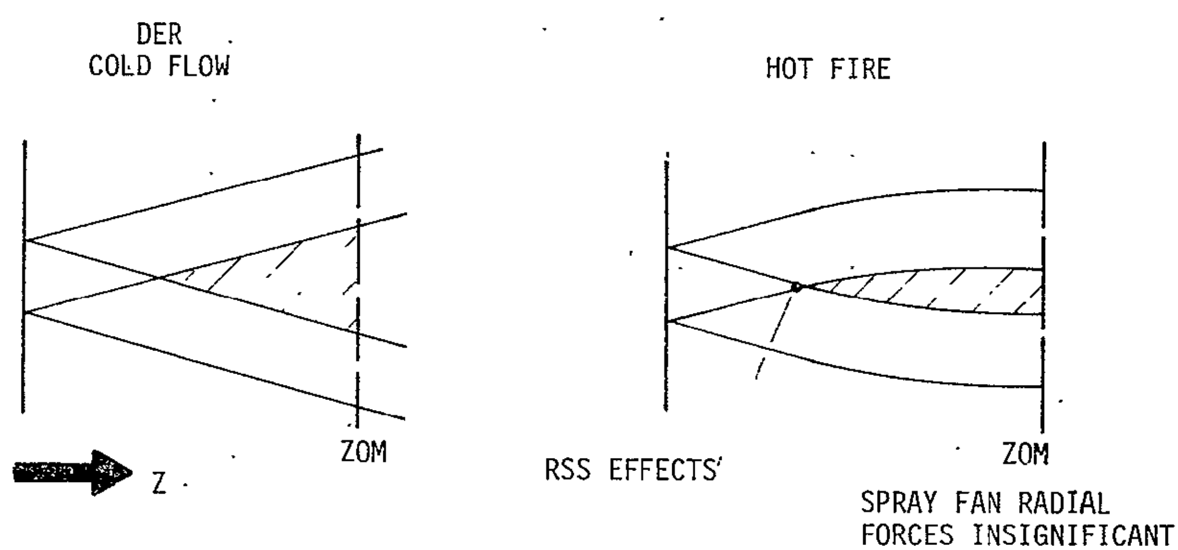

FIGURE A-4. COMBUSTION EFFECTS ON COLD FLOW SPRAY FAN PROFILE

Finite mixing losses are experienced in hot firings because combustion gas acceleration and reactive stream separation (RSS) forces (if any) combine to impede inter spray fan mixing. It therefore seems reasonable that selection of the ZOM plane should account for the influence of combustion on the chamber spray fan mass distribution. As combustion gas is formed and accelerated significant axial droplet drag forces are generated. These forces result in an effective bending of the cold flow spray fan, as shown in Figure A-4. Eventually, the axial spray fan drag forces dominate any radial droplet velocity forces and inter spray fan mixing stops. During Task II of the IP program a methodology for accounting for combustion effects and for a priori selection of the ZOM plane location was developed. The current status of this model is detailed in Section V of this report.

Recent work (Ref. 18) indicates that, in addition to normal combustion gas acceleration effects, Reactive Stream Separation (RSS or "blow-apart") can also significantly affect chamber mixing performance. RSS has been successfully correlated as a function of the injector element design and operating point. Section B.5 of this appendix expands the RSS topic and suggests ways of incorporating RSS modeling in the LISP mass distribution formulation. A proposed overall development plan for general improvement and update of the LISP ZOM plane mixing technique is included in Section C.7 of this appendix.

A final limitation of the ZOM plane methodology is the relatively narrow parametric range over which spray distribution coefficients have been catelogued in LISP. Currently, if the design point to be analyzed is not within the spray coefficient range for the element type in question the spray coefficients for the nearest available design point are selected. No technique currently exists for extrapolation of the spray coefficients. The current parametric range for the LISP coefficients for the five primary liquid/liquid element types is shown below in Table A-I. Expansion of the spray coefficient matrix is required if the ZOM technique is retained in DER.

TABLE A-I

LISP SPRAY COEFFICIENTS PARAMETRIC RANGE

	Element	Orif. Dia. (in.)	Imping. Angle (deg)	Momentum Ratio (f/o)
(1)	Unlike Doublet	0.020-0.079	45-70	9.42-1.0
(2)	Like Doublet	0.020-0.079	45-70	1.0
(3)	Like Doublet Pair	0.020-0.028	60 Like, 40 Unlike	Not Correlated
(4)	Triplet	0.085-0.067 Outer 0.043-0.067 Inner	70	0.3-8.0
(5)	4-on-1 (Pentad)	0.21-0.47 Inner 0.1-0.22 Outer	60	0.2-1.25

3. DER Vaporization Sensitivity Study

The previous subsections have detailed the three most critical DER analysis input parameters; the mass median drop diaemter, the LISP spray distribution coefficients, and the LISP/STC interface plane, ZOM. The specification of these LISP inputs controls, in large part, the accuracy of the DER calculation. The most important function of the Streamtube Combustion (STC) subprogram is to compute propellant vaporization to the chamber throat plane, after correct input is established and STC has segregated the LISP calculated mass distribution into a finite number of axisymmetric streamtubes. The third subtask of the DER review was a vaporization sensitivity study conducted to determine the influence of engine design and operating variables on the DER vaporization calculation. DER predictions were compared to similar calculations made with the simplified Priem L-General model (Ref. 17) for reference. The Priem L-General model is an empirical correlation of an analytical vaporization model that accounts for droplet heating. The L-General model accounts for the effect of chamber length, contraction ratio, chamber pressure, injection velocity, drop size, initial propellant temperature and propellant properties on vaporization rate.

The vaporization sensitivity study was conducted by running single stream calculations with STC. The NTO/MMH propellant combination was selected because of experience obtained during the Space Shuttle OMS Engine program. Oxidizer and fuel mass median drop diameter, initial velocity, and total flowrates were input to STC. A log normal drop size distribution (σ = 2.3), with five size groups for each propellant, was used throughout the study, except during the phase of the study which evaluated the effect of the specified drop distribution on the vaporization efficiency prediction. The independent design and program input variables evaluated during the study included chamber length, mass median drop diameter, chamber pressure, droplet initial (injection) velocity, chamber contraction ratio, propellant inlet temperature, and the propellant drop size distribution. The study nominal calculation point and the parametric range of the independent variables is detailed in Table A-II.

TABLE A-II

DER VAPORIZATION SENSITIVITY STUDY
VARIABLE RANGES

Variable	Nominal Value	Range
Chanber Length, L' (in)	6	6-14
Mass Median Drop Diameter, $\overline{D}$ (in)	.002	.001-.004
Chamber Pressure, Pc (psia)	120	60-240
Injection Velocity, V_j (ft/sec)	65	65-200
Contraction Ratio, ϵ_c	1.9	1.9-5
Propellant Temp., T_p (°F)	70	40-130

In addition to the DER vaporization sensitivity study, the recent comprehensive combustion model evaluation conducted by Bracco (Ref. 7) was reviewed. This study resulted in three conclusions that are relevant to the DER review. First, the Priem vaporization model, used as the reference technique in the sensitivity study, was judged to be capable of accurate correlation of empirical ethanol mass vaporization profiles. Secondly, the Priem

C-2

technique was most accurate if the droplet drag coefficient was assigned a low but finite value ($0 < C_D < 24/Re$). A major conclusion by Bracco was that low drag coefficients give better results than higher drag equations, such as the Rabin equations (See Section C.3.d. of this appendix) used in DER. In support of lower drag coefficients he cites Eisenklam's suggestion (Ref. 29) that burning droplets actually have lower drag coefficients than solid spheres. The final significant conclusion of Braccos work is that a drop size distribution function is not necessary to accurately reproduce the steady combustion profile, although it does tend to improve the results.

The results of the vaporization study are presented below for each design variable shown in Table A-II.

a. Chamber Length

Propellant vaporization was calculated at three chamber lengths (6, 10, and 14 inches) with DER and the Priem L-General model. Figure A-5 shows that both models predict similar trends of propellant vaporization versus chamber length. The calculated absolute levels differ somewhat for the MMH vaporization characteristic. This difference is believed to be related to the fact that DER does not allow for the finite time required to heat the liquid propellant to the chamber "wet bulb" condition. This omission is described more fully in the section dealing with propellant inlet temperature considerations. The trend agreement versus chamber length for the Priem and DER models suggests that both model the gas dynamic, droplet ballistic, and steady state heat and mass transfer processes similarly. This result is clouded somewhat by the chamber pressure sensitivity result presented in the next paragraph.

b. Chamber Pressure

Propellant vaporization was calculated for chamber pressures ranging from approximately 60 to 240 psia. The results of this phase of the sensitivity study are shown in Figure A-6. The figure indicates a significant difference exists between the predicted effect of chamber pressure on propellant vaporization for the DER and Priem models. The DER model indi-

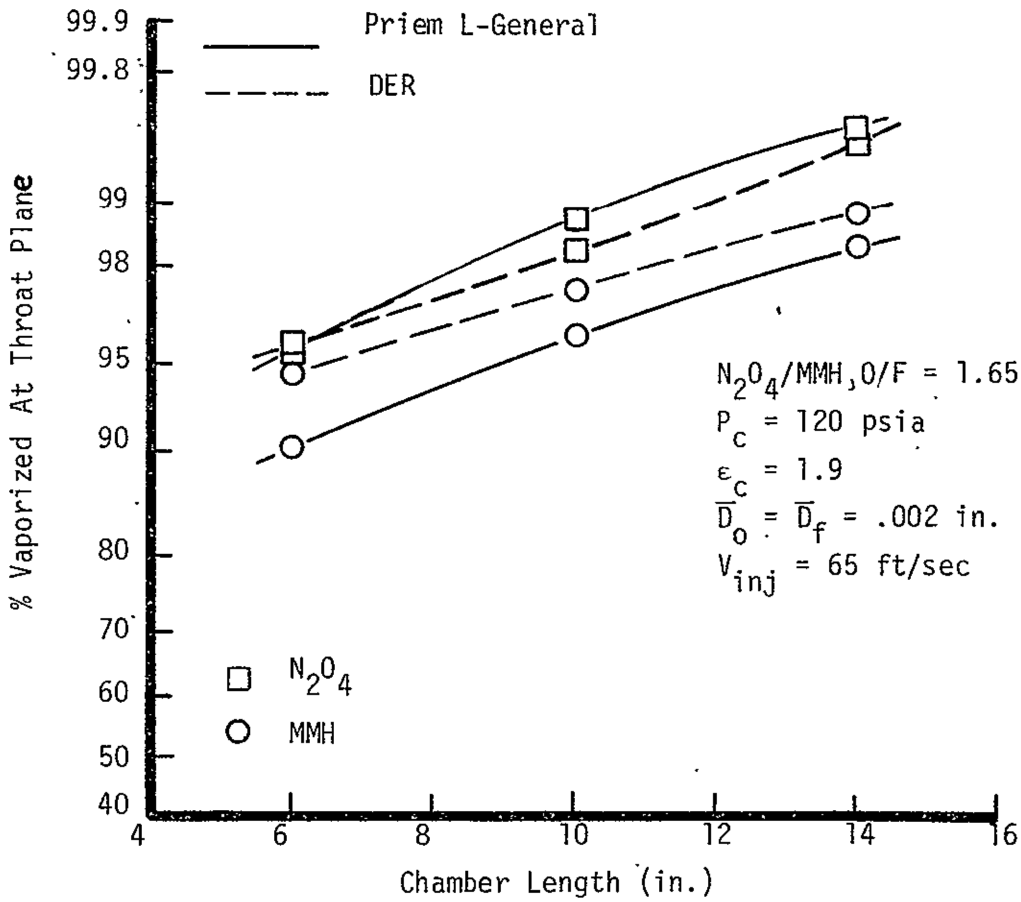

FIGURE A-5. CHAMBER LENGTH EFFECT ON VAPORIZATION

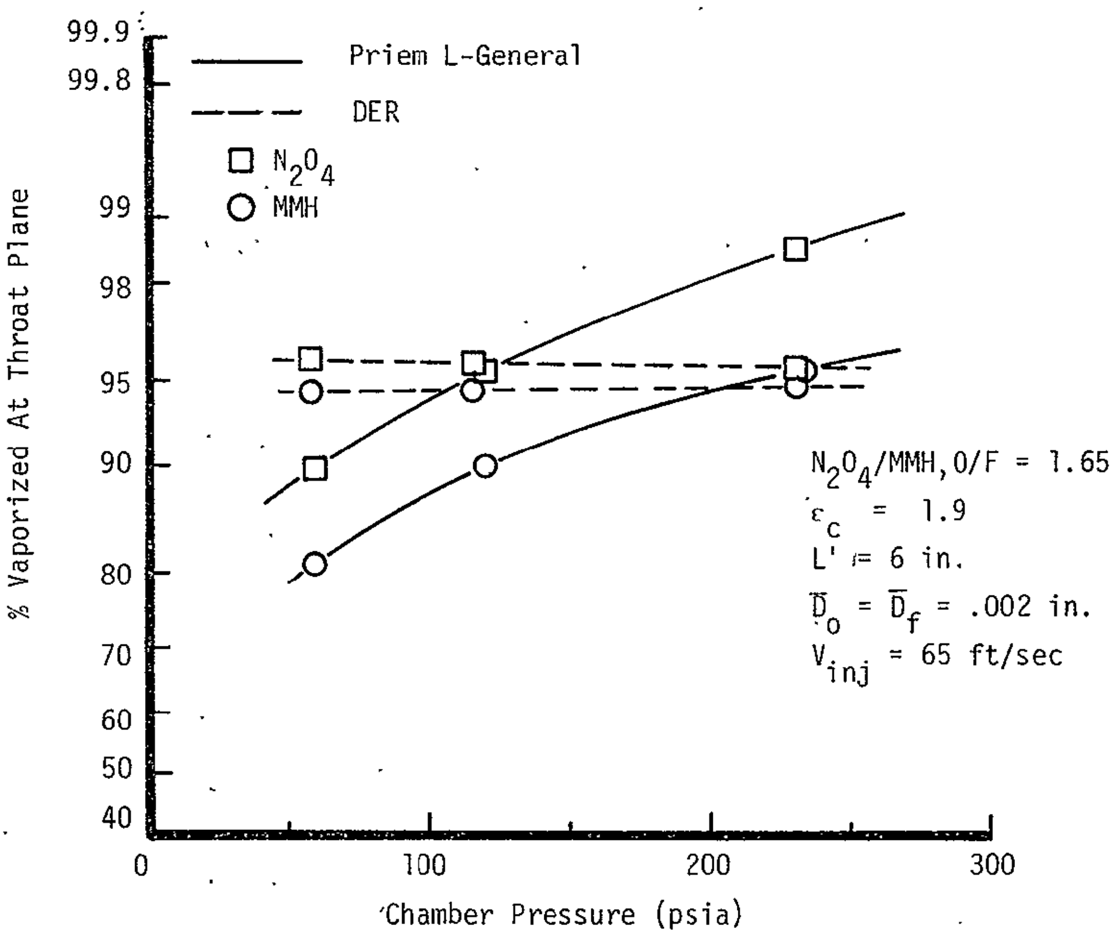

FIGURE A-6. CHAMBER PRESSURE EFFECT ON VAPORIZATION cates no sensitivity to chamber pressure, while the Preim model shows a significant influence*. The DER and Priem vaporization formulations were briefly investigated to determine the reason for the chamber pressure influence difference. The DER K-Prime model is based on the early work of El Wakil and others (Ref. 30). An admitted weakness of this model was the need for a correction factor accounting for unidirectional, as opposed to equimolal, droplet vapor diffusion in the mass transfer equations. The Priem model accomplishes the transformation through the following equation.

$$(j_{a,s})_{unidirectional} = (j_{a,s})_{equimolal} \times (\alpha)$$

where: $$\alpha = \frac{p_s}{p_{a,s}} \ln \left[\frac{p_s}{p_s - p_{a,s}} \right] \qquad \text{(A-12)}$$

The mass transfer rate equation without the unidirectional diffusion correction is written as:

$$w = A_s K \quad p_{a,s} \qquad \text{(A-13)}$$

Including the α term yields the following, which results in a term showing a directly proportional relationship between the mass transfer rate and the local static pressure.

$$W = A_s K p_s \quad \ln \left[\frac{p_s}{p_s - p_{a,s}} \right] \qquad \text{(A-14)}$$

It is suggested that possibly the DER K-Prime model does not accurately account for the effect of chamber pressure on the vaporization rate because of this omission. Complete resolution of this question was beyond the scope of the current work.

---

*Priem correlated an effective chamber length (L_{gen}) as being proportional to $p_c^{0.66}$.

c. Mass Median Droplet Diameter

Propellant vaporization was calculated for mass median driplet diameters of .001, .002, .003, and .004 inches. Relatively small droplets were selected because state-of-the-art injector designs are attaining performance consistent with such drop sizes. The results of the drop diameter study are plotted in Figure A-7. The trends for the DER and Priem models are nearly identical. The figure indicates that both formulations account for the influence of drop diameter on mass transfer, heat transfer, and droplet ballistics.

d. Droplet Initial (Injection) Velocity

Propellant vaporization was calculated for droplet initial velocities of 65, 100, and 200 ft/sec. The results are shown in Figure A-8. The Priem model indicates a much greater sensitivity to initial velocity than does DER. Two differences in the droplet ballistic equations of the two models have been discovered.

First, the DER integration technique (a simple step-by-step Euler approach) often predicts a droplet downstream station velocity greater than the downstream gas velocity. When this occurs DER sets the downstream station droplet velocity equal to the upstream station droplet velocity, resulting in an unrealistically long droplet chamber residence time and increased propellant vaporization. This result is indicated in Figure A-8 by the high DER vaporization efficiencies predicted for high droplet initial velocities.

The second droplet ballistics difference between the two models is in the formulation of the droplet drag coefficient. The Priem model employs the empirical correlation developed by Ingebo (Ref. 16).

$$C_d = 27 \, Re_D^{-0.84} \tag{A-15}$$

DER uses a variation of the Ingebo result, developed by Rabin (Ref. 31) above Reynolds numbers of 80.

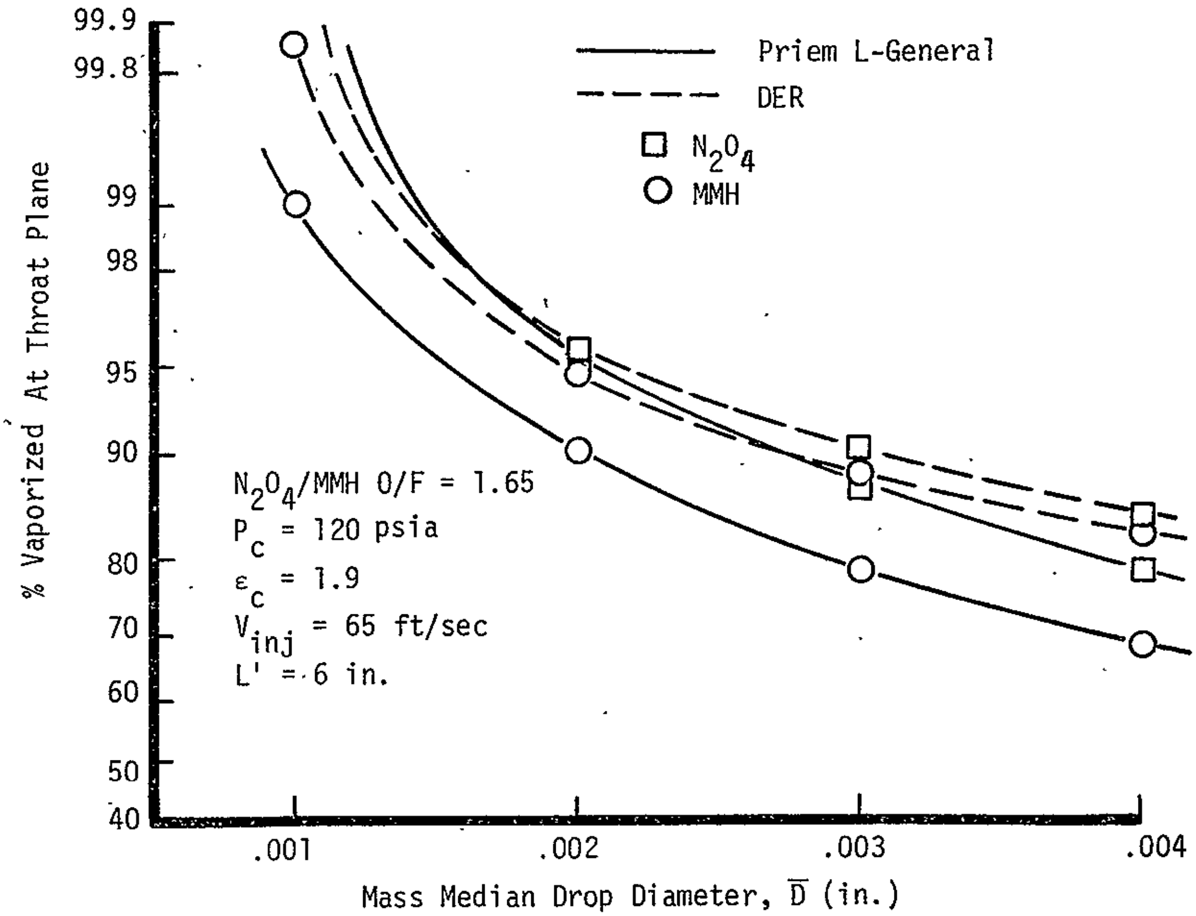

FIGURE A-7.MASS MEDIAN DROP DIAMETER EFFECT ON VAPORIZATION

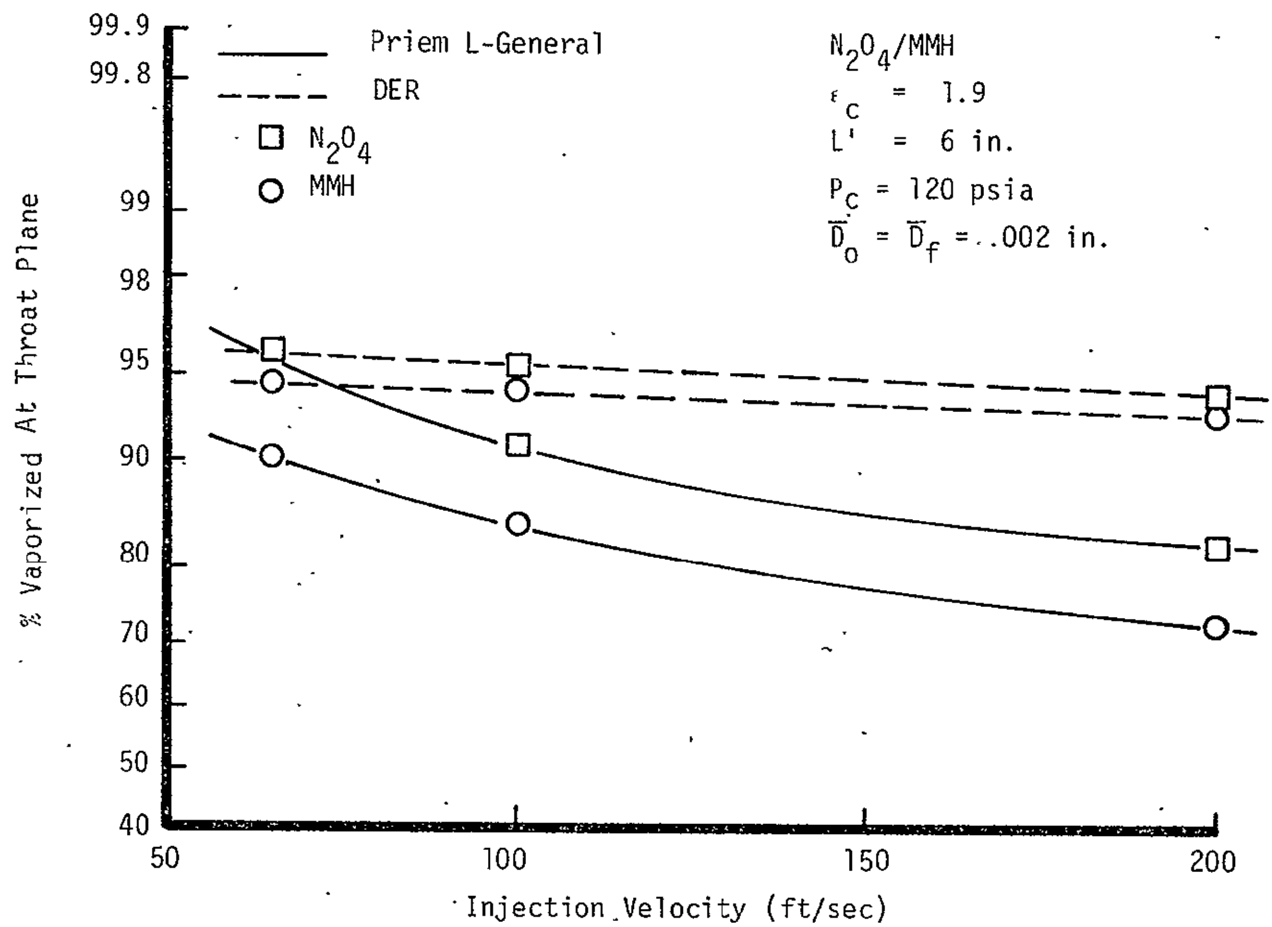

FIGURE A-8. INJECTION VELOCITY EFFECT ON VAPORIZATION

$$C_d = 27\ Re_D^{-0.84} \qquad Re_D < 80 \qquad (A\text{-}16)$$

$$C_d = 0.271\ Re_D^{.217} \qquad 80 \le Re_D \le 10^4 \qquad (A\text{-}17)$$

$$C_d = 2 \qquad Re_D > 10^4 \qquad (A\text{-}18)$$

Considerable discussion occurs in the literature over the validity of the two models. As introduced previously, Bracco (Ref. 7) has concluded that high C_D's (such as the Rabin equations) give erroneous mass vaporization profile results. Also, an excellent synopsis of relatively current thought is contained in Ref. 32.

The effect of substituting the Ingebo correlation for the Rabin correlation on DER vaporization predictions is shown in Figures A-9 and A-10. In Figure A-9 the predicted vaporization efficiencies are plotted versus injection velocity for both drag coefficient correlations. The Ingebo equation increases the absolute vaporization efficiency level and results in a slope more nearer the Priem model result. In Figure A-10 DER predictions for both models are plotted versus chamber length. The slope of the predictions are nearly equivalent, while the Ingebo equation results in a significantly higher rate of propellant vaporization.

e. Chamber Contraction Ratio

Propellant vaporization was calculated for chamber contraction ratios of 1.9, 3, and 5:1 for a constant chamber length of 10 inches. The results are shown in Figure A-11. The differences in the slope of the predicted DER and Priem model results are likely to be attributable to the two droplet ballistic model inconsistencies commented on in the previous paragraphs.

f. Propellant Temperature

The DER K-Prime model does not allow for the finite time required for a droplet to heat from its injection temperature to the "wet bulb" state. DER has no prescribed method for accounting for the effect of the

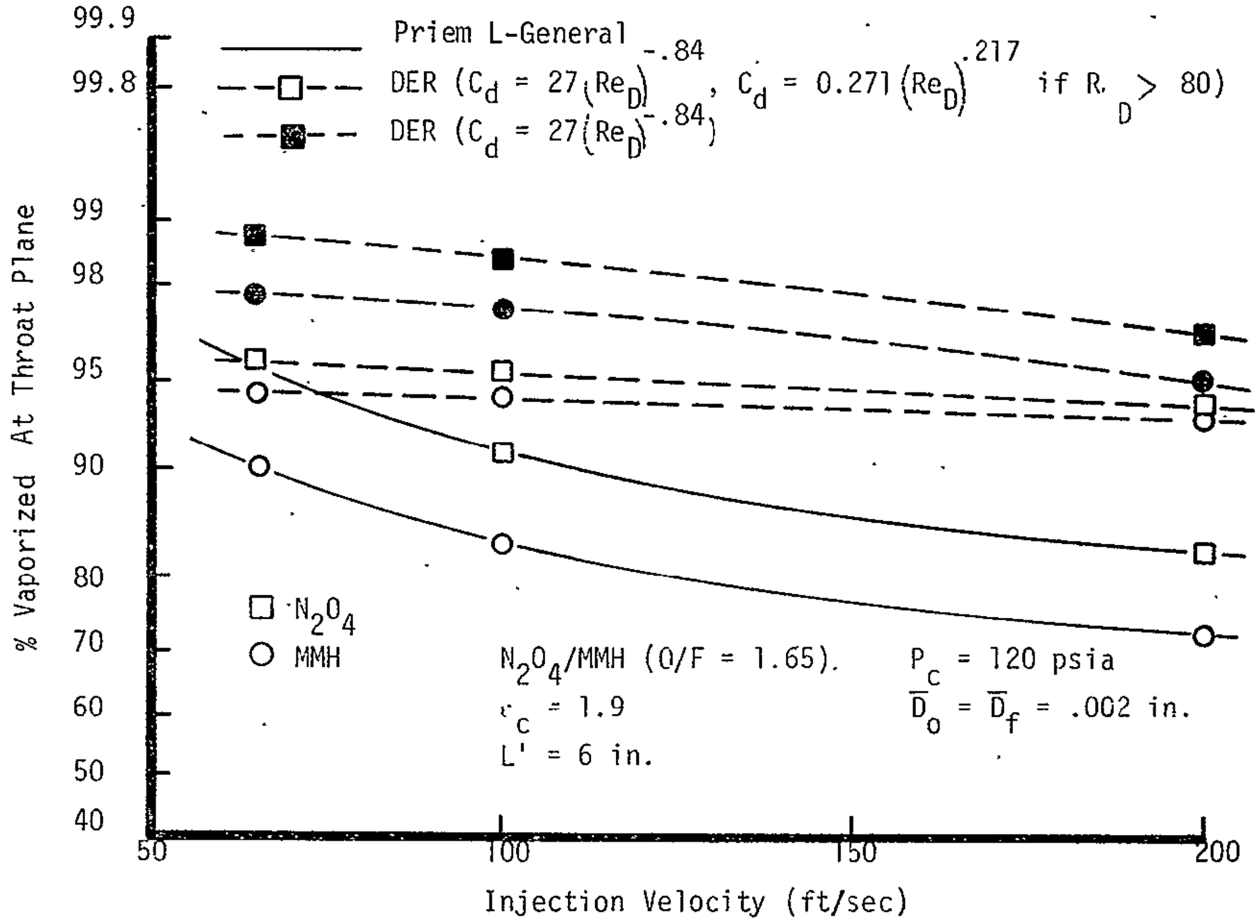

FIGURE A-9. INJECTION VELOCITY EFFECT ON VAPORIZATION FOR DIFFERENT DROPLET DRAG COEFFICIENTS

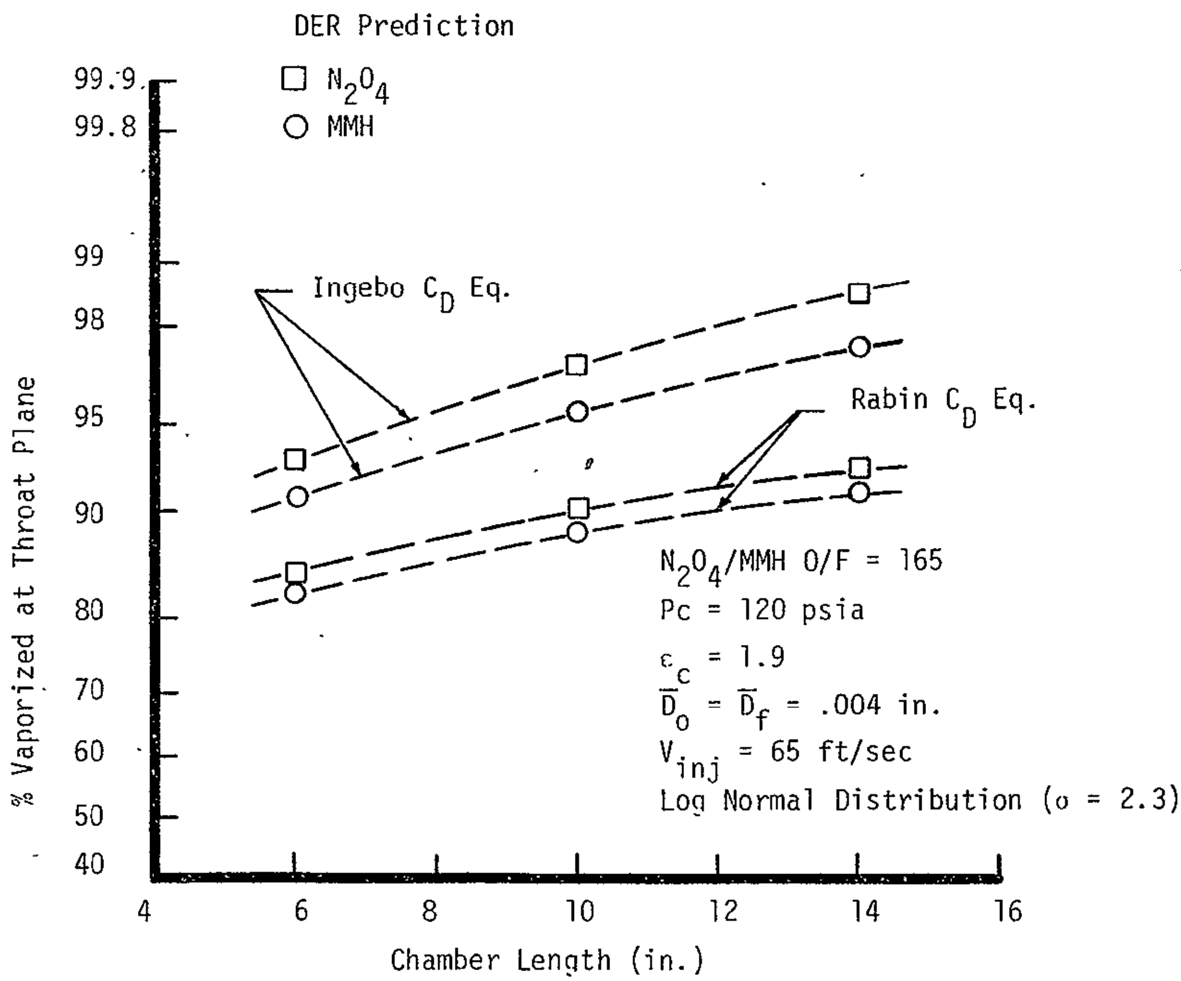

FIGURE A-10. CHAMBER LENGTH EFFECT ON VAPORIZATION FOR DIFFERENT DROPLET DRAG COEFFICIENTS

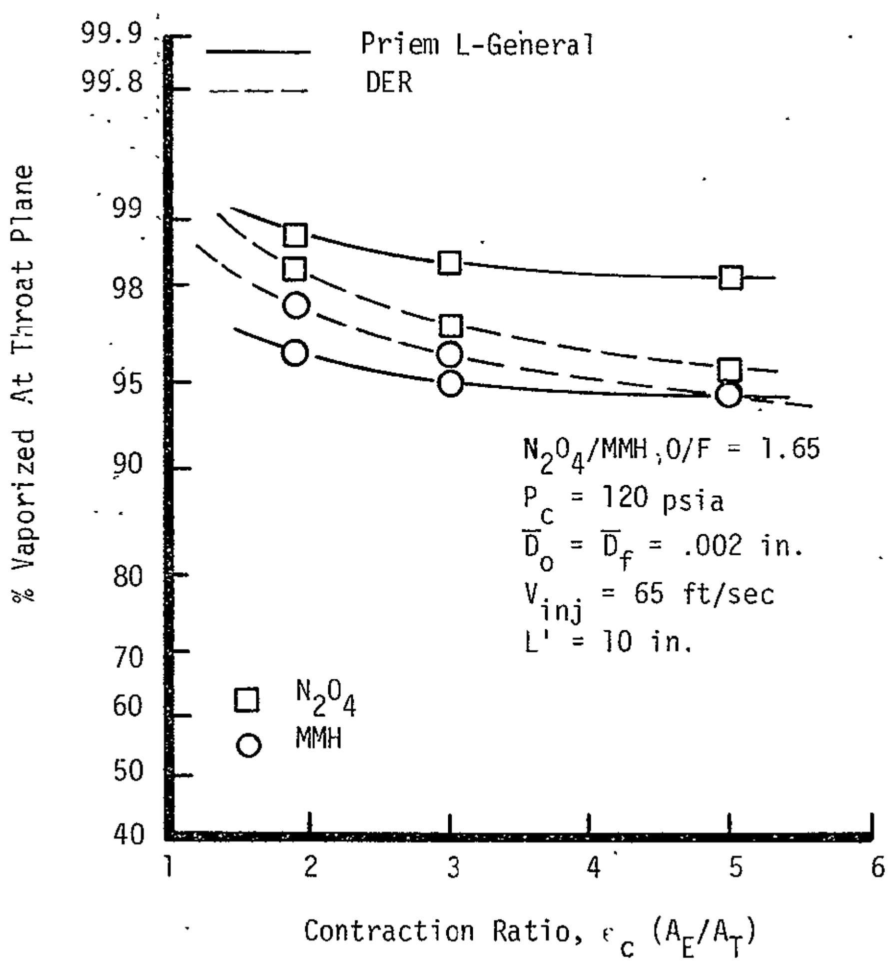

FIGURE A-11. CONTRACTION RATIO EFFECT ON VAPORIZATION propellant inlet temperature on vaporization efficiency because of this model simplification. Priem used his time based mass and heat transfer equations to compare the time to reach the "wet bulb" condition to the time to vaporize 99 percent of the mass for several different propellants. The results are shown below.

TABLE A-III

PROPELLANT HEAT-UP TIME CHARACTERISTICS

Propellant	Length to Wet Bulb / Length to Vaporize (Pc = 300 psia)
Heptane	1/5
Hydrazine	1/12
Ammonia	1/16
Oxygen	1/10
Fluorine	1/10

It is apparent that this initial unsteady state can be significant when accounting for a complete droplet time history. The time to reach the "wet bulb" condition is primarily dependent on the droplet diameter and the initial propellant temperature.

Figure A-12 shows the Priem model predicted effect of propellant temperature on vaporization for the study baseline calculation point. An attempt to allow for this effect with DER was made by adjusting the MMH input latent heat of vaporization. This result, shown in the figure, is considered to be unsatisfactory. The most physically correct way to solve this shortcoming of DER would be to adopt a time dependent vaporization model.

g. Drop Size Distribution

The importance of the droplet size distribution on propellant vaporization has long been recognized. The DER user should realize that the DER builtin drop size distribution may not be physically accurate for his particular injector design*. Figure A-13 shows various drop size distributions found in the literature. The builtin DER drop size dis-

*The DER user can override the builtin distribution through input.

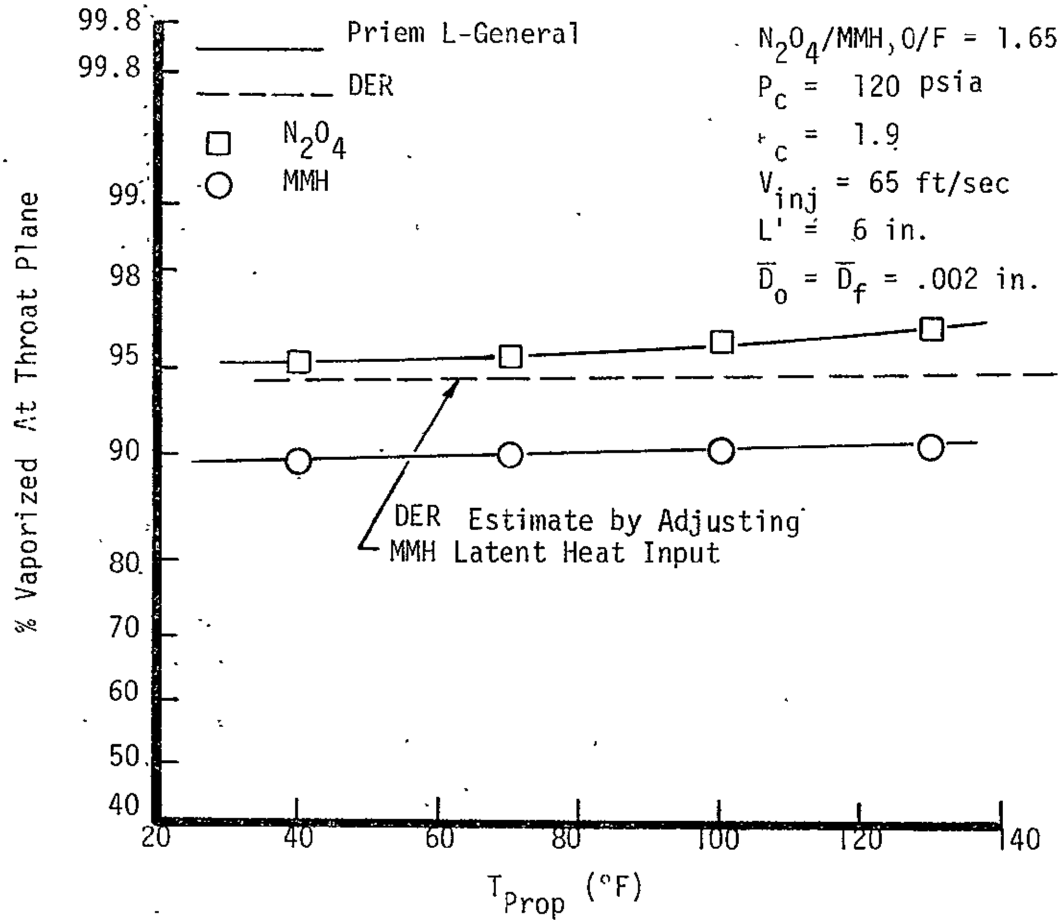

FIGURE A-12. PROPELLANT TEMPERATURE EFFECT ON VAPORIZATION

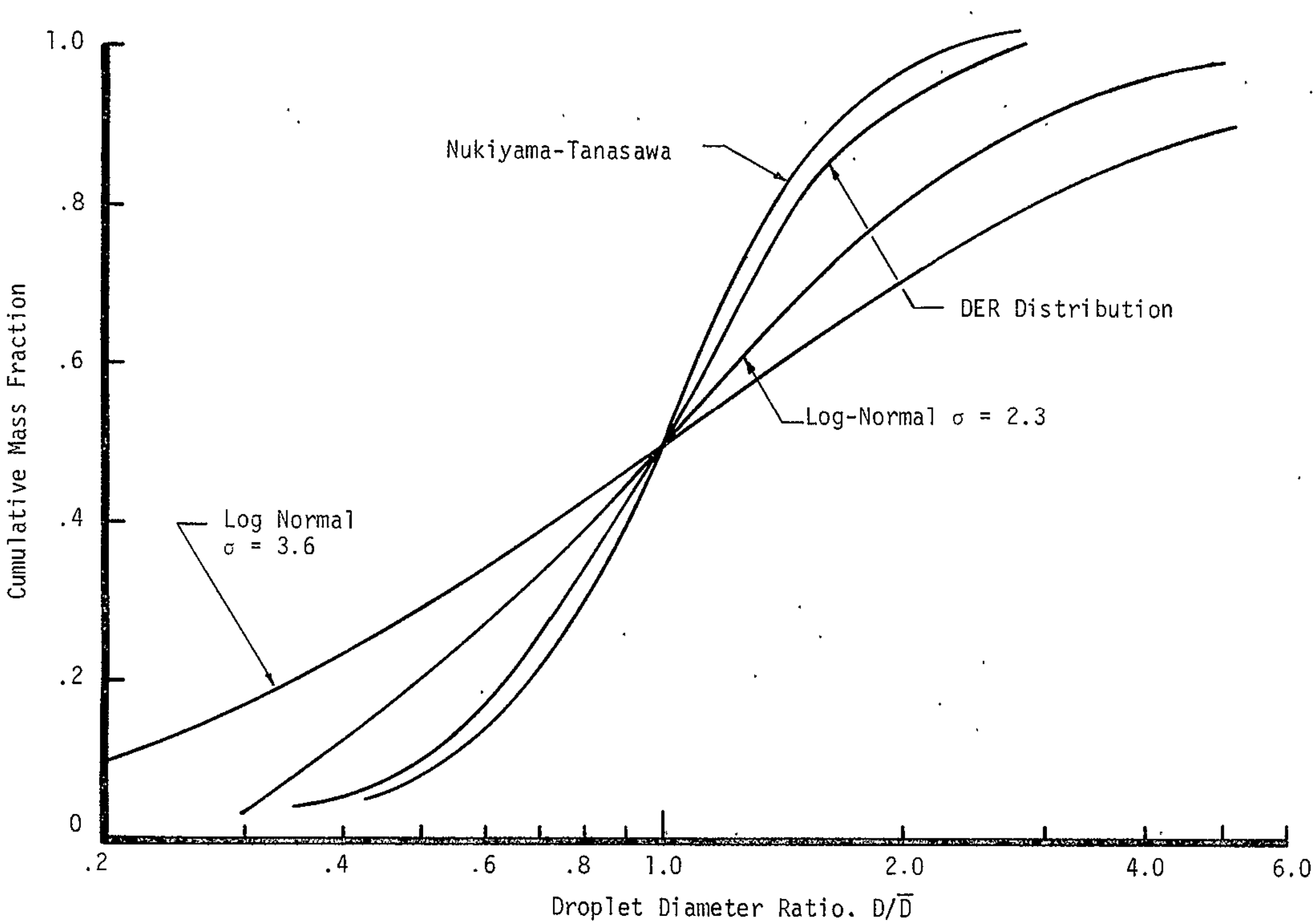

FIGURE A-13.DROPLET SIZE DISTRIBUTIONS

tribution is based on the Rocketdyne molten wax experimental results (Ref. 24). It is quite similar to the well-known Nukiyama-Tanasawa empirically determined cold flow distribution which is also shown in the figure. Priem correlated his hot fire data with log-normal distribution equations.

$$\frac{dR}{dD} = \frac{e^{-1/2\left[\frac{\text{Ln } D/\bar{D}}{\text{Ln } \sigma}\right]^2}}{2\pi \quad D \quad \ln \quad \sigma} \tag{A-19}$$

Priem determined that doublets and triplet hot test sprays were best described with standard deviations of 2.3 and 3.6, respectively. These two distributions are also shown in Figure A-13. The effect of the drop size distribution on propellant vaporization is shown in Figure A-14. The significance of the distribution on the predicted level of vaporization is evident. The DER and Nukiyama-Tanasawa distributions are cold flow (i.e., gas static) distributions. The implication of the Priem correlations is that a dynamic (i.e., accelerating) gas environment affects the atomization process thus resulting in a different hot test distribution.

4. Near-Zone Combustion and Monopropellant Flame Considerations

Monopropellant decomposition burning for hydrazine based fuels has been verified by several investigators. Decomposition burning results in higher energy release than the bipropellant reaction in the injector face near zone. A recommendation has been made recently (Ref. 33) not to include a decomposition flame model in the "standardized" DER program. Two reasons for this recommendation were cited: (1) "Two Flame" effects are only important close to the injector face and do not significantly affect the vaporized propellant mass fraction at the chamber throat plane, and (2) the combustion chamber near-zone flow field can not be well defined analytically.

Monopropellant burning does not significantly affect performance for most thrust chamber designs. However, a valid DER performance model would extend itself naturally to combustion stability and chamber compatibility analytical modeling. Accurate stability and compatibility predictions hinge on a realistic representation of the near zone flow field, where monopropellant effects are significant. Also, the new ZOM mass distribution model described in Section V of this report depends on an accurate vaporization rate calculation near the injector face.

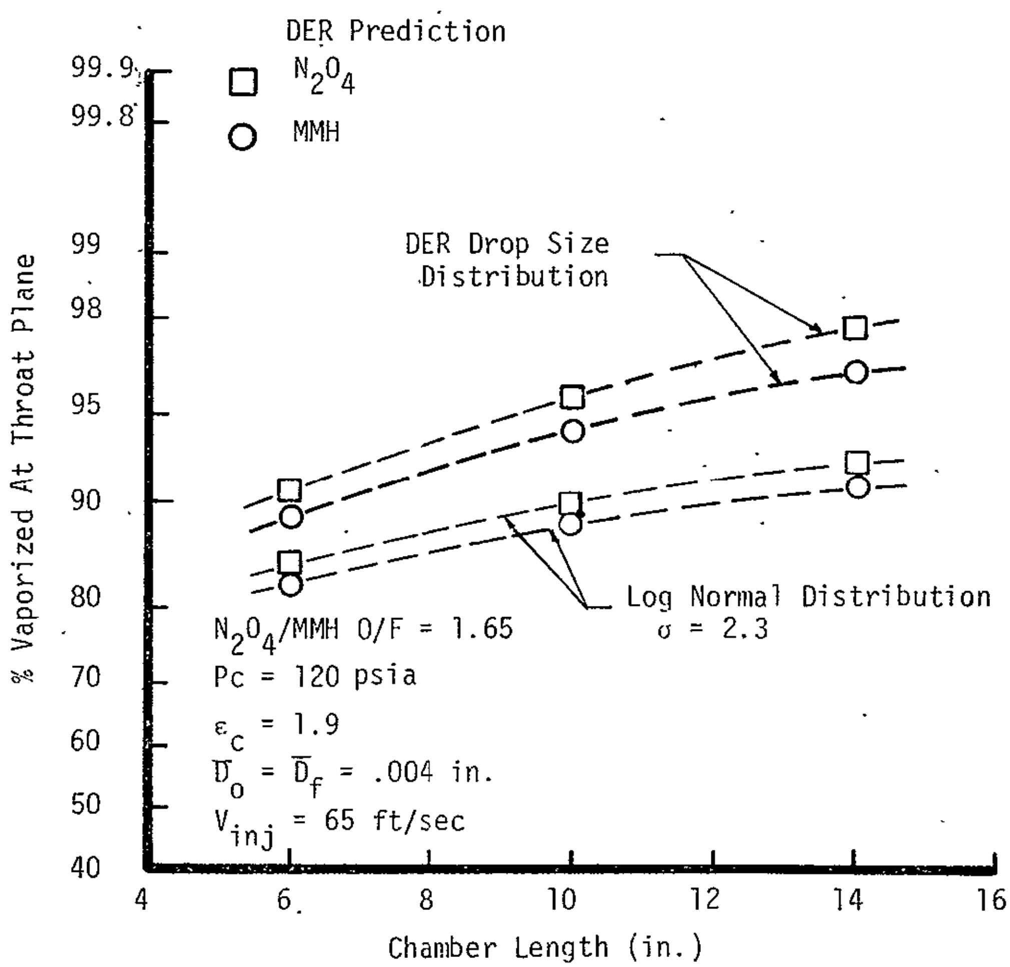

FIGURE A-14. CHAMBER LENGTH EFFECT ON VAPORIZATION FOR DIFFERENT DROP DISTRIBUTIONS

Recent work on the Space Shuttle OMS engine program (Ref. 14) indicates that the near combustion zone can be well modeled. This conclusion was reached through correlation of analytical predictions made with the Priem model with empirically measured energy release rate data. Figure A-15 shows actual and predicted energy release data for a subscale platelet V-doublet injector. The analytical prediction was made with a "two flame" transformation to the simplified Priem L-general model. The OMS engine utilizes the Nitrogen Tetroxide (N_2O_4)/Monomethyl Hydrazine (MMH) propellant combination, thus justifying a two flame correction to the MMH vaporization calculation. Excellent agreement between prediction and test was obtained for the injector near zone, from 0-2 inches from the injector face, as shown in the plot. The correlation continued to be valid to the throat plane, 8 inches from the injector face plane (not shown). The predicted vaporized propellant (gas) mixture ratio profile for the two flame model prediction is also shown in the figure, along with the mixture ratio profile made with the Priem model without the "two flame" correction. The difference is quite significant, indicating the near zone is not modeled correctly unless decomposition burning is accounted for. The local gas composition is directly related to the local gas mixture ratio, indicating the importance of the "two flame" correction to chamber stability and compatibility modeling.

The semi-empirical technique developed to convert measured chamber axial static pressure profiles to injector energy release rate profiles is graphically illustrated in Figure A-16. The measured static pressure at any chamber axial location is used to calculate the local gas velocity and flowrate through isentropic relationships. The cumulative energy release to the same plane is calculated knowing the percentage of the total propellant burned. The energy release rate is predicted by taking the first derivative of the cumulative energy release profile. It has been determined that the resulting injector energy release rate characteristic can be directly related to the injector combustion stability characteristic. Additionally, data obtained in this manner for OMS multi-element subscale like-doublet pair injectors are being used to develop and verify the new ZOM mass distribution model described in Section V of this report.

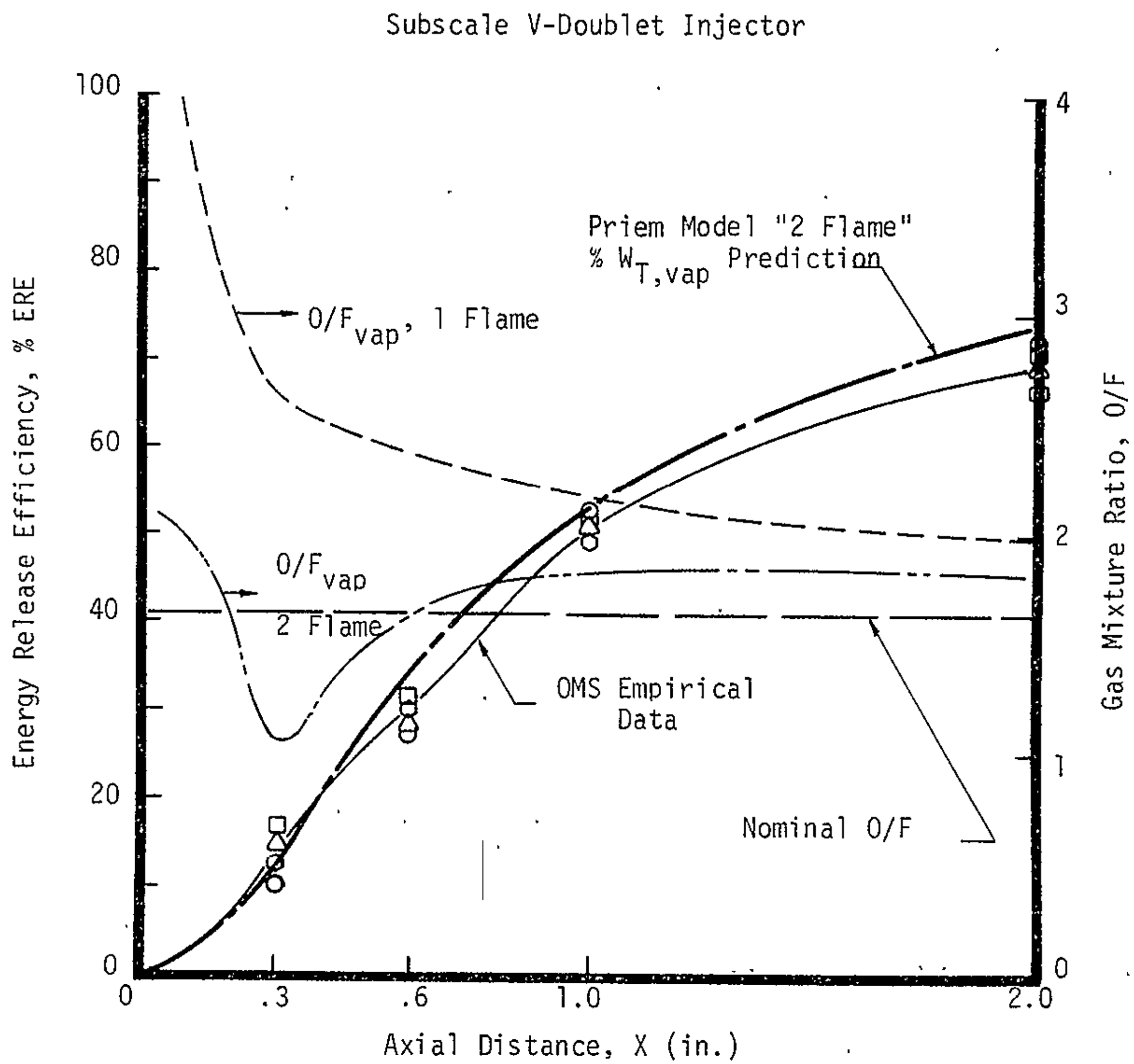

FIGURE A-15.CORRELATION OF PRIEM AND OMS SEMI-EMPIRICAL NEAR ZONE MODEL RESULTS

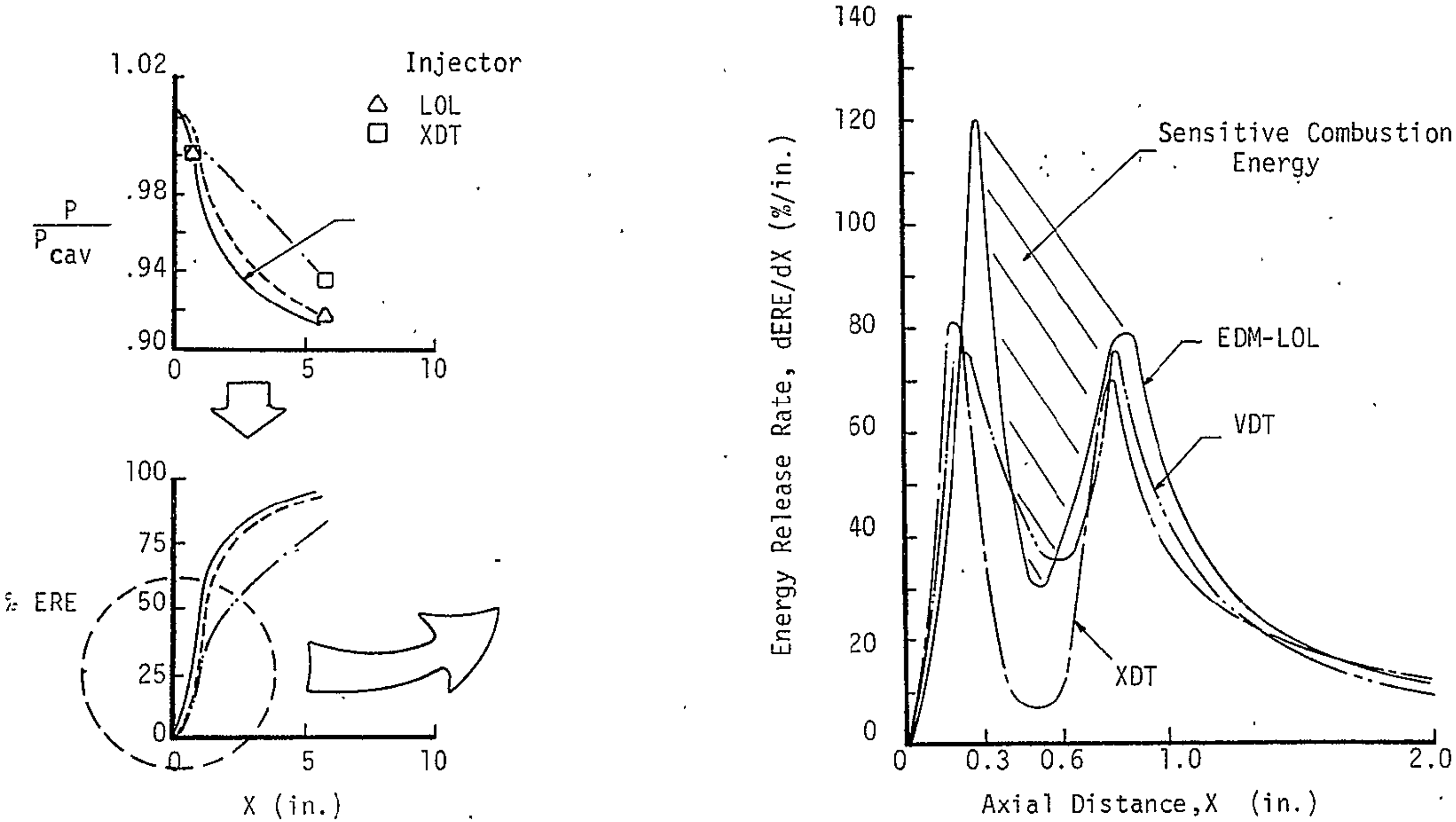

FIGURE A-16. SEMI-EMPIRICAL NEAR ZONE COMBUSTION MODEL

The OMS test results indicate a "two flame" model is required to accurately model the injector near zone for injectors employing hydrazine based fuels. Examples of available models are Refs. 34 through 37.

5. Combustion Gas Acceration and Reactive Stream Separation Effects on Cold Flow Mass Distribution

The LISP mass distribution calculation technique does not allow for the influence of combustion on the elemental cold flow mixing characteristics. The formation and acceleration of combustion gas affects spray distribution for all liquid propellant injectors. Additionally, dependent on the injector operating point, the phenomenon termed Reactive Stream Separation (RSS or "blowapart") can also alter the hot fire case mass distribution from one measured under cold flow conditions.

A model has been proposed to account for the influence of combustion gas acceleration on the calculated chamber mass distribution. Also, inherent in the proposed model is a technique for a priori estimation of the ZOM plane location for mass distribution characterization. The model is described, along with a report on the current status of a model verification effort, in Section V of this report.

The effect of RSS on injector performance can be significant. Figure A-17 indicates the influence of RSS on the energy release efficiency (ERE) for platelet "splash plate" injectors as a function of engine chamber pressure. For one particular injector tested RSS decreased injector ERE approximately 10 percent for a chamber pressure range of from 50 to 110 psia.

A recently completed investigation (Ref. 18) indicates that RSS phenomenon can be accurately modeled and predicted in terms of injector/chamber design and operating variables. Single element unlike doublet, F-O-F triplet, and platelet injectors were tested. The mode of operation of a particular test (i.e., mixed, mixed-separated, or separated) was determined through filming of the combustion with a high speed motion picture camera. Results were correlated with the test design and operating point to result in a mechanistic RSS model.

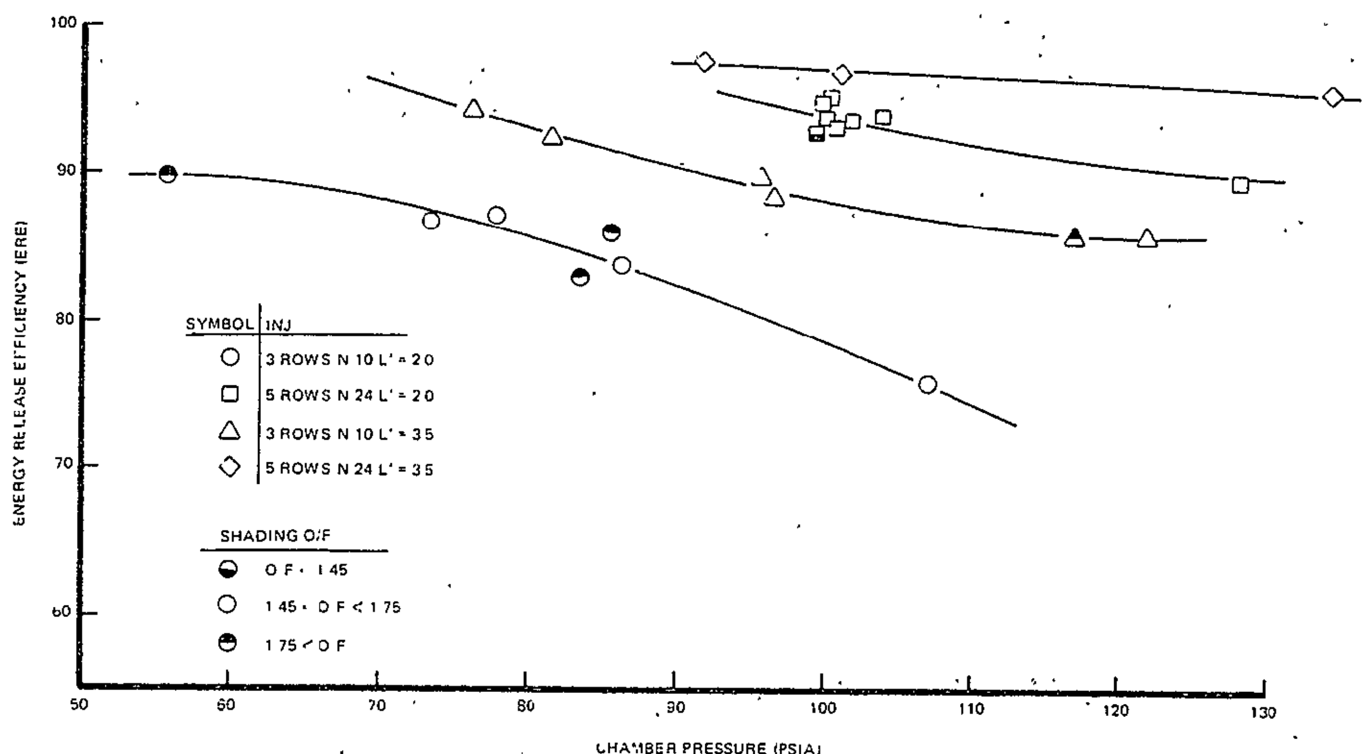

Figure A-17. RSS Effect on Injector Performance

An example RSS correlation is shown in Figure A-18. The occurrence of RSS is plotted for a single unlike doublet element as a function of chamber pressure and a parameter containing Weber Number, Reynolds Number, and a propellant temperature influence term. The Weber number relates the jet aerodynamic drag force to the liquid surface tension force. The results indicate that the occurrence of RSS can be accurately predicted if the injector operating point is well characterized.

Inclusion of RSS results, such as shown in Figure A-18, in LISP could provide a significant improvement in the DER performance prediction capabilities under conditions where RSS occurs. There appears to be two types of RSS models that could be incorporated into LISP. (1) A simple "warning" model that could tell the user that the occurrence of RSS is predicted for his input injector design and operating point, and (2) a model that would predict the occurrence of RSS and would adjust the LISP ZOM plane mass distribution based on actual hot test mass distribution results.

The first model would serve only to provide the designer with more information. It would not provide a quantitative estimate of the effect of RSS on injector performance.

The second model approach represents the most quantitatively accurate approach to RSS performance modeling. Testing would have to be performed that would result in measured hot fire mixed and separated mass distributions. LISP mass distribution coefficients would be developed to account for the influence of RSS. Such measurements have been performed for a gas/gas swirl coaxial element at ambient chamber pressure (Ref. 38). A double-walled, hot hydrogen cooled probe was used to withdraw the gas sample. The gas sample mass composition was measured by a mass spectrometer. Measured mixed and separated mass distribution coefficients could be correlated as a function of the injector design and operating point, to result in an experimentally verified model to be readily inserted into DER.

An additional RSS model approach exists that is adaptable to the JANNAF simplified performance prediction methodology, but not necessarily compatible with the DER program computational techniques. This model would

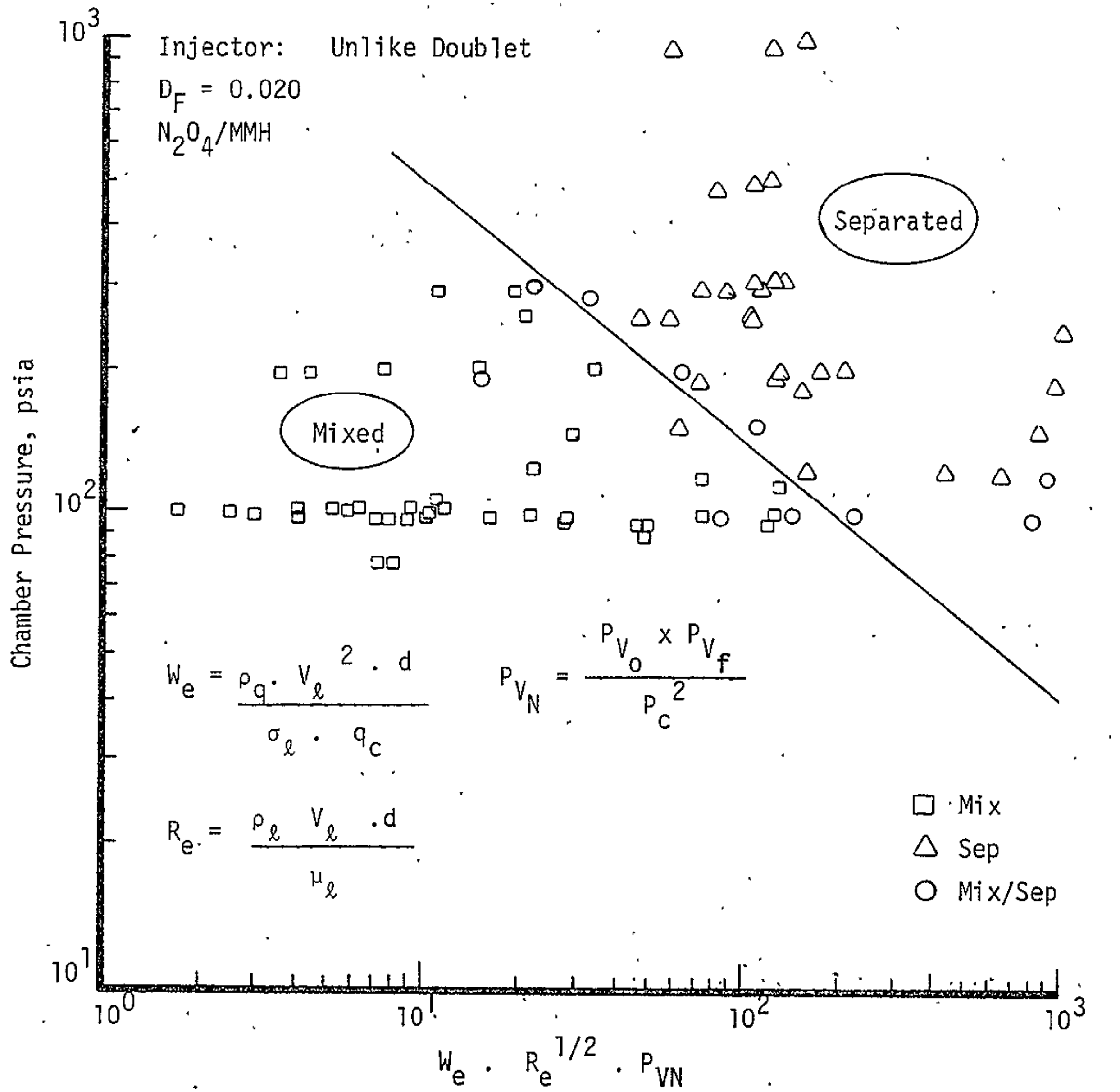

Figure A-18. Correlation of RSS Test Data predict the occurrence of RSS and adjust the performance prediction through an empirically based performance correlation technique. The model would require development of a correlation between a RSS prediction parameter (such as the abscissa of Figure A-18) and actual injector performance. A possible technique would be to relate mixed and separated mass and mixture ratio distributions through stream tube performance relationships.

6. Turbulent Mixing Model

The LISP cold flow mass distribution calculated at the ZOM plane should account for the influences of combustion gas acceleration and RSS, as previously suggested. Another significant omission in DER mass distribution modeling is the characterization of turbulent mixing effects on performance and chamber compatibility (remembering that DER is the computational base for the Injector/Chamber Compatibility (ICC) model). Turbulent mixing effects downstream of ZOM could range from minimal (for uniform patterns with a large number of injector elements) to substantial (coarse patterns or film cooled chambers). The DER streamtube modeling does not calculate any inter-streamtube mass exchange downstream of the ZOM plane. The characterization of turbulent mixing effects would provide a large step in the direction toward providing DER with the desired a priori prediction capability. The effect of streamtube mixture ratio changes due to turbulent mixing on propellant vaporization efficiency can be shown to be a second order influence for most chamber designs. Therefore, the turbulent mixing and vaporization calculations could be separated, resulting in a relatively simplified computational approach. Conversely, a simultaneous mixing with vaporization model would result in a more accurate solution with an inherent increase in programming complexity and computer run time.

Two test programs have been conducted that resulted in the development of semi-empirical models for the prediction of mixing limited injector performance. The programs investigated gas/gas intraelement (Ref. 11) and film cooling/injector core mixing (Ref. 38). The physically mechanistic analytical modeling developed on both programs is naturally extendible to the DER program.

O'Hara, et. al., (Ref. 39) have recently completed work that resulted in a quantification of the intensity of turbulence and Lagrangian correlation for turbulent mixing in rocket combustion chambers. The analysis was based on gas sample measurements taken from a oxygen/heptane 300 psia chamber pressure small rocket engine. It is concluded that the Lagrangian correlation could be used in rocket engine diffusion calculations. Another significant discovery of the work was that turbulence intensity was very high near the injector face due to the rapid rate of combustion and presence of liquid spray in this area.

7. Development of an A Priori DER Mixing Model

Two primary weaknesses in the DER ZOM plane mixing technique were determined during the DER review. (1) No methodology exists for calculating the correct ZOM plane value on an *a priori* basis, and (2) RSS and turbulent mixing effects can significantly alter the correct mass distribution for chamber throat plane mixing loss calculations.

Recent research indicates that RSS is a near-zone phenomenon. That is, combustion gas mass distribution is affected by RSS within an inch or two of the injector face plane. Combustion gas acceleration effects on spray distribution are also predominant in the near zone. (See Section V of this report). Conversely, turbulent mixing effects can extend to the chamber throat plane. For these reasons modeling of gas acceleration effects, RSS, and turbulent mixing can be easily adapted to the current DER computational methodology, as graphically suggested in Figure A-19.

New DER mixing methodology could be executed in the following three steps.

(1) ZOM is calculated with the gas acceleration effects model presented in Section V of this report. The ZOM mass distribution would be calculated based on empirical cold flow spray coefficients (identically to the current model).

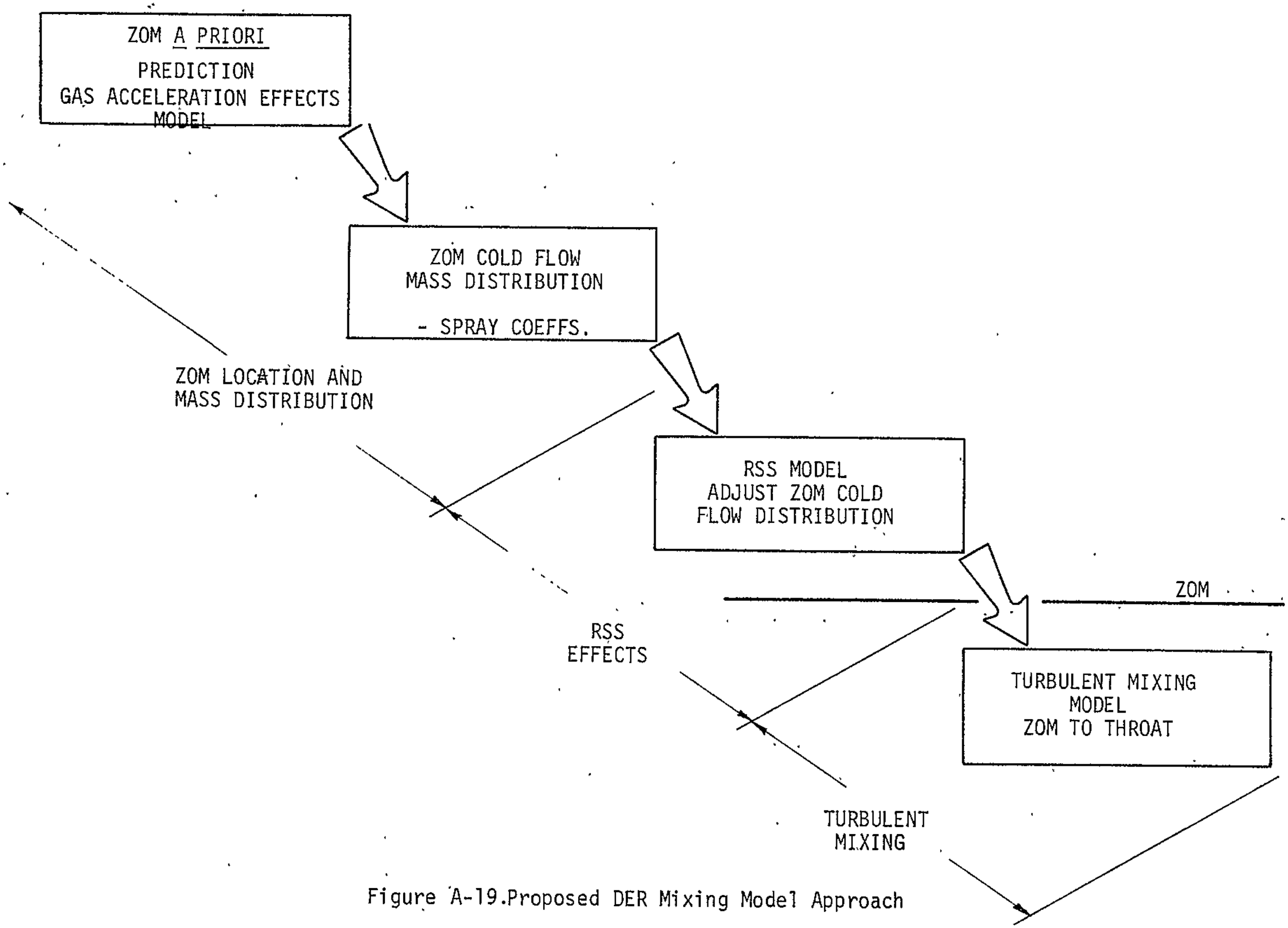

Figure A-19. Proposed DER Mixing Model Approach

(2) The ZOM cold flow distribution would be adjusted for RSS effects.

(3) The turbulent mixing model would adjust the new ZOM mass distribution in axial increments to the chamber throat plane.

D. Inconsistencies Between JANNAF Procedures and DER Computer Program Operations

The JANNAF Performance Prediction Procedures described in CPIA 246 were reviewed with regard to use of the DER computer program. The primary functional purpose of DER in the rigorous JANNAF procedure is to provide STC output which can be directly input to the Two Dimensional Kinetic (TDK) Reference Program (Ref. 5). TDK analyzes the supersonic nozzle expansion process in the JANNAF methodology. During Task II of this program the STC/TDK interface problem was to be objectively evaluated. Rescoping of Task II eliminated STC and TDK analyses that would have determined if the interface is easily accomplished.

Review of CPIA 246 indicated several inconsistencies between the JANNAF methodology and the results of the DER review. Each point is elaborated on to the extent that task scope allowed. It is hoped that the significant questions will be resolved with future DER review and applications work.

1. The DER Review results indicate that the intended predictive accuracy of the JANNAF rigorous procedure to within 1 percent for predicted specific impulse) is out of the question for <u>a priori</u> performance prediction. ZOM plane, mass median drop size, drop size distribution, droplet drag coefficient, and combustion effects on mixing considerations can each affect the prediction on the order of 1 percent.

2. Section 2.8.1 of CPIA 246 suggests that the DER subcritical K-Prime vaporization model is valid for chamber pressures 20 percent below propellant critical pressures in which the droplet heating time to the "wet bulb" temperature is negligible and combustion gas solubility is low. For other cases the DER supercritical version is recommended for use. The problem is that the

JANNAF methodology includes no formulation for predicting the significance of the droplet unsteady temperature state or gas solubility effects.

3. Section 2.8.3 of CPIA 246 recommends that the most physically realistic technique for selection of ZOM is to run LISP to a ZOM plane value at which the spray patterns from different elements start to overlap. It is almost impossible to recognize this point in a typical LISP output unless one possesses an intimate knowledge of the injector element spray characteristics. Also, this technique ignores interelement mixing effects on injector performance.

APPENDIX B

CICM COMPUTER MODEL REVIEW RESULTS

APPENDIX B

CICM COMPUTER MODEL REVIEW RESULTS

TABLE OF CONTENTS

This appendix details the results of the critical review of the JANNAF CICM computer model. Three subtasks were accomplished during the review. (1) Identification of Operational Problems Including a Code Review and Inclusion of Diagnostic Print-Out Statements, (2) Identification of Inadequate Formulations and Model Technical Shortcomings, (3) Review of the JANNAF Performance Prediction Procedure (CPIA 246) with Regard to the Use of CICM and Identification of Inconsistencies Between the Procedure and Program Operations. A complete summary of recommendations resulting from the CICM review is included in Section III.B. of this report.

A. Coding Errors and Diagnostic Statements

The review of the CICM computer code consisted of verification of the key model equations. The equations checked in the code were: (1) jet stripping rate, (2) mass median drop size, (3) droplet drag coefficient, (4) droplet drag force and acceleration, (5) droplet heating, and (6) droplet vaporization. These formulations were all coded correctly.

One possible code (or formulation) error was discovered during the review. Examination of the documented sample case output revealed that periodically, in the chamber vaporization calculation, drop size groups that should not have been completely vaporized are dropped from the calculation. As an example, refer to pages 117-122 of the Appendix C sample case output in the user's manual (Ref. 4). At the 0.75 inch axial station there are 22 drop size groups. At the 1.00 inch axial station the number 2 drop size group is missing, though the smaller drops in group number 1 still remain. At the 0.75 inch station the group 1 $\overline{D}$ was 75 microns and the group 2 $\overline{D}$ was 88 microns. It is physically incorrect that the group 2 drops would vaporize more quickly than group 1 drops. This error occurs again at the 1.250 axial station when the number 3 drop size group vanishes, but the group 1 still exist. The source of this computation error was not discovered during the review. It should be added that, for the following reason, this possible error was not expected to affect the CICM analysis of the M-1 engine reported in report Section IV. The drop size groups in question were consistently vaporized completely long before the chamber throat plane calculation station was reached.

B. Identification of Inadequate Formulations and Model Technical Shortcomings

The purpose of this subtask of the CICM review was to identify model technical problem areas and, if possible, to propose approaches for improvement. Incorporation of the improvements was, for the most part, beyond the scope of the program, but their identification provides a basis for future CICM work. The CICM user's manual states that the model controlling processes are: (1) the local stripping rate of the liquid jet, M_A, (2) the local mean drop size produced when M_A is stripped from the jet, $\overline{D}$, (3) the droplet heating and vaporization rates, (4) the assumed droplet drag coefficient formulation, and (5) for the chamber flow, the rate of mixing of the external "rigimesh" face flow. Careful review of the program input requirements and model analytical assumptions indicated that two additional important controlling CICM parameters should be defined, (6) the input specification of the intra-element fuel and oxidizer mass and mixture ratio distribution, and (7) the input specification of separate flow analysis zones to allow for manifold mass and mixture ratio maldistribution. The CICM program does not calculate mixing and requires that mass distribution input be user justified. Currently no standard guidelines exist in the CICM user's manual or the JANNAF Performance Prediction Manual (CPIA 246, Ref. 3) for measurement or input specification of these propellant mass distributions. The results of the CICM formulations review are presented below in seven sub-sections that deal with the model controlling processes defined above.

1. Jet Stripping Rate Correlation

The circular stripping rate correlation used by CICM is defined below.

$$M_A = C_A \left[\frac{\mu_j \, (\rho_g \, U_r^{\,2})^2}{\sigma_j/\rho_j} \right]^{1/3} \pi D_j \, (\Delta z) \qquad \text{(B-1)}$$

The CICM and JANNAF open literature does not include a derivation of the stripping rate correlation. A cursory examination of the literature on the atomization of liquid jets injected concurrently into gas streams yielded no directly applicable correlation for jet disintegration rate. The scope of the CICM review did not allow for a comprehensive literature review on liquid jet atomization. Qualitatively, the equation appears to be correctly formulated. As the jet to gas relative velocity increases the stripping rate increases due to aerodynamic drag. The stripping rate will also increase as the jet density, viscosity, and surface area ($\pi D_j \; \Delta z$) and the gas density increase. It is also correct that the stripping rate should decrease as the jet liquid surface tension increases. For the atomization constant (C_A) to be a universal constant the respective terms in the atomization equations must be raised to the correct power. Also, no physical variables that have a significant influence on the stripping rate can be omitted from the equation and still result in development of a universally applicable value of C_A. Variables that could possibly fall in this category are the absolute liquid jet velocity, the absolute gas stream velocity, and the gas stream viscosity.

The stripping rate equation calculates the time lag between jet initial contact with a concurrent gas stream and final jet disintegration. For a coaxial injector, the initial contact can occur in the recessed portion of the element cup or at the injector face plane. Typical gas/liquid coaxial injector designs require relatively long chamber lengths to reduce mixing and vaporization performance losses. Therefore, the atomization time lag is usually small compared to the total chamber residence time. As an example, the M-1 engine design analyzed during Task II has a conical chamber length (face plane to throat plane) of nearly 30 inches. Based on documented previous CICM runs it was expected that the element oxidizer jet would be completely atomized from 2 to 4 inches of the injector face. It was apparent that the drop sizes calculated to be shed from the oxidizer jet will have a far more significant effect on M-1 predicted engine performance than the rate of jet atomization.

2. <u>Mass Median Drop Size Correlation</u>

The mass median drop size correlation used by CICM is defined below.

$$\bar{D}_j = B_A \left[\frac{\mu_j \, (\sigma_j/\rho_j)^{1/2}}{\rho_g \, U_r^{\,2}} \right]^{2/3} \qquad \text{(B-2)}$$

Similarly to the jet stripping rate correlation described previously, the open literature does not include explanation of development of the CICM drop size correlation equution. However, a number of investigations are documented that concentrated on measurement of drop sizes generated from injection of liquid jets into non-accelerating concurrent gas streams. Table B-I summarizes the results of three of these investigations and compares their correlation results to the CICM equation. The table shows the power exponent correlated by each study for nine different independent variables. The Ingebo study (Ref. 13) developed the most mathematically stringent correlation by assuming that the measured maximum drop size was controlled by six non-dimensional parameters that characterized liquid hydraulics, gas dynamics, gas acceleration, and liquid hydrostatic and surface tension forces. The CICM correlation accounts for five of the nine variables modeled by Ingebo. The most significant CICM omission identified by Ingebo appears to be that the absolute gas velocity (not just the velocity differential) has a significant influence on the atomized drop size. Comparison of the exponents of the variables modeled by both Ingebo and CICM shows that the exponent sign agrees for all variables except the liquid jet viscosity. The Ingebo result is inconsistent with other atomization models that indicate drop size increases with increasing liquid viscosity. For example, Priem (Ref. 17) uses a propellant properties grouping that results in a liquid jet viscosity exponent of + 0.25. The other variable exponents shown agree in sign but consistently disagree on the absolute magnitude. It is apparent that the cited jet drop size equations differ because of the influence of measurement technique, measurement error, and the method of data correlation.

The CICM code was examined to determine the drop size distribution relationship used by CICM as an addition to the drop size equation review. During the DER review (Appendix A) it was shown that the assumed drop size distribution, about the mass median diameter, significantly influences the predicted total mass vaporization rate. Review of the CICM code indicated that subroutine ATOM calculates the portion of the liquid jet that is atomized over one axial computational increment. ATOM calculates a droplet spray group based on the total jet mass shed during the axial step. All the drops in the group are assigned an initial diameter equal to the mass median diameter calculated with the previously introduced drop size correlation equation. Thus,

TABLE B-I. COMPARISON OF LIQUID JET BREAKUP CORRELATIONS IN NONACCELERATING GAS STREAMS

Investigator	Characteristic Drop Diameter	Exponent for -								
		Orifice Diameter, D_o	Differential Velocity, U_r	Liquid-Jet Velocity, V_j	Gas Stream Velocity, V_g	Gas Stream Density ρ_g	Liquid-Jet Density, ρ_j	Gas Stream Viscosity, μ_g	Liquid-Jet Viscosity, μ_j	Surface Tension, σ_j
Ingebo (Ref. 13)	Maximum	0.08	-1.6	0.1	-0.5	-0.3	-0.76	0.5	-0.1	0.66
Weiss & Worsham (Ref. 26)	Mass-Median	.16	-1.33	.08	---	---	-.84	.09	.34	.41
Nukiyama Tanasawa (Ref. 28)	Sauter	---	-1.0	---	---	---	-.5	---	---	.5
Sutton (CICM)	Mass-Median	---	-1.33	---	---	-.67	-.33	---	.67	.33

in reality, CICM does not calculate a real droplet size distribution. CICM assumes that all the mass shed during a finite time period, defined by the axial step distance, is shed with a constant diameter defined by the $\overline{D}$ equation. The influence of this calculational assumption on the total liquid vaporization rate can not be estimated simply. It is apparent, though, that the drop size distribution tabulated at the end of a CICM run is only the summation of several constant mass median diameter groups, each group being calculated over a particular axial step. This resultant distribution is quite different than a drop size group calculated with distributions typically used to model rocket combustor sprays.

3. Droplet Heating and Vaporization Rate Formulations

CICM contains an advanced droplet heat-up and vaporization model that is described in detail in the program user's manual. The CICM formulation is far superior to the DER K-Prime model in that the droplet temperature transient and continuous vaporization through subcritical and supercritical propellant states are allowed for. The CICM/STC interface procedure review reported in Section C.2 of this appendix resulted in a recommendation that, in the JANNAF performance prediction methodology, CICM should compute to the chamber plane at which all the calculated drop size groups have reached the chamber "wet bulb" temperature. For oxygen this temperature transient typically takes place over a time period equal to about 10 percent of the total time required to vaporize 99 percent of the propellant (Ref. 17). After CICM has calculated the transient the STC program calculates droplet steady state burning from the interface plane to the chamber throat plane. Therefore, STC is responsible for calculating droplet vaporization rates over approximately 90 percent of the total droplet chamber residence time.

The two most important functions of CICM in the JANNAF methodology, based on the information in the previous paragraph, are to; (1) calculate liquid drop sizes resulting from aerodynamic stripping of the liquid jet; the bulk of which will be vaporized in STC, and (2) calculate the droplet temperature time transients. The CICM drop size correlation was discussed in the previous sub-section. The CICM droplet heat-up formulations were checked by comparing, for reference, CICM calculated heating rates for oxygen to heat-up rates calculated in Ref. 17. The results of the comparison are shown in Figure B-1. Initially, heat-up rates were compared, as a function of

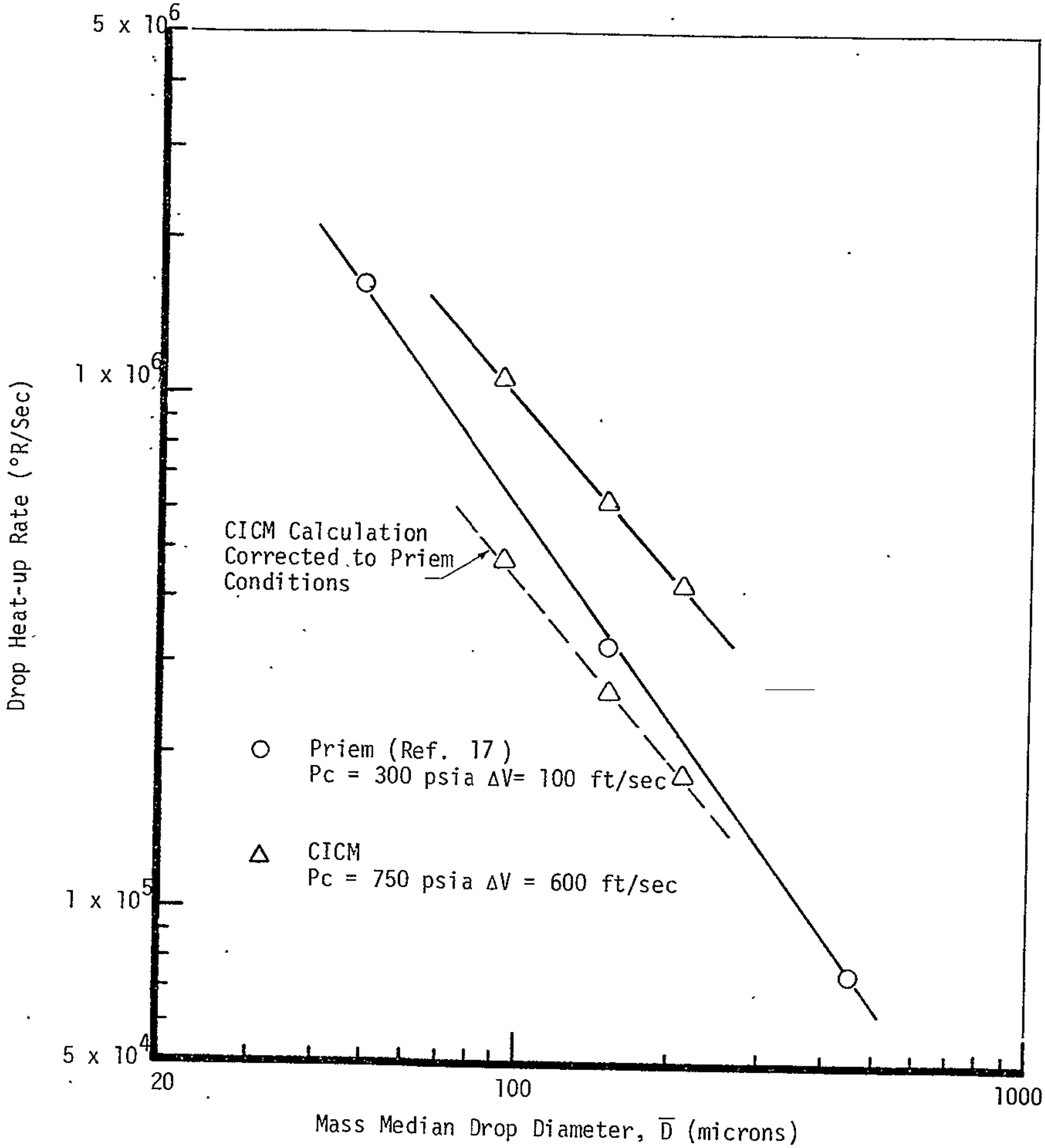

FIGURE B-1. COMPARISON OF OXYGEN HEATING RATE CALCULATIONS mass median drop diameter, for the solid line conditions shown in the figure. The agreement between the two models improved when chamber pressure and velocity differential effects on the local drop heat transfer rate were accounted for in the CICM calculation. Since no attempt was made to ensure that both model predictions were made with exactly the same gas and liquid properties the agreement can be considered to be excellent. The results of the droplet heating rate comparison verify the CICM droplet heat-up model.

4. Droplet Drag Coefficient Correlation

CICM employs the droplet drag correlation equations developed by Rabin (Ref. 31).

$$C_d = 27\ Re_D^{-0.84} \qquad Re_D < 80 \tag{B-3}$$

$$C_d = 0.271\ Re_D^{.217} \qquad 80 \leq Re_D \leq 10^4 \tag{B-4}$$

$$C_d = 2 \qquad Re_D > 10^4 \tag{B-5}$$

The influence of the assumed droplet drag correlation on the vaporization rate was examined during the DER review. This investigation indicated that the droplet drag correlation significantly affects the final performance prediction made by STC. The review recommended that the Rabin drag coefficient correlation be reviewed and compared to other available correlations.

5. Chamber Mixing of Face "Rigimesh" Flow

The CICM program calculates mixing of any face rigimesh flow by assuming the rate of mixing to be a linear function between the face and an input downstream distance. The mixed flow is spread uniformly over the cross-sectional area of the element flow field and becomes part of the propellant (usually fuel) to be reacted. The CICM user's manual states that calculations have been performed for rigimesh mixing that indicate that rapid acceleration reduces the rigimesh flow area to only approximately 3 percent of its injection area. This rarefaction occurs on the order of only 2 inches from the injector face plane. The rigimesh area reduces to an annulus trapped between coaxial element flows; the average thickness of the annulus was calculated to typically be on the order of .01 inch. It is therefore argued that turbulence sweeps the flow into adjacent element flow fields. This calculational technique would seem to be satisfactory for ordinary amounts of rigimesh flow (on the order of five percent of the total fuel flow) because the axial variation of the expansion area of the combusting flow field of adjacent elements will not be affected significantly. As an example of a typical case in point, the M-1 injector design analyzed during Task II of the program has 3 percent of the total hydrogen fuel flowing through the rigimesh portion of the injector face.

6. Intra-Element Mass Distribution Specification

CICM allows for the effect of intra-element mass and mixture ratio distribution through user input specification. For each zone (i.e., single element) analyzed by CICM, the user is instructed to input radial zonal oxidizer and fuel mass fractions based on single element cold flow data. An example of such input is shown in Figure B-2 , taken from the CICM J-2S sample case in CPIA 246. There are several problems associated with accounting for intra-element mass non-uniformities in this manner.

(1) There is no available standard technique for measuring single element cold flow gas/liquid coaxial mass distribution.

(2) The JANNAF methodology does not specify the axial plane (i.e., collection plane) at which the intra-element mass distribution should be specified. Face plane measurements are most easily accomplished but will be significantly altered by the high ΔV shear mixing inherent to coaxial element designs.

(3) The test cases used to back out the recommended atomization and drop size input constants to CICM assumed that the thrust chamber in question had uniform throat plane mixtue ratio distributions. For

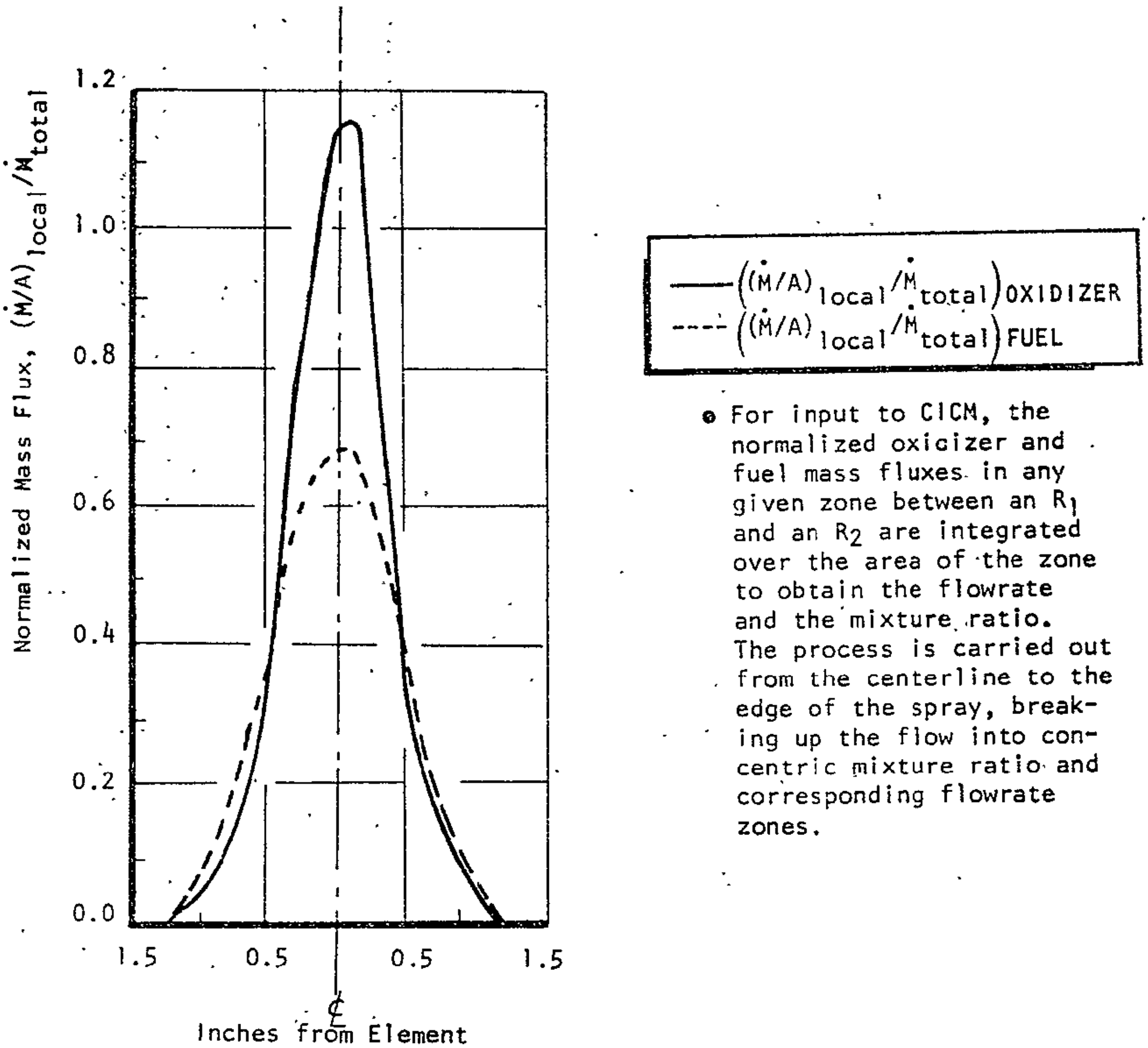

- For input to CICM, the normalized oxidizer and fuel mass fluxes in any given zone between an R_1 and an R_2 are integrated over the area of the zone to obtain the flowrate and the mixture ratio. The process is carried out from the centerline to the edge of the spray, breaking up the flow into concentric mixture ratio and corresponding flowrate zones.

FIGURE B-2. COAXIAL ELEMENT COLD-FLOW SPRAY MASS FLUX DISTRIBUTION most real coaxial injectors there will be a finite mixing loss because the coaxial element is a relatively slow mixing element. It is apparent that the correct values for the C_A and B_A coefficients will be directly dependent on the assumed single element mixture ratio distribution. Unless a standard method for measuring or calculating single element mixture ratio distributions is developed it is extremely doubtful that universal values for the C_A and B_A constants can be verified.

(4) Similarly to the DER program for liquid/liquid injectors, CICM does not allow for the influence of combustion on the single element mass and mixture ratio distribution.

Currently, it appears that, without a standard coaxial element mixing model or approach, standardization of the parameters that influence the propellant vaporization rate will be difficult. That is, two processes affect coaxial injector performance (mixing and vaporization) and each process must be physically modeled to a comparable degree to result in a model that can calculate an accurate superimposed solution. At this stage CICM has been verified for engines that apparently have only one effective performance loss mechanism, i.e., incomplete propellant mass vaporization.

7. Manifold Mass Distribution Zone Specification

The CICM user's manual recommends that measured or calculated manifold mass maldistributions should be accounted for by modeling separate chamber flow field zones when executing the program. Since the manifold distribution is usually calculated at the injector face plane, this technique assumes that the mass maldistribution will persist to the chamber throat plane. The manifold mass maldistribution performance loss is inevitably overpredicted with this technique, since turbulent mixing is ignored. Also, there is no recommended methodology for dividing the measured distribution into analysis zones. Therefore, the method of zone mass fraction assignment also becomes an user controlled input that affects the final performance prediction.

The solution of this problem is more complicated than the intra-element mixing problem discussed in the previous sub-section. It would be difficult to generalize a chamber zonal mixing model. Measurement of performance for thrust chamber assemblies having negligible vaporization and intra-element mixing losses would seem to provide a reasonable approach for solution of this problem. That is, if the engine vaporization and single element mixing losses are small (or can be accurately calculated) the manifold induced maldistribution loss can be backed out from the performance data.

C. Inconsistencies Between JANNAF Procedures and Program Operations

1. Background

CICM was developed as a rigorous analytical model that describes the atomization, vaporization and combustion of gas/liquid coaxial jets in a rocket engine environment. In the context of the JANNAF series of performance prediction models, CICM is intended to replace the LISP subprogram of DER for gas/liquid coaxial elements.

CICM is a highly specialized program intended to be used for one specific injector design concept. Additionally, the model has only been applied, to this date, to coaxial injectors using a central liquid O_2 circular core surrounded by a gaseous H_2 or H_2/O_2 combustion gas mixture annulus. The program input requires an extensive group of propellant property cards (644 cards for the CICM user's manual sample case) that will have to be generated for each propellant combination analyzed in the future. Another factor that currently limits the generality of CICM in the JANNAF methodology is that key empirical atomization rate and drop size constants, that control program performance predictions, have only been determined from test data for the LO_2/GH_2 propellant combination. Detailed discussion on these program inputs is included in Section B of this appendix. The CICM analysis documented in Section IV of this report was also restricted to a LO_2/GH_2 injector. Therefore, there are no current plans for testing the ability of CICM to model gas/liquid coaxial designs using other propellant combinations.

During this phase of the review task CICM was critiqued for its ability to function as documented in the JANNAF rigorous performance prediction procedure described in CPIA 246. The evaluation emphasized two areas; (1) test and evaluation of the CICM/STC interface procedure by running the CICM sample case and subsequently using the CICM input to generate an input deck for STC, and (2) development of a criteria for specifying the chamber axial location of the CICM/STC interface plane.

2. Evaluation of the CICM/STC Interface Procedure

The CICM/STC interface procedure was examined carefully to ensure that the JANNAF performance prediction methodology accuracy and utilization time is not being compromised by the currently recommended interface technique. It was determined that the CICM interface routine DERINI was incomplete and punched improperly formated cards for input to the STC subcritical K-Prime version. The CICM user's manual states that DERINI punches input for the supercritical version of the DER program. No check was made to see if the punched output was compatible with the input requirements of that DER version. The next section of this appendix completely details the interface evaluation and development of a new interface procedure. This new DERINI version was successfully utilized during the program Task II CICM analysis effort.

3. Description of Improved CICM/STC Interface Procedure

The JANNAF Performance Prediction Manual (CPIA 246) specifies that CICM will replace the LISP model for the analysis of gas/liquid coaxial elements. In this function, CICM must be capable of calculating spray formation, vaporization,and gaseous combustion and of generating output which is consistent with STC input and operational requirements.

The CICM/STC interface procedure was critically evaluated during the CICM review task of the Injection Processes Program. The CICM sample case documented in the user's manual was executed to determine if an interface with the STC program could be easily accomplished. The documented CICM sample case considers two injector zones (elements) which are each divided into two intra-element mixture ratio zones through input mass fraction distributions. This input specification results in four separate sets (2 interelement zones x 2 intraelement zones) of streamtube input for the STC subprogram of DER. The DER user's manual was then used to determine that this four streamtube case required an input deck consisting of eight-six separate cards. The CICM interface subroutine (DERINI) was designed to punch only the streamtube flowrate and drop size input cards required by STC (cards 6720, 7010-7016, 7020-7026, 7030-7036, and 7040-7046 for this case). These cards comprised twenty-nine of the eighty-six cards required to correctly interface the CICM output and the DER input. Also, the cards punched to designate the streamtube and drop size group droplet flowrates (GWSPR (I, J)), velocities (VELD1 (I, J)), and diameters (GDIAD1 (I, J)) were improperly formated to be input to STC. The format error occurred because the interface subroutine DERINI also punched droplet temperatures for each streamtube and drop size group, while STC (in the subcritical DER K' version) does not require or allow for this input.

This attempt to join the CICM sample case output with the subcritical STC program indicated that the interface procedure required improvement. The six improvements that were grouped to result in the new interface procedure are detailed below.

(1) The streamtube and droplet size group input cards were properly formated and labeled with their correct sequence numbers, as indicated in the DER user's manual.

(2) A number of STC inputs that have constant values when LISP execution does not precede STC execution (e.g., when CICM interfaces with STC) were assigned values in the CICM interface routine DERINI and included in the STC input cards to be punched.

(3) All STC inputs that are also input or internally calculated in CICM (e.g., combustion gas transport properties as a function of mixture ratio) were included in the DERINI output deck for input to STC.

(4) STC inputs that could not be specified as constants and are not set by CICM input or calculation were grouped into a new namelist input set for DERINI.

(5) Coding was included in DERINI to result in each STC input card having its correct sequence number, as specified in the DER user's manual, punched in columns 73-80.

(6) An option was included in the new DERINI namelist input group to allow for writing the DERINI formulated STC input deck on a computer system drum file (or stratch tape) without having to punch an actual card deck.

The listed improvements resulted in an interface technique, completely internal to CICM, that allows generation of all required STC input. The new CICM/STC interface procedure is detailed in the following three paragraphs that include in turn; (1) a listing of the new CICM interface routine DERIN and specification of required line changes and additions to generate the new routine from the old verison, (2) a description of the required namelist input for DERINI, and (3) a description of the STC input deck generated with the new procedure for the CICM sample case documented in the program user's manual.

A compilation of the new version of the CICM subroutine DERINI, designed to provide punched card or mass storage file input to the DER subprogram STC, is shown in Table B-II. The line modifications that were applied to the original version of DERINI are detailed in Table V-III. No other changes are required to any CICM routine to develop the new interface procedure.

The required namelist input variables for DERINI are defined in Table B-IV. The DERINI namelist variable inputs must be preceded by a $\not{S}$STC specification and followed by a $\not{S}$END specification (or the system equivalent to these Univac 1108 Exec-8 designations). The first three variables listed in the table designate forms by which the STC input data may be output from DERINI. Any combination of these three output forms may be specified. The remaining input variables listed are identical to descriptions given in the DER user's manual. The oxidizer latent heat input, DHVO, should be consistent with the droplet "wet bulb" temperature calculated by CICM at the interface plane axial chamber location. Any STC variables not listed are either input to, internally set within, or calculated by CICM. Liquid fuel properties are not included in the namelist because CICM requires that one propellant be gaseous and one liquid. The namelist input set used to check the new interface technique for the CICM sample case is shown in Table B-V.

The STC input generated by DERINI for the CICM sample case is listed in Table B-VI. The STC program was successfully executed with the data set shown.

TABLE B-II MODIFIED CICM/STC INTERFACE SUBROUTINE (DERINI)

```
@FOR,S DERINI
FORTRAN V, IBD VERSION 4,68-02/26/76-08:52:12 (6,)

   SUBROUTINE DERINI    ENTRY POINT 002334

   STORAGE USED: CODE(1) 002370; DATA(0) 006755; BLANK COMMON(2) 000000

    COMMON BLOCKS:

    0003    TCPLF   001514
    0004    PROP1   000013
    0005    CGTABC  000135
    0006    CHCOM   000072

   EXTERNAL REFERENCES (BLOCK, NAME)

    0007    LOCFAC
    0010    XVDHV
    0011    EQSTAT
    0012    CGPROP
    0013    RHOGF
    0014    NRDU$
    0015    NIO1$
    0016    NIO2$
    0017    SQRT
    0020    NRNL$
    0021    XPRR
    0022    NWDU$
    0023    NERR3$

   STORAGE ASSIGNMENT  (BLOCK, TYPE, RELATIVE LOCATION, NAME)

    0000    006503 1F        0001    000003 10L       0001    002224 1057G     0001    002244 1071G     0000    006545 11F
    0001    002273 1100G     0001    001330 12L       0001    000270 120L      0001    001334 13L       0001    001340 14L
    0001    000307 140L      0001    000027 145G      0001    001343 15L       0001    000042 154G      0001    001316 16L
    0001    000312 160L      0001    000066 166G      0000    006550 17F       0000    006551 18F       0000    006506 2F
    0001    000466 200L      0001    000523 210L      0001    000160 217G      0001    000170 224G      0001    000227 241G
    0001    000246 247G      0001    000272 261G      0001    000327 276G      0000    006511 3F        0001    000647 300L
    0001    000346 307G      0001    000537 340G      0001    000653 355G      0001    000674 362G      0000    006514 4F
    0001    001054 414G      0001    001100 426G      0001    001273 472G      0000    006516 5F        0001    001404 556G
    0001    001441 563G      0001    001461 576G      0000    006520 6F        0001    001067 610L      0001    001512 620G
    0001    001073 620L      0001    001257 640L      0001    001574 660G      0001    001624 670G      0001    001650 677G
    0000    006522 7F        0001    001267 700L      0001    001712 715G      0001    001721 720G      0001    001751 727G
    0001    002004 741G      0001    002013 744G      0001    002043 753G      0000    006532 8F        0000    006534 9F
    0000    006651 9000F     0001    002310 9999L     0006 R  000046 ACHAMC    0006    000014 ACSC      0000 R  004110 AGO
    0005    000002 AMRT      0000 R  004350 AREA1     0000 R  006424 AHK       0000 R  006353 ARTOLD    0000 R  006425 BRK
    0006    000012 BSPRC     0000 R  006442 C         0006    000017 CCANGC    0006    000015 CLNTC     0006    000016 CONRAC
    0000 R  006255 CPVO      0000 R  006352 CRTOL     0006    000013 CSPRC     0000 R  006203 CSTR      0004    000011 CXOV
    0006    000011 DELTXC    0000 R  006423 DHV       0000 R  006470 DHVF      0000 R  006357 DHVO      0000 R  005107 DOD
    0000 R  006430 DRLDT     0000 R  006431 DWS       0000 R  006372 EMRCG     0006    000004 EMRGJC    0000 R  006432 EMRI
    0000 R  004160 EMW       0000 R  006377 EMWCG     0006    000006 EMWGJC    0004 R  000004 EMWL      0004    000012 EMWPR
    0004 R  000006 EMWV      0000 R  006443 FA        0000 R  006400 FCHA      0000 R  006362 FCHAM     0000 R  004610 FFMIX
    0000 R  006417 FN        0000 R  004660 FUMIX     0000 R  004730 FSDER     0000 R  006406 F1        0000 R  003770 GAM
```

```
0006     000007 GAMGJC    0000 R 000000 GASFL     0000 R 001060 GDIAD1    0000 R 005607 GMR       0000 R 006413 G8W8
0000 R 005763 GTK       0000 R 002020 GTOD1     0000 R 002760 GVELD1    0000 R 000120 GWSPR     0000 R 006421 HD
0000 I 006365 I         0000 I 006440 IC        0000 I 006472 ICARD     0000 I 006347 ICRC      0000 I 006355 IDRUM
0000 I 006450 IFILE     0000 I 006410 II        0000 I 006420 IJ        0000 I 006451 ILISP     0000   006715 INJP$
0000 I 006351 IPRMST    0000 I 006350 IPRSST    0000 I 006356 IPUNCH    0000 I 006467 IPUN3D    0000 I 006455 IST
0000 I 006452 ISTC      0000 I 006454 ITDK      0000 I 006453 ITRANS    0000 I 006354 IWRITE    0000 I 006405 I1
0000 I 006360 J         0000 I 006407 JJ        0000 I 006412 JJJ       0000 I 006335 JK1       0000 I 006336 JSPC
0000 I 006411 K         0000 I 006500 L         0000 I 006475 M         0006     000001 M2C       0000 I 006476 N
0000 I 006447 NASEG     0000 I 006474 NC        0006 I 000000 NCHAMC    0006     000002 NCON4C    0000 I 006361 NDER
0000 I 006366 NOSC      0000 I 006367 NELEM     0000 I 006446 NGF       0000 I 006364 NGO       0000 I 006444 NGT
0000 I 006363 NMIXZ     0000 I 006346 NMSTI     0000 I 006464 NOZUN     0000 I 006344 NP        0003 I 001512 NPCP
0000 I 006345 NSSTI     0000 I 006445 NST       0000 I 006465 NSTPZ     0005 I 000000 NTAB      0003 I 001510 NTCP
0000 I 006337 NTK       0000 I 006466 NUG       0000 R 003720 P         0000 R 006370 PC        0000 R 006441 PCI
0004     000000 PCRIT     0000 R 006436 PHIGH     0000 R 006437 PLOW      0000 R 004230 PUS       0006     000020 RCBCC
0006     000021 RCTC      0000 R 006427 RG        0000 R 006426 RHOD      0000 R 004540 RHOG      0013 R 000000 RHOGF
0000 R 006461 RHOLF     0000 R 006343 RHOLO     0000 R 006460 RHONBF    0000 R 006342 RHONBO    0000 R 000050 SMRG
0000     006553 STC       0006     000005 STGJC     0004     000010 STOCMR    0005     000001 STT       0000 R 006414 SUM1
0000 R 006415 SUM2      0000 R 006416 SUM3      0000 R 006373 SWSPR     0000 R 006456 TBF       0000 R 006341 TBO
0000 R 006305 TCONVO    0003     000050 TCP       0004 R 000002 TCRIT     0005 R 000047 TGAM      0000 R 004470 TGAS
0000 R 005563 THL       0003 R 000670 THOL      0000 R 006376 TLI       0005 R 000003 TMR       0005 R 000071 TMW
0000 R 006457 TNBF      0000 R 006340 TNBO      0000 R 004040 TO        0000 R 005253 TOD       0003 R 000024 TPCPL
0003 R 000000 TTCPL     0005 R 000025 TTO       0005 R 000113 TVIS      0000 R 006225 TVO       0000 R 006374 VCG
0000 R 004420 VGAS      0000 R 006433 VISC      0000 R 006375 VLJI      0000 R 005417 VOD       0000 R 004300 VUS
0000 R 006371 WCG       0000 R 006403 WFE       0006     000003 WGJC      0000 R 006402 WUXE      0000 R 006404 WSPE
0000 R 004743 WSPR      0000 R 006435 WT        0000 R 006401 WTE       0000 R 006462 WTMLLF    0000 R 006463 WTMLVF
0006 R 000022 XCHAMC    0006     000010 XLMC      0000 R 006473 XNAP      0000 R 006502 XNGT      0000 R 006477 XNMR
0000 R 006501 XNTK      0000 R 006434 XOV       0000 R 006422 XV        0000 R 006471 ZSTART


00101          SUBROUTINE  DERINI(IDER,ACHAM,XMINDE,IRDER)                           00000010
00103          DIMENSION  GASFL(40), SMRG(40), GWSPR(12,40), GDIAD1(12,40),          00000020
00103         1     GTOD1(12,40), GVELD1(12,40), P(40), GAM(40), TO(40),             00000030
00103         2     AGO(40), EMW(40), PUS(40), VUS(40), AREA1(40), VGAS(40),         00000040
00103         3     TGAS(40), RHOG(40)                                               00000050
00104          DIMENSION  FFMIX(40), FOMIX(40), FSDER(11)                            00000060
00105          DIMENSION  WSPR(100), DOD(100), TOD(100), VOD(100), THL(20)          00000070
00106          DIMENSION GMR(6,18),GTK(6,24),CSTR(18),TVO(24),CPVO(24),TCONVO(24)
00107          COMMON  /TCPLF/  TTCPL(20,1), TPCPL(20,1), TCP(20,20,1),             00000080
00107         1     THOL(20,20,1), NTCP(2), NPCP(2)                                  00000090
00110          COMMON  /PROP1/  PCRIT(2), TCRIT(2), EMWL(2), EMWV(2),                00000100
00110         1     STOCMR, CXOV, EMWPR                                               00000110
00111          COMMON/CGTABC/NTAB,STT,AMRT,TMR(18),TTO(18),TGAM(18),TMW(18),
00111         *            TVIS(18)
00112          COMMON/CHCOM/NCHAMC,M2C,NCON4C,WGJC,EMRGJC,STGJC,EMWGJC,GAMGJC,
00112         *            XLMC,DELTXC,BSPRC,CSPRC,ACSC,CLNTC,CONRAC,CCANGC,
00112         *            RCBCC,RCTC,XCHAMC(20),ACHAMC(20)
00113
00113          DATA  JK1,JSPC/0,1/                                                   00000120
00116        1 FORMAT(4I12,24X,I8)
00117        2 FORMAT(3E12,6,36X,I8)
00120        3 FORMAT(4E12,6,24X,I8)
00121        4 FORMAT(12I6,I8)
00122        5 FORMAT(6E12,6,I8)
00123        6 FORMAT(6I12,I8)
00124        7 FORMAT(6X,'STC INPUT FROM CICM PROGRAM CASE',T73,I8)
```

```
00125          8 FORMAT(72X,I8)
00126          9 FORMAT(6X,'O2/H2 GAS PROPERTIES FROM CICM INPUT',T77,I8)
00127         11 FORMAT(2E12.6,48X,I8)
00130         17 FORMAT(12I6)
00131         18 FORMAT(6E12.6)
00132            NAMELIST/STC/TVO,TCONVO,NTK,TNBO,TBO,RHONBO,RHOLO,NP,NSSTT,NMSTT,
00132           *             ICRC,IPRSST,IPRMST,CRTOL,ARTOLD,IWRITE,IDRUM,IPUNCH,
00132           *             CPVO,DHVO
00133            CSTAR(XMW,TO,GAM)=SQRT(49677.*GAM*TO/XMW/((2./(GAM+1.))**((GAM+1.)
00133           */(GAM-1.))))/GAM
00134            J = 0                                                          00000190
00135            NDER = 0                                                       00000200
00136            FCHAM = 0.0                                                    00000220
00137         10 READ(IRDER,17) NMIXZ,NGO                                                  000003
00143            READ(IRDER,18) (FFMIX(I),FOMIX(I),I=1,NMIXZ)                              000014
00152            READ(IRDER,18) (FSDER(I),I=1,NGO)                                         000033
00160            READ(IRDER,17) NDSC,NELEM                                                 000045
00164            READ(IRDER,18) (WSPR(I),DOD(I),TOD(I),VOD(I),I=1,100)                     000054
00175            READ(IRDER,18) PC,WCG,EMRCG,SWSPR,VCG,VLJI,TLI,EMWCG,FCHA                 000074
00210            WTE = (SWSPR+WCG)*NELEM                                        00000310   000112
00211            WOXE = (SWSPR+WCG*EMRCG/(1.+EMRCG))*NELEM                      00000320   000116
00212            WFE = WTE-WOXE                                                 00000330   000126
00213            WSPE = SWSPR*NELEM                                             00000340   000130
00214            CALL LOCFAC(JK1,PC,TPCPL,NPCP(1),I1,F1)                        00000350   000133
00215            NP = NTCP(1)                                                   00000360   000143
00216            DO 20 I=1,NP                                                   00000370   000151
00221         20 THL(I) = THOL(I1,I,1)+F1*(THOL(I1+1,I,1)-THOL(I1,I,1))         00000380   000160
00223            DO 100 JJ=1,NMIXZ                                              00000390   000170
00226            I = J+JJ                                                       00000400   000174
00227            GASFL(I) = FFMIX(JJ)*WFE+FOMIX(JJ)*(WOXE-WSPE)                 00000410   000177
00230            SMRG(I) = FOMIX(JJ)*(WOXE-WSPE)/(FFMIX(JJ)*WFE)                00000420   000203
00231            GWSPR(1,I) = 0.0                                               00000430   000205
00232            GDIAD1(1,I) = 0.0                                              00000440   000210
00233            GTOD1(1,I) = 100.0                                             00000450   000211
00234        100 GVELD1(1,I) = 100.0                                                       000213
00236            IF(NGO.LT.NDSC) GO TO 160                                      00000490   000216
00240            DO 140 II=1,NGO                                                00000500   000222
00243            I = II+1                                                       00000510   000234
00244            IF(II.GT.NDSC) GO TO 120                                       00000520   000237
00246            DO 110 K=1,NMIXZ                                               00000530   000246
00251            JJ = J+K                                                       00000540   000246
00252            GWSPR(I,JJ) = WSPR(II)*NELEM*FOMIX(K)                          00000550   000251
00253            GDIAD1(I,JJ) = DOD(II)                                         00000560   000256
00254            GTOD1(I,JJ) = TOD(II)                                          00000570   000260
00255        110 GVELD1(I,JJ) = VOD(II)                                                    000262
00257            GO TO 140                                                      00000600   000266
00260        120 DO 130 K = 1,NMIXZ                                                        000272
00263            JJ = J+K                                                       00000630   000272
00264            GWSPR(I,JJ) = 0.0                                              00000640   000277
00265            GDIAD1(I,JJ) = 0.0                                             00000650   000300
00266            GTOD1(I,JJ) = 100.0                                            00000660   000301
00267        130 GVELD1(I,JJ) = 100.0                                                      000303
00271        140 CONTINUE                                                       00000690   000310
00273            GO TO 300                                                      00000700   000310
00274        160 JJJ = 1                                                        00000720   000312
00275            DO 230 II=1,NGO                                                00000730   000313
00300            I = II+1                                                       00000740   000332
```

```
00301              GSWS = 0.0                                                        00000750   000335
00302              SUM1 = 0.0                                                        00000760   000336
00303              SUM2 = 0.0                                                        00000770   000337
00304              SUM3 = 0.0                                                        00000780   000340
00305              FN = FSDER(II)                                                    00000790   000341
00306              DU 170 IJ=JJJ,NDSC                                                00000800   000346
00311              JJ = IJ                                                           00000810   000346
00312              CALL LUCFAC(JK1,TOD(IJ),TTCPL,NTCP(1),I1,F1)                      00000820   000350
00313              HD = THL(I1)+F1*(THL(I1+1)-THL(I1))                               00000830   000362
00314              CALL XVDHV(XV,DHV,ARK,BRK,PC,TOD(IJ),JSPC)                        00000840   000370
00315              CALL EQSTAT(RHOD,RG,DRLDT,PC,TOD(IJ),XV,EMWL(JSPC),EMWCG,         00000850   000403
00315             1     ARK,BRK,JSPC)                                                00000860   000403
00316              IF(WSPR(IJ).GT.FN*SWSPR) GO TO 200                                00000870   000425
00320              GSWS = GSWS+WSPR(IJ)                                              00000880   000432
00321              SUM1 = SUM1 + WSPR(IJ)*VOD(IJ)                                    00000890   000435
00322              SUM2 = SUM2 + WSPR(IJ)*HD                                         00000900   000441
00323              SUM3 = SUM3 + WSPR(IJ)/(VOD(IJ)**2*RHOD*DOD(IJ)**2)               00000910   000445
00324         170  FN = FSDER(II) - GSWS/SWSPR                                                  000457
00326              GO TO 210                                                         00000940   000464
00327          200 DWS = FN*SWSPR                                                    00000950   000466
00330              GSWS = GSWS+DWS                                                   00000960   000470
00331              JJJ = JJ                                                          00000970   000472
00332              WSPR(JJ) = WSPR(JJ)-DWS                                           00000980   000474
00333              SUM1 = SUM1 + DWS*VOD(JJ)                                         00000990   000500
00334              SUM2 = SUM2 + DWS*HD                                              00001000   000504
00335              SUM3 = SUM3 + DWS/(VOD(JJ)**2*RHOD*DOD(JJ)**2)                    00001010   000510
00336         210  SUM2 = SUM2/GSWS                                                             000523
00337              DO 230 K = 1,NMIXZ                                                           000525
00342              JJ = J+K                                                          00001050   000537
00343              GWSPR(I,JJ) = SWSPR*FSDER(II)*NELEM*FOMIX(K)                      00001060   000542
00344              GVELD1(I,JJ) = SUM1/GSWS                                          00001070   000547
00345              CALL LUCFAC(JK1,SUM2,THL,NTCP(1),I1,F1)                           00001080   000551
00346              GTOD1(I,JJ) = TTCPL(I1,1)+F1*(TTCPL(I1+1,1)-TTCPL(I1,1))          00001090   000563
00347              CALL XVDHV(XV,DHV,ARK,BRK,PC,GTOD1(I,JJ),JSPC)                    00001100   000571
00350              CALL EQSTAT(RHOD,RG,DRLDT,PC,GTUD1(I,JJ),XV,EMWL(JSPC),           00001110   000604
00350             1     EMWCG,ARK,BRK,JSPC)                                          00001120   000604
00351         230  GDIAD1(I,JJ) = SQRT(GSWS/(GVELD1(I,JJ)**2*RHOD*SUM3))                        000626
00354         300  DU 500 K = 1,NMIXZ                                                           000647
00357              JJ = J+K                                                          00001200   000656
00360              GSWS = 0.0                                                        00001210   000666
00361              DO 400 I=1,NGO                                                    00001220   000674
00364          400 GSWS = GSWS+GWSPR(I,JJ)                                           00001230   000674
00366              P(JJ) = PC                                                        00001240   000677
00367              EMRI = SMRG(JJ)                                                   00001242   000701
00370              CALL CGPROP(SMRG(JJ),TO(JJ),EMW(JJ),GAM(JJ),VISC,GASFL(JJ),       00001250   000703
00370             1     0.0,0,XOV,EMRI,PC,NGO,VLJI,GTOD1(1,JJ),GVELD1(1,JJ),         00001260   000703
00370             2     GWSPR(1,JJ),GSWS,TLI)                                        00001270   000703
00371              AREA1(JJ) = FCHA*(FFMIX(K)*WFE+FOMIX(K)*WOXE)/WTE*ACHAM           00001280   000750
00372              PUS(JJ) = PC                                                      00001290   000761
00373              VUS(JJ) = VCG                                                     00001300   000763
00374              VGAS(JJ) = VCG                                                    00001310   000765
00375              AGO(JJ) = SQRT(32.2*GAM(JJ)*1545.*TO(JJ)/EMW(JJ))                 00001320   000766
00376              TGAS(JJ) = TO(JJ)*(1.-(GAM(JJ)-1.)*0.5*(VGAS(JJ)/AGO(JJ))**2)     00001330   001000
00377         500  RHOG(JJ) = RHOGF (TGAS(JJ),PC,EMW(JJ),2)                                     001012
00401              FCHAM = FCHAM+FCHA                                                00001360   001027
00402              J = J+NMIXZ                                                       00001370   001032
00403              NDER = NDER+1                                                     00001380   001035
```

```
      IF(NDER.LT.IDER) GO TO 10
      SUM1 = 0.0
      WT = 0.0
      PHIGH = 0.0
      PLOW = 0.0
      IC = 0
      DO 600 I=1,J
      SUM1 = SUM1+GASFL(I)*P(I)
  600 WT = WT + GASFL(I)
      PCI = SUM1/WT
      GO TO 620
  610 PCI = (PLOW+PHIGH)/2.0
  620 SUM1 = 0.0
      DO 630 I=1,J
      C = -144.*(PUS(I)-PCI)*32.2/RHOG(I)
      IF(VUS(I)*VUS(I).LT.4.*C) GO TO 640
      VGAS(I) = (VUS(I)+SQRT(VUS(I)*VUS(I)-4.*C))/2.0
      TGAS(I) = TO(I)*(1.-(GAM(I)-1.)*0.5*(VGAS(I)/AGO(I))**2)
      RHOG(I) = RHOGF(TGAS(I),PCI,EMW(I),2)
      AREA1(I) = 144.*GASFL(I)/(VGAS(I)*RHOG(I))
  630 SUM1 = SUM1 + AREA1(I)
      FA = SUM1/(FCHAM*ACHAM)
      IF(ABS(FA-1.).LE.0.001) GO TO 700
      IF(FA.LT.1.0) PLOW = PCI
      IF(FA.GE.1.0) PHIGH = PCI
      IC = IC+1
      IF(IC.GT.60) GO TO 700
      IF(IC.GE.2) GO TO 610
      IF(PHIGH.LE.0.0.OR.PLOW.LE.0.0) IC = 0
      IF(PLOW.LE.0.0) PCI = PCI-1.0
      IF(PHIGH.LE.0.0) PCI = PCI+1.0
      GO TO 620
  640 PHIGH = PCI
      IF(PLOW.GT.0.0) GO TO 610
      PCI = PCI-1.0
      GO TO 620
  700 DO 710 I=1,J
  710 AREA1(I) = AREA1(I)/FA
      NGT = NGO+1
      NST = J
      NGF = 1
      NASEG = 1
      IWRITE=1
      IDRUM=0
      IPUNCH=0
C     INPUT TO CICM THROUGH $STC
      READ(5,STC)
   16 CONTINUE
      IF(IWRITE.EQ.1) GO TO 12
      IF(IDRUM.EQ.1) GO TO 13
      IF(IPUNCH.EQ.1) GO TO 14
      GO TO 9999
   12 CONTINUE
      IFILE=6
      IWRITE=0
      GO TO 15
```

```
00525        IFILE=11                                                  001334
00526        IDRUN=0                                                   001335
00527        GO TO 15                                                  001336
00530     14 CONTINUE                                                  001340
00531        IFILE=7                                                   001340
00532        IPUNCH=0                                                  001341
00533     15 CONTINUE                                                  001343
00534        ILISP=0                                                   001343
00535        ISTC=1                                                    001343
00536        ITRANS=0                                                  001345
00537        ITDK=0                                                    001346
00540        IST=1                                                     001347
00541        TBF=0.0                                                   001350
00542        TNBF=0.0                                                  001351
00543        RHONBF=0.0                                                001352
00544        RHOLF=0.0                                                 001353
00545        WTMLLF=0.0                                                001354
00546        WTMLVF=0.0                                                001355
00547        NOZON=0                                                   001356
00550        NSTPZ=0                                                   001357
00551        NUG=0                                                     001360
00552        IPUN3D=0                                                  001361
00553        DHVF=0.0                                                  001362
00554        ZSTART=XMINDE                                             001363
00555        DO 31 I=1,NTAB                                            001404
00560     31 CSTR(I)=CSTAR(TMW(I),TTO(I),TGAM(I))                      001405
00562        DO 715 J=1,NTAB                                           001441
00565        GMR(1,J)=TMR(J)                                           001441
00566        GMR(2,J)=TTO(J)                                           001442
00567        GMR(3,J)=TVIS(J)                                          001444
00570        GMR(4,J)=TGAM(J)                                          001446
00571        GMR(5,J)=TMW(J)                                           001450
00572        GMR(6,J)=CSTR(J)                                          001452
00573    715 CONTINUE                                                  001461
00575        DO 716 J=1,NTK                                            001461
00600        GTK(1,J)=0.0                                              001461
00601        GTK(2,J)=0.0                                              001461
00602        GTK(3,J)=0.0                                              001462
00603        GTK(4,J)=TVO(J)                                           001463
00604        GTK(5,J)=CPVO(J)                                          001465
00605        GTK(6,J)=TCONVO(J)                                        001467
00606    716 CONTINUE                                                  001472
00610   9000 FORMAT(1H1,///,23X,'CICM GENERATED INPUT DATA FOR DER SUBPROGRAM S   001472
00610       *TC'///)                                                   001472
00611        WRITE(6,9000)                                             001472
00613        ICARD=10                                                  001477
00614        WRITE(IFILE,7) ICARD                                      001501
00617        DO 720 I=2,4                                              001512
00622        ICARD=I*10                                                001512
00623    720 WRITE(IFILE,8) ICARD                                      001515
00627        ICARD=50                                                  001525
00630        WRITE(IFILE,1) ILISP,ISTC,ITRANS,ITDK,ICARD               001527
00637        ICARD=5010                                                001541
00640        WRITE(IFILE,1) NOZON,NSTPZ,NUG,IPUN3D,ICARD               001543
00647        ICARD=5020                                                001555
00650        WRITE(IFILE,1) NP,NCHAMC,NTAB,NTK,ICARD                   001557
00657        DO 725 I=1,NCHAMC                                         001574
```

```
00662          ACHAMC(I)=SQRT(4./3.14159*CHAMC(I))                   001574
00663      725 CONTINUE                                              001603
00665          XNAP=NCHAMC                                           001603
00666          NC=XNAP/3.+.9                                         001606
00667          DO 730 I=1,NC                                         001620
00672          ICARD=5020+I*10                                       001624
00673          M=I*3-2                                               001630
00674          N=M+2                                                 001634
00675      730 WRITE(IFILE,5) (XCHAMC(J),ACHAMC(J),J=M,N),ICARD      001636
00706          ICARD=5100                                            001660
00707          WRITE(IFILE,9) ICARD                                  001662
00712          XNMR=NTAB                                             001670
00713          NC=XNMR/6.+.9                                         001673
00714          DO 740 I=1,6                                          001705
00717          DO 740 J=1,NC                                         001721
00722          ICARD=5000+I*100+J*10                                 001721
00723          M=J*6-5                                               001725
00724          N=M+5                                                 001731
00725      740 WRITE(IFILE,5) (GMR(I,L),L=M,N),ICARD                 001736
00736          XNTK=NTK                                              001762
00737          NC=XNTK/6.+.9                                         001765
00740          DO 750 I=1,6                                          001777
00743          DO 750 J=1,NC                                         002013
00746          ICARD=5600+I*100+J*10                                 002013
00747          M=J*6-5                                               002017
00750          N=M+5                                                 002023
00751      750 WRITE(IFILE,5) (GTK(I,L),L=M,N),ICARD                 002030
00762          ICARD=6510                                            002054
00763          WRITE(IFILE,5) TNBF,TBF,RHONBF,RHOLF,EMWL(2),EMWV(2),ICARD    002056
00774          ICARD=6520                                            002072
00775          WRITE(IFILE,5) TNBO,TBO,RHONBO,RHOLO,EMWL(1),EMWV(1),ICARD    002074
01006          ICARD=6530                                            002110
01007          WRITE(IFILE,3) TCRIT(2),TCRIT(1),DHVF,DHVO,ICARD      002112
01016          ICARD=6540                                            002124
01017          WRITE(IFILE,6) IST,NSSTI,NMSTI,ICRC,IPRSST,IPRMST,ICARD       002126
01030          ICARD=6550                                            002142
01031          WRITE(IFILE,11) CRTOL,ARTOLD,ICARD                    002144
01036          ICARD=6710                                            002154
01037          WRITE(IFILE,11) PCI,ZSTART,ICARD                      002156
01044          ICARD=6720                                            002166
01045          WRITE(IFILE,1) NGT,NGF,NST,NASEG,ICARD                002170
01054          XNGT=NGT                                              002202
01055          NC=XNGT/2.+.9                                         002205
01056          DO 800 J=1,NST                                        002217
01061          ICARD=7000+J*10                                       002224
01062          WRITE(IFILE,2) AREA1(J),GASFL(J),SHRG(J),ICARD        002230
01070          DO 800 I=1,NC                                         002244
01073          ICARD=ICARD+1                                         002244
01074          M=I*2-1                                               002247
01075          N=M+1                                                 002253
01076      800 WRITE(IFILE,5) (GWSPR(L,J),GVELD1(L,J),GDIAD1(L,J),L=M,N),ICARD   002260
01111          GO TO 16                                              002306
01112     9999 CONTINUE                                              002310
01113          RETURN                                      00002170  002310
01114          END                                         00002180  002367
```

TABLE B-III CARD CHANGES TO CICM ROUTINE
DERINI FOR IMPROVED STC INTERFACE

```
@FOR,URS DERINI
-7
      DIMENSION GMR(6,18),GTK(6,20),CSTR(18),TVO(24),CPVO(24),TCONVO(24)
-11
      COMMON/CGTABC/NTAB,STT,AMRT,TMR(18),TTO(18),TGAM(18),TMW(18),
     *              TVIS(18)
      COMMON/CHCOM/NCHAMC,M2C,NCON4C,WGJC,EMRGJC,STGJC,EMWGJC,GAMGJC,
     *              XLMC,DELTXC,BSPRC,CSPRC,ACSC,CLNTC,CONRAC,CCANGC,
     *              RCBCC,RCTC,XCHAMC(20),ACHAMC(20)
-13,17
    1 FORMAT(4I12,24X,I8)
    2 FORMAT(3E12.6,36X,I8)
    3 FORMAT(4E12.6,24X,I8)
    4 FORMAT(12I6,I8)
    5 FORMAT(6E12.6,I8)
    6 FORMAT(6I12,I8)
    7 FORMAT(6X,'STC INPUT FROM CICM PROGRAM CASE',T73,I8)
    8 FORMAT(72X,I8)
    9 FORMAT(6X,'O2/H2 GAS PROPERTIES FROM CICM INPUT',T73,I8)
   11 FORMAT(2E12.6,48X,I8)
   17 FORMAT(12I6)
   18 FORMAT(6E12.6)
      NAMELIST/STC/TVO,TCONVO,NTK,TNBO,TBO,RHONBO,RHOLO,NP,NSSTI,NMSTI,
     *              ICRC,IPRSST,IPRMST,CRTOL,ARTOLD,IWRITE,IDRUM,IPUNCH,
     *              CPVO,DHVO
      CSTAR(XMW,TO,GAM)=SQRT(49677.*GAM*TO/XMW/((2./(GAM+1.))**((GAM+1.)
     */(GAM-1.))))/GAM
-20,20
-22,27
   10 READ(IRDER,17) NMIXZ,NGO
      READ(IRDER,18) (FFMIX(I),FOMIX(I),I=1,NMIXZ)
      READ(IRDER,18) (FSDER(I),I=1,NGO)
      READ(IRDER,17) NOSC,NELEM
      READ(IRDER,18) (WSPR(I),DOD(I),TOD(I),VOD(I),I=1,100)
      READ(IRDER,18) PC,WCG,EMRCG,SWSPR,VCG,VLJI,TLI,EMWCG,FCHA
-165,187
      IWRITE=1
      IDRUM=0
      IPUNCH=0
C     INPUT TO CICM THROUGH $STC
      READ(5,STC)
   16 CONTINUE
      IF(IWRITE.EQ.1) GO TO 12
      IF(IDRUM.EQ.1) GO TO 13
      IF(IPUNCH.EQ.1) GO TO 14
      GO TO 9999
   12 CONTINUE
      IFILE=6
      IWRITE=0
      GO TO 15
   13 CONTINUE
      IFILE=11
      IDRUM=0
      GO TO 15
   14 CONTINUE
```

```
      IFILE=7
      IPUNCH=0
   15 CONTINUE
      ILISP=0
      ISTC=1
      ITRANS=0
      ITDK=0
      IST=1
      TBF=0.0
      TNBF=0.0
      RHONBF=0.0
      RHOLF=0.0
      WTMLLF=0.0
      WTMLVF=0.0
      NOZON=0
      NSTPZ=0
      NUG=0
      IPUN3D=0
      DHVF=0.0
      ZSTART=XMINDE
      DO 31 I=1,NTAB
   31 CSTR(I)=CSTAR(TMW(I),TTO(I),TGAM(I))
      DO 715 J=1,NTAB
      GMR(1,J)=TMR(J)
      GMR(2,J)=TTO(J)
      GMR(3,J)=TVIS(J)
      GMR(4,J)=TGAM(J)
      GMR(5,J)=TMW(J)
      GMR(6,J)=CSTR(J)
  715 CONTINUE
      DO 716 J=1,NTK
      GTK(1,J)=0.0
      GTK(2,J)=0.0
      GTK(3,J)=0.0
      GTK(4,J)=TVO(J)
      GTK(5,J)=CPVO(J)
      GTK(6,J)=TCONVO(J)
  716 CONTINUE
 9000 FORMAT(1H1,///,23X,'CICM GENERATED INPUT DATA FOR DER SUBPROGRAM S
     *TC'///)
      WRITE(6,9000)
      ICARD=10
      WRITE(IFILE,7) ICARD
      DO 720 I=2,4
      ICARD=I*10
  720 WRITE(IFILE,8) ICARD
      ICARD=50
      WRITE(IFILE,1) ILISP,ISTC,ITRANS,ITDK,ICARD
      ICARD=5010
      WRITE(IFILE,1) NOZON,NSTPZ,NUG,IPUN3D,ICARD
      ICARD=5020
      WRITE(IFILE,1) NP,NCHAMC,NTAB,NTK,ICARD
      DO 725 I=1,NCHAMC
      ACHAMC(I)=SQRT(4./3.14159*ACHAMC(I))
  725 CONTINUE
      XNAP=NCHAMC
      NC=XNAP/3.+.9
```

```
      DO 730 I=1,NC
      ICARD=5020+I*10
      M=I*3-2
      N=M+2
  730 WRITE(IFILE,5) (XCHAMC(J),ACHAMC(J),J=M,N),ICARD
      ICARD=5100
      WRITE(IFILE,9) ICARD
      XNMR=NTAB
      NC=XNMR/6.+.9
      DO 740 I=1,6
      DO 740 J=1,NC
      ICARD=5000+I*100+J*10
      M=J*6-5
      N=M+5
  740 WRITE(IFILE,5) (GMR(I,L),L=M,N),ICARD
      XNTK=NTK
      NC=XNTK/6.+.9
      DO 750 I=1,6
      DO 750 J=1,NC
      ICARD=5600+I*100+J*10
      M=J*6-5
      N=M+5
  750 WRITE(IFILE,5) (GTK(I,L),L=M,N),ICARD
      ICARD=6510
      WRITE(IFILE,5) TNBF,TBF,RHONBF,RHOLF,EMWL(2),EMWV(2),ICARD
      ICARD=6520
      WRITE(IFILE,5) TNBO,TBO,RHONBO,RHOLO,EMWL(1),EMWV(1),ICARD
      ICARD=6530
      WRITE(IFILE,3) TCRIT(2),TCRIT(1),DHVF,DHVO,ICARD
      ICARD=6540
      WRITE(IFILE,6) IST,NSSTI,NMSTI,ICRC,IPRSST,IPRMST,ICARD
      ICARD=6550
      WRITE(IFILE,11) CRTOL,ARTOLD,ICARD
      ICARD=6710
      WRITE(IFILE,11) PCI,ZSTART,ICARD
      ICARD=6720
      WRITE(IFILE,1) NGT,NGF,NST,NASEG,ICARD
      XNGT=NGT
      NC=XNGT/2.+.9
      DO 800 J=1,NST
      ICARD=7000+J*10
      WRITE(IFILE,2) AREA1(J),GASFL(J),SMRG(J),ICARD
      DO 800 I=1,NC
      ICARD=ICARD+1
      M=I*2-1
      N=M+1
  800 WRITE(IFILE,5) (GWSPR(L,J),GVELD1(L,J),GDIAD1(L,J),L=M,N),ICARD
      GO TO 16
 9999 CONTINUE
```

TABLE B-IV
NAMELIST INPUT VARIABLES FOR
IMPROVED CICM/STC INTERFACE ROUTINE

VARIABLE NAME	DEFINITION	UNITS
IWRITE*	STC input data generated by CICM will be printed out when IWRITE = 1	-
IDRUM*	STC input data generated by CICM will be written on system drum file 11 when IDRUM = 1	-
IPUNCH*	STC input data generated by CICM will be punched on cards when IPUNCH = 1	-
NP	Total number of z-planes between z=ZSTART and nozzle throat	-
NSSTI	Maximum number of complete passes, marching from z = ZSTART to throat, in single tube analysis	-
NMSTI	Maximum number of passes in multiple stream tube analysis	-
ICRC	Number of corrector cycles calculated at each Δz interval	-
IPRSST	Number of Δz intervals between single stream tube printouts	-
IPRMST	Number of Δz intervals between multiple stream tube printouts	-
CRTOL	Decimal tolerance, deviation of computed single stream tube throat contraction ratio from unity	-
ARTOLD	Decimal tolerance, deviation of computed multiple stream tube throat contraction ratio from unity	-
NTK	Number of temperatures at which propellant vapor specific heats and film thermal conductivity are tabulated	-
TVO (20)	Temperatures at which oxidizer CPVO and TCONVO are tabulated	°R
CPVO (20)	Oxidizer vapor specific heat at constant pressure	Btu/lbm-°R
TCONVO (20)	Thermal conductivity of vapor/gas film surrounding oxidizer droplets	Btu/ft-sec-°R
DHVO	Oxidizer latent heat of vaporization at chamber "wet bulb" temperature calculated by CICM	Btu/lbm
TNBO	Oxiidzer normal boiling point	°R

VARIABLE NAME	DEFINITION	UNITS
TBO	Oxidizer droplet saturation temperature at Pc	°R
RHONBO	Oxidizer density at normal boiling point	lbm/in^3
RHOLO	Oxidizer density at saturation temperature corresponding to Pc	lbm/in^3

NOTE: All parameters except those asterisked are identical to descriptions given in the DER users manual (Ref. 2).

TABLE B-V NAMELIST INPUT FOR MODIFIED C1CM/STC INTERFACE SUBROUTINE

```
$STC
CRTOL=0.01, ARTOLD=0.01, IWRITE=1, IDRUM=0, IPUNCH=0,
NP=50, NSSTI=3, NMSTI=3, ICRC=1, IPRSST=25, IPRMST=25,
TNBO=162., TBO=265., RHONBO=.0413, RHOLO=.0271, DHVO=45.,
NTK=20,
TVO(1)=200.,265.,275.,285.,300.,340.,400.,600.,1200.,1800.,
       2400.,3000.,3400.,3800.,4200.,4600.,5000.,5600.,
       6000.,6400.,
CPVO(1)=.94,.94,.55,.43,.356,.286,.257,.226,.245,.260,.269,
        .276,.280,.284,.288,.292,.2955,.301,.304,.307,
TCONVO(1)=.00000917,.00000917,.0000108,.00001105,.00001130,
          .00001167,.00001389,.00001806,.00002778,.000035,
          .00004028,.00004444,.00004583,.00004681,.00004722,
          .00004639,.000045,.00003806,.00001917,.0,
$END
```

TABLE B-VI CICM SAMPLE CASE GENERATED INPUT ELEMENT FOR STC

@ELT,L STC
PROCESSED BY UNIVAC 1100 SERIES ELT PROCESSOR LEVEL H8 AT 8:52:18 AM ON THURSDAY, FEBRUARY 26, 1976 (CYCLE 2)

1.	STC INPUT FROM CICM PROGRAM CASE						10
2.							20
3.							30
4.							40
5.	0	1	0	0			50
6.	0	0	0	0			5010
7.	50	2	16	20			5020
8.	.000000+00	.463300+01	.500000+01	.255300+01			5030
9.	O2/H2 GAS PROPERTIES FROM CICM INPUT						5100
10.	.000000	.100000+00	.500000+00	.100000+01	.150000+01	.200000^01	5110
11.	.250000+01	.300000+01	.350000+01	.400000+01	.450000+01	.500000+01	5120
12.	.550000+01	.600000+01	.700000+01	.800000+01	.000000	.000000	5130
13.	.540000+03	.723514+03	.143978+04	.226954+04	.300818+04	.366881+04	5210
14.	.425866+04	.477364+04	.520902+04	.556641+04	.585309+04	.607691+04	5220
15.	.624526+04	.636535+04	.648942+04	.650686+04	.000000	.000000	5230
16.	.599022-05	.751828-05	.133827-04	.209151-04	.281415-04	.349234-04	5310
17.	.411218-04	.466813-04	.514907-04	.555499-04	.589147-04	.616405-04	5320
18.	.638106-04	.654806-04	.675984-04	.686049-04	.000000	.000000	5330
19.	.140500+01	.139700+01	.138000+01	.133800+01	.130100+01	.127400+01	5410
20.	.125400+01	.124000+01	.122900+01	.122000+01	.121400+01	.120900+01	5420
21.	.120500+01	.120200+01	.119900+01	.119800+01	.000000	.000000	5430
22.	.201600+01	.221800+01	.302400+01	.403200+01	.504000+01	.604700+01	5510
23.	.705000+01	.804000+01	.900700+01	.994100+01	.108370+02	.116920+02	5520
24.	.125020+02	.132660+02	.146520+02	.158620+02	.000000	.000000	5530
25.	.532077+04	.588331+04	.713801+04	.784513+04	.815831+04	.828650+04	5610
26.	.831491+04	.827652+04	.819444+04	.808436+04	.795385+04	.781410+04	5620
27.	.766980+04	.752364+04	.723488+04	.696488+04	.000000	.000000	5630
28.	.000000	.000000	.000000	.000000	.000000	.000000	5710
29.	.000000	.000000	.000000	.000000	.000000	.000000	5720
30.	.000000	.000000	.000000	.000000	.000000	.000000	5730
31.	.000000	.000000	.000000	.000000	.000000	.000000	5740
32.	.000000	.000000	.000000	.000000	.000000	.000000	5810
33.	.000000	.000000	.000000	.000000	.000000	.000000	5820
34.	.000000	.000000	.000000	.000000	.000000	.000000	5830
35.	.000000	.000000	.000000	.000000	.000000	.000000	5840
36.	.000000	.000000	.000000	.000000	.000000	.000000	5910
37.	.000000	.000000	.000000	.000000	.000000	.000000	5920
38.	.000000	.000000	.000000	.000000	.000000	.000000	5930
39.	.000000	.000000	.000000	.000000	.000000	.000000	5940
40.	.200000+03	.265000+03	.275000+03	.285000+03	.300000+03	.340000+03	6010
41.	.400000+03	.600000+03	.120000+04	.180000+04	.240000+04	.300000+04	6020
42.	.340000+04	.380000+04	.420000+04	.460000+04	.500000+04	.560000+04	6030
43.	.600000+04	.640000+04					6040
44.	.940000+00	.940000+00	.550000+00	.430000+00	.356000+00	.286000+00	6110
45.	.257000+00	.226000+00	.245000+00	.260000+00	.269000+00	.276000+00	6120
46.	.280000+00	.284000+00	.288000+00	.292000+00	.295500+00	.301000+00	6130
47.	.304000+00	.307000+00					6140
48.	.917000-05	.917000-05	.108000-04	.110500-04	.113000-04	.116700-04	6210
49.	.138900-04	.180600-04	.277800-04	.350000-04	.402800-04	.444400-04	6220
50.	.458300-04	.468100-04	.472200+04	.463900-04	.450000-04	.380600-04	6230
51.	.191700-04	.000000					6240
52.	.000000	.000000	.000000	.000000	.201600+01	.201600+01	6510
53.	.162000+03	.265000+03	.413000-01	.271000-01	.320000+02	.320000+02	6520
54.	.590000+02	.278600+03	.000000	.450000+02			6530

55.	1	3	3	1	25	25	6540
56.	.100000-01	.100000-01					6550
57.	.741407+03	.150000+01					6710
58.	12	1	4	1			6720
59.	.289392+01	.184291+01	.235410+01				7010
60.	.000000	.100000+03	.000000	.167655+00	.369139+03	.553597-02	7011
61.	.167655+00	.338165+03	.797571-02	.167655+00	.317580+03	.921044-02	7012
62.	.167655+00	.295141+03	.108685-01	.167655+00	.271784+03	.128331-01	7013
63.	.167655+00	.250306+03	.148369-01	.167655+00	.227946+03	.171472-01	7014
64.	.167655+00	.205843+03	.195475-01	.167655+00	.189710+03	.193214-01	7015
65.	.838276-01	.184154+03	.153935-01	.838276-01	.162630+03	.126132-01	7016
66.	.330055+01	.213035+01	.287724+01				7020
67.	.000000	.100000+03	.000000	.204912+00	.369139+03	.553597-02	7021
68.	.204912+00	.338165+03	.797571-02	.204912+00	.317580+03	.921044-02	7022
69.	.204912+00	.295141+03	.108685-01	.204912+00	.271784+03	.128331-01	7023
70.	.204912+00	.250306+03	.148369-01	.204912+00	.227946+03	.171472-01	7024
71.	.204912+00	.205843+03	.195475-01	.204912+00	.189710+03	.193214-01	7025
72.	.102456+00	.184154+03	.153935-01	.102456+00	.162630+03	.126132-01	7026
73.	.332128+01	.220514+01	.318061+01				7030
74.	.000000	.100000+03	.000000	.228233+00	.367647+03	.518475-02	7031
75.	.228233+00	.334501+03	.797777-02	.228233+00	.314769+03	.911975-02	7032
76.	.228233+00	.291444+03	.108120-01	.228233+00	.268513+03	.126896-01	7033
77.	.228233+00	.246842+03	.146856-01	.228233+00	.223920+03	.170421-01	7034
78.	.228233+00	.201528+03	.194719-01	.228233+00	.183104+03	.197896-01	7035
79.	.114116+00	.175840+03	.158903-01	.114116+00	.152905+03	.126287-01	7036
80.	.382225+01	.246888+01	.212041+01				7040
81.	.000000	.100000+03	.000000	.228233+00	.367647+03	.518475-02	7041
82.	.228233+00	.334501+03	.797777-02	.228233+00	.314769+03	.911975-02	7042
83.	.228233+00	.291444+03	.108120-01	.228233+00	.268513+03	.126896-01	7043
84.	.228233+00	.246842+03	.146856-01	.228233+00	.223920+03	.170421-01	7044
85.	.228233+00	.201528+03	.194719-01	.228233+00	.183104+03	.197896-01	7045
86.	.114116+00	.175840+03	.158903-01	.114116+00	.152905+03	.126287-01	7046

END ELT. TIME: 0.3866 SECONDS.

@FIN

4. Criteria for Specifying the CICM/STC Interface Plane Location

In Section 2.1.2 of CPIA 246 it is recommended that for CICM/STC analyses the CICM program should be executed to the axial plane at which the liquid jet has disappeared for all flow zones. At this point CICM output is transferred into STC input. There are two problems with specifying the interface plane in this manner.

(1) The CICM program contains an advanced droplet heat-up and vaporization model. The subcritical K-Prime STC version assumes a constant "wet bulb" propellant temperature. If CICM execution is limited to the point of liquid jet dissipation a significant percentage of the liquid droplets will not have yet heated to the "wet bulb" temperature. It is physically incorrect to ignore this effect and to characterize all the liquid droplets with a constant temperature and latent heat of vaporization in the STC input.

(2) CICM performance predictions are controlled, in large part, by two empirically correlated input constants, C_A and B_A. C_A is an atomization (jet stripping) rate constant and B_A is a drop size constant. The recommended input values for these coefficients were backed out from CICM by correlating hot test data. In these instances, CICM was allowed to compute to the chamber throat plane. Thus, the technique used to derive the constant input values is inconsistent with the recommended procedure of joining the CICM and STC analyses at an intermediate chamber axial plane.

CICM improves the JANNAF methodology for subcritical propellants because it allows for the droplet temperature transient. However, it is economically unrealistic to use CICM to the chamber throat plane because of the high computation time this technique requires. Also, using CICM to the throat plane would cause the coaxial injector analysis technique to be inconsistent with the JANNAF conventional liquid/liquid injector methodology, which utilizes STC. The most physically realistic technique is to have CICM execute until all the calculated oxidizer drop size groups have been heated to the chamber "wet bulb" temperature. As previously cited, for oxygen the unsteady state typically comprises only approximately 10 percent of the total time required to vaporize 99 percent of the propellant. Thus, STC would still be responsible for calculating the majority of the liquid mass transfer to the gaseous phase. Importantly, the STC assumption of constant liquid drop temperature is verified when CICM calculates the complete unsteady state time period.

5. Specification of Intra-Element and Manifold Zone Mass Distributions

There is one additional technical problem in interfacing the CICM and STC programs. CICM does not contain formulations for calculating intra or inter-element mixing. The subjects were previously discussed in Sections B.6-7 of this appendix. CPIA 246 and the CICM user's manual recommend the following two solutions.

(1) Manifold mass maldistributions should be accounted for by modeling separate chamber flow field zones.

(2) Intra-element mass maldistributions are modeled by using empirical single element cold flow data to input distinct radial mass distribution sub-zones to CICM for each chamber flow field zone designated as described in (1) above.

There are at least the following four limitations to these suggested solution techniques.

(1) The JANNAF programs can not allow for the dissipation, due to diffusion mixing, of the face plane measured manifold distributions.

(2) The JANNAF methodology does not recommend where the single element mass and mixture ratio distribution should be specified. If the distribution is measured at the face plane the solution will be in error because coaxial elements rely on shear (gas/liquid ΔV) mixing to produce nearly uniform mass distribution at the chamber throat plane.

(3) The CICM and DER literature list only one example of application of the recommended coaxial mass distribution specification technique (the J-2S sample case that is included in CPIA 246). The method that was used to specify the given flow distribution is not described. However, it was stated

that the given distribution was known to result in low performance predictions. This would be expected if the given distribution did not account for shear mixing to the chamber throat plane.

(4) As previously cited in Section B.6 of this appendix, the test cases used to back out the recommended atomization and drop size inputs to DER assumed that the thrust chambers in question had uniform throat plane mixture ratio distributions. For most real coaxial injectors there will be a finite mixing loss because the coaxial element is a relatively slow mixing element. It is apparent that the correct values for the C_A and B_A coefficients will be directly dependent on the assumed single element mixture ratio distribution. Unless a standard method for measuring or calculating single element and chamber mixture ratio distributions is developed it is extremely doubtful that universal values for the C_A and B_A constants can be verified.

APPENDIX C

JANNAF SIMPLIFIED PREDICTION PROCEDURE FOR CICM ANALYSIS

The M-1 sea-level, pressure fed facility for ablative chamber testing is shown in Figure C-1. The corresponding instrumentation code sheet follows Figure 1. Figure C-2 specifies chamber pressure tap axial and circumferential locations.

The M-1 injector design layout is shown in Figure C-3. The injector contained 3248 coaxial elements with gaseous hydrogen being injected annularly around the oxidizer. A row of orifices, drilled through the porous face, was located around the injector periphery and provided the chamber wall film cooling. Approximately 3.7% of the total fuel flow rate was used for chamber wall film cooling. Total fuel element flow rate was 89.8% of the thrust chamber fuel flow rate with a baffle fuel film cooling flow rate of 3.9%. The remaining 2.6% of the fuel flowed through the rigimesh injector face. The element consisted of two basic components which were threaded together. An oxidizer tube was recessed within the fuel sleeve producing a fuel annulus between the two parts. The fuel annulus was fed by four holes having an area four times that of fuel annulus. The oxidizer tube was flared at a fifteen degree included angle and was recessed 0.231 inches from the injector face. Elements were arrayed in 33 concentric rows.

The low area ratio combustion chamber used for testing with the M-1 injector is comprised of an outer steel shell and an inner ablative liner. The assembled combustion chamber (Figure C-4) consists of an upper fuel torous and a lower conical combustion chamber. The thrust chamber design parameters, as related to the ODK input parameters, are identified in Figure C-5.

The test 009 nominal computer input decks for the JANNAF programs utilized during the M-1 analysis are shown in Figures C-6 through C-9.

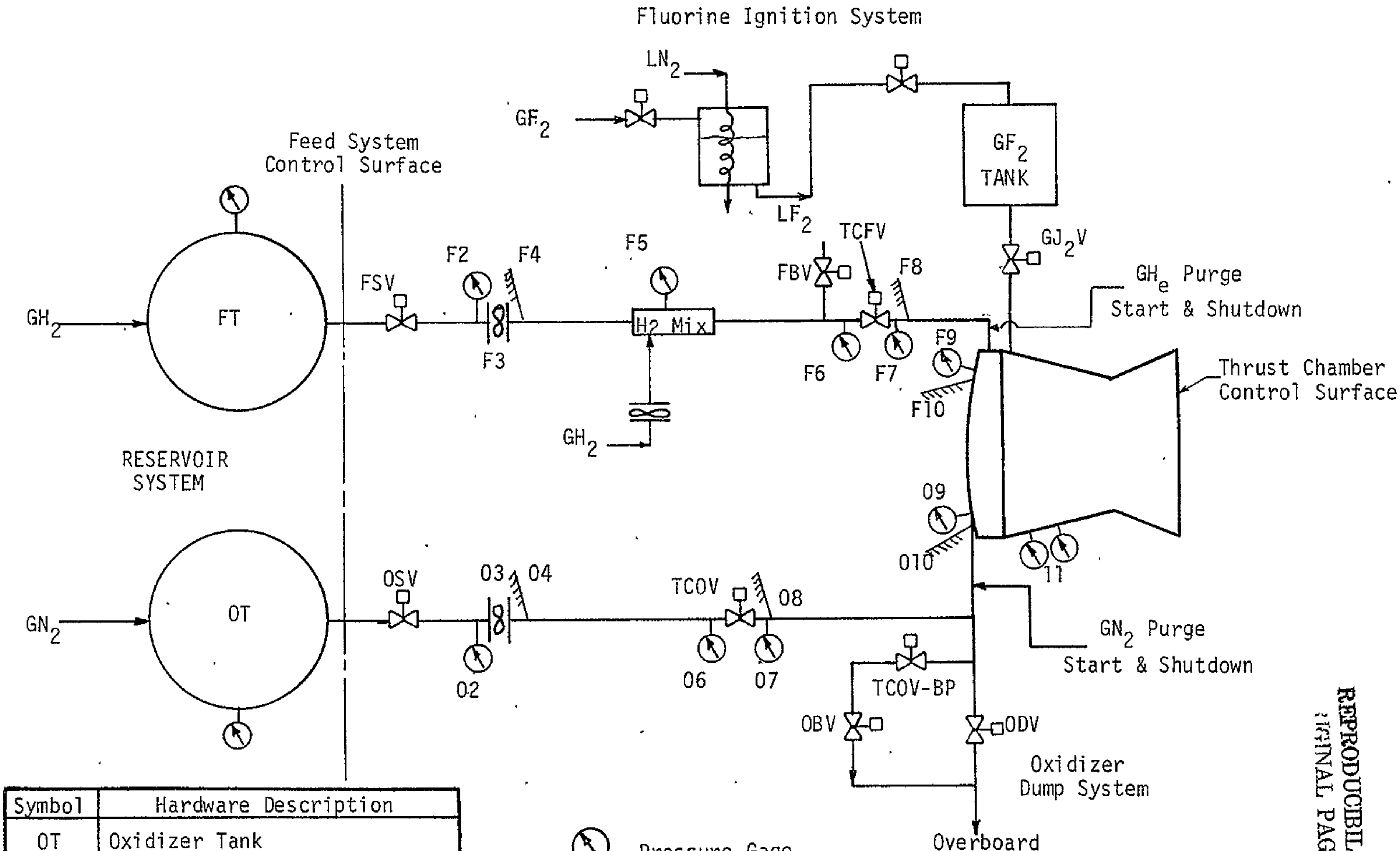

Symbol	Hardware Description
OT	Oxidizer Tank
FT	Fuel Tank
OSV	Oxidizer Safety Valve
FSV	Fuel Safety Valve
OBV	Oxidizer Bypass Valve
FBV	Fuel Bypass Valve
TCOV	Thrust Chamber Oxidizer Valve
TCFV	Thrust Chamber Fuel Valve

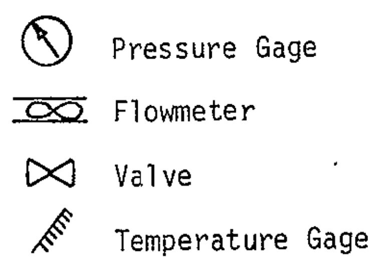

FIGURE C-1. M-1 TEST FACILITY SCHEMATIC

M-1 INSTRUMENTATION TAP LOCATIONS

Measurement	Oxid. Tap Loc.	Fuel Tap Loc.
Tank Pressure (POT, PFT)	01	F1
Flow Meter Pressure (POFM, PFFM)	02	F2
Flow Meter Temperature (TOFM, TFFM)	04	F4
GH_2 Mixer Pressure (PFMIX-2)		F5
Thrust Chamber Pressure-1 (POTCV-1, PFTCV-1)	06	F6
Thrust Chamber Pressure-2 (POTCV-2, POTCV-2)	07	F7
Thrust Chamber Temperature (TOTCV-2, TFTCV-2)	08	F8
Thrust Chamber Injector Pressure (POJ, PFJ)	09	F9
Thrust Chamber Injector Temperature (TOJ, TFJ)	010	F10
Thrust Chamber Pressure (Pc4B-1 & 2)	11	11

FIGURE C-1.(cont.) INSTRUMENTATION CODE

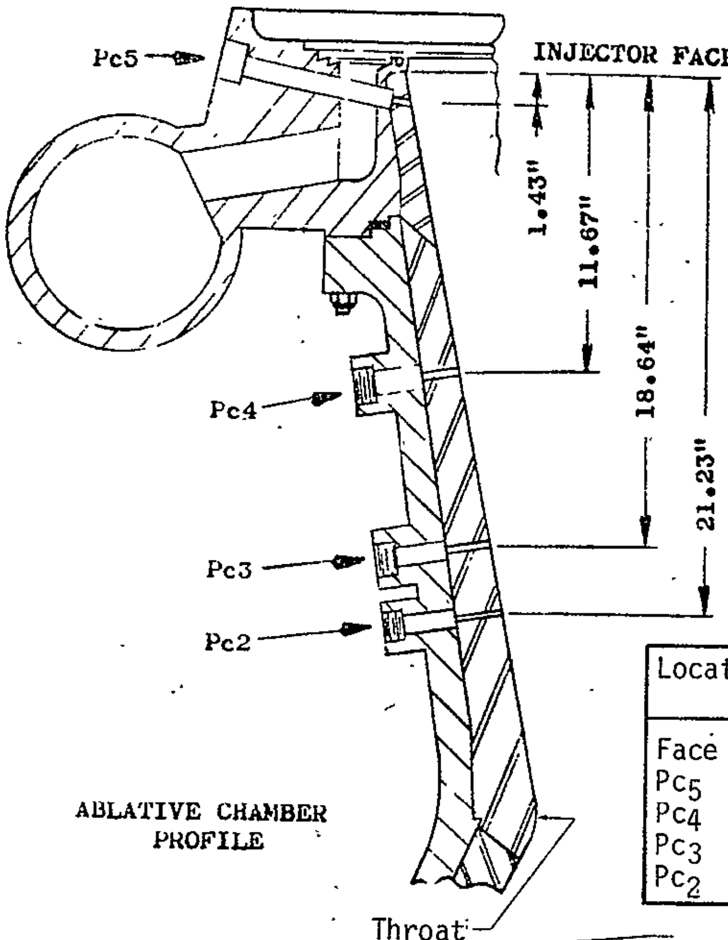

Location	Dist. Face (in.)	D (in.)	Cham. Area (in.^{2})	ε_c
Face	0.00	40.62	1296.	1.833
Pc_5	1.43	40.05	1260.	1.782
Pc_4	11.67	35.96	1016.	1.437
Pc_3	18.64	33.18	864.6	1.223
Pc_2	21.23	32.15	811.6	1.148

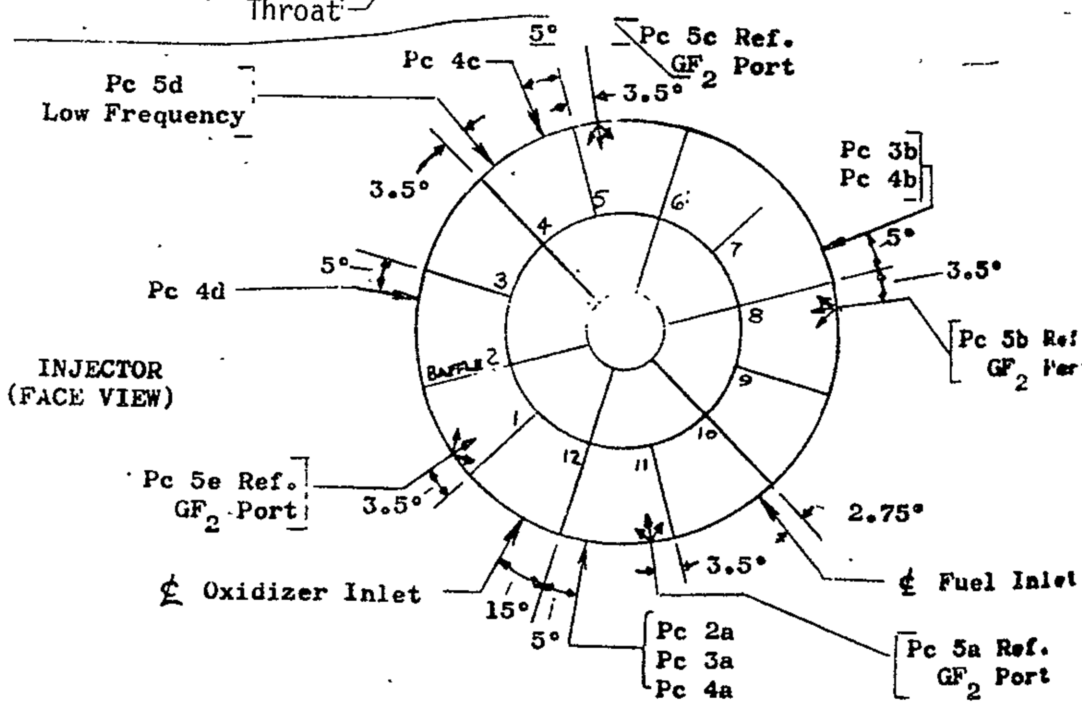

FIGURE C-2. PRESSURE TAP LOCATIONS

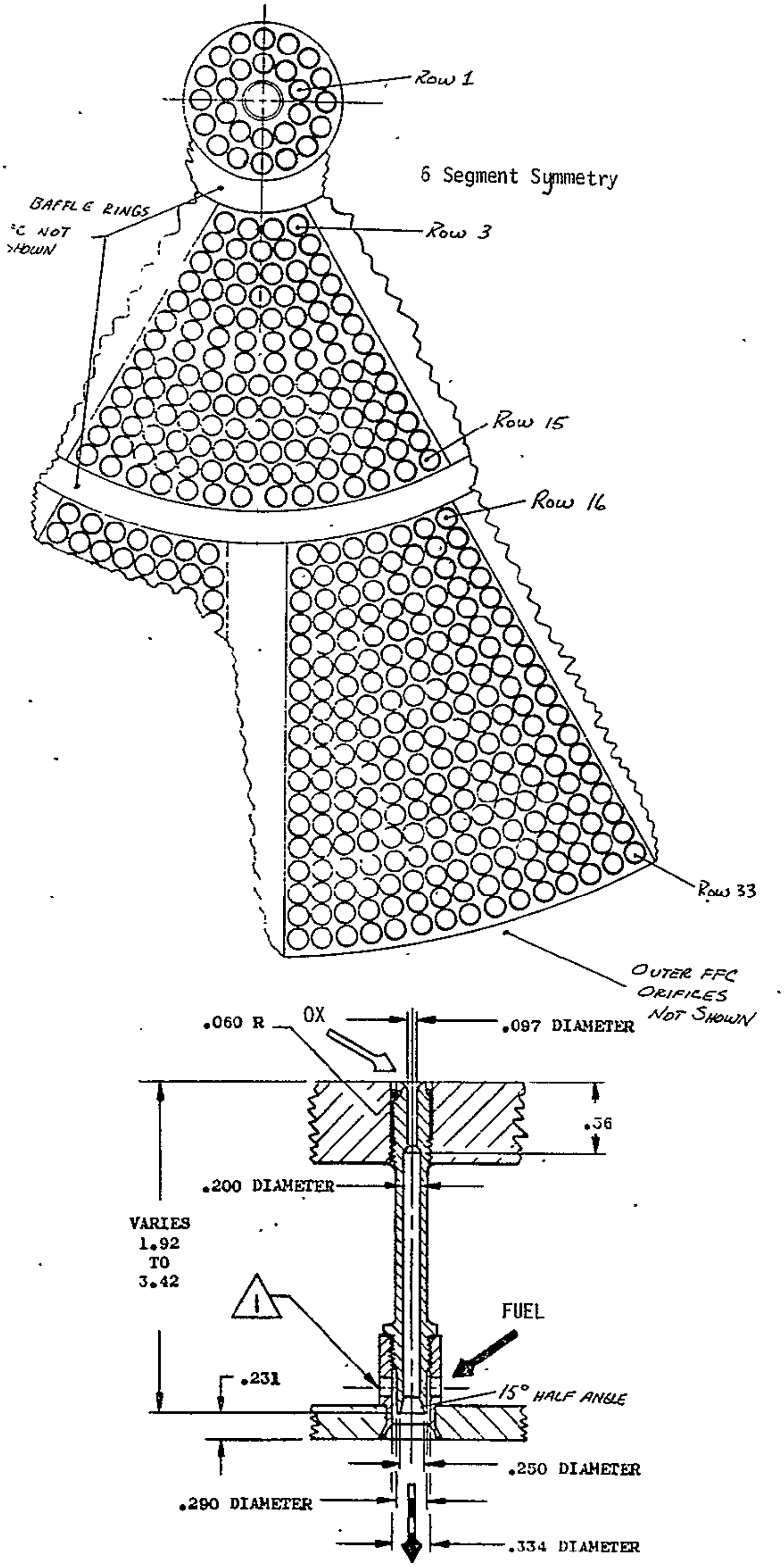

Row No.	Number of Orifices Req'd per Row
1	10
2	16
3	24
4	30
5	36
6	42
7	48
8	48
9	48
10	66
11	72
12	76
13	84
14	90
15	84
16	84
17	96
18	96
19	108
20	108
21	120
22	120
23	132
24	132
25	144
26	144
27	156
28	156
29	168
30	168
31	180
32	180
33	180

FIGURE C-3. M-1 INJECTOR DESIGN

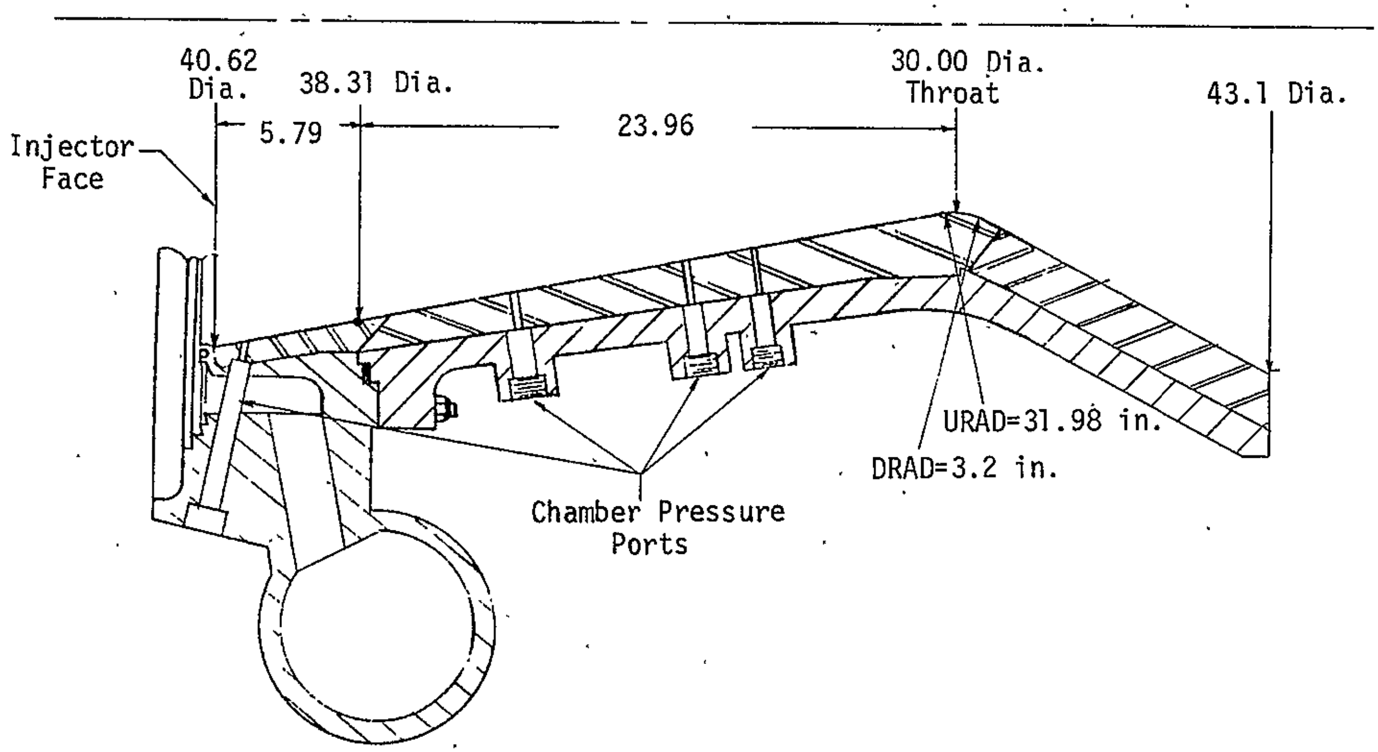

FIGURE C-4. M-1 ABLATIVE CHAMBER FUEL TORUS ASSEMBLY

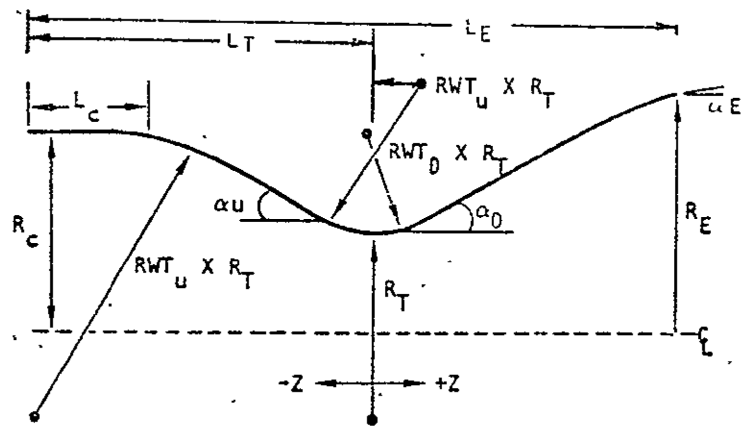

PARAMETER	ODK INPUT NAME	DESIGN VALUE
Chamber Radius, R_C	-	20.31 in.
Throat Radius, R_T	RSTAR	15.0 in.
Contraction Ratio	ECRAT	1.833
Inlet Angle, αu	THETAI	11.3°
Cylindrical Length, L_C	-	0.0 in.
Chamber Length, L_T	-	29.75 in.
Normalized Inlet Radius $RWTU/R_T$	RWTU	2.132
Normalized Outlet Radius $RWTD/R_T$	RWTD	.213
Expansion Angle, αD	THETA	29.9°
Exit Angle, αE	THE	29.9°
Exit Radius	-	21.55
Expansion Ratio	EPS	2.06:1

Figure C-5 M-1 Thrust Chamber Design Parameters

```
625.              18                                                                        5
626.       .0          97.           2.016        1.4          .215E-05                    10
627.       .5         973.           3.024        1.389       1.039E-05                    20
628.      1.         1835.           4.032        1.356       1.819E-05                    30
629.      1.5        2611.           5.040        1.314       2.558E-05                    40
630.      2.4        3805.           6.853        1.261       3.809E-05                    50
631.      2.8        4260.           7.653        1.239       4.337E-05                    60
632.      3.2        4667.           8.444        1.219       4.830E-05                    70
633.      3.6        5021.           9.219        1.199       5.284E-05                    80
634.      4.0        5326.           9.973        1.183       5.692E-05                    90
635.      4.4        5579.          10.702        1.169       6.052E-05                   100
636.      4.8        5788.          11.404        1.157       6.366E-05                   110
637.      5.2        5957.          12.078        1.148       6.635E-05                   120
638.      5.6        6089.          12.721        1.142       6.858E-05                   130
639.      6.0        6190.          13.333        1.136       7.040E-05                   140
640.     7.0         6323.          14.726        1.130       7.337E-05                   150
641.      8.0        6344.          15.937        1.128       7.464E-05                   160
642.     10.0        6233.          17.930        1.129       7.462E-05                   170
643.     12.0        6053.          19.514        1.132       7.327E-05                   180
644.              1          1          0          10          3                           10
645.     23.874        .0          97.           2.016        1.4          4.05            30        12
646.       .05       120.           .08          4.05                                      40
647.     1295.9        29.75         1.833        11.29         .0          31.98          50
648.         INJECTION PROCESSES PROGRAM TASK IIB M-1 TEST DATA CORRELATION               110
649.         TEST 009 XMINDE=4.05                                                                    12
650.              0         3248          0          2          0                         120
651.              1          0          3          1                                      130
652.       .087616       .231         .57265     -22.5         .0          .0             140
653.      .071221      .0          .021564      .0        97.          .0                 160        12
654.      .428879   169.          -.049087 6000.         3.0553       .037854             170        12
655.      .0         .0          97.           2.016       1.4          4.05              180        12
656.    556.6       26.09         0.5          0.031       0.010        1.                190        12
657.         .2207        .0        600.                                                  191
658.              1          11                                                           300
659.      1.         1.                                                                   320
660.       .1         .1          .1          .1          .1          .1                  330
661.       .1         .1          .1          .05         .05                             331
```

NOTE: FIRST 624 CARDS IDENTICAL TO SAMPLE CASE IN REF. 6

FIGURE C-6. CICM INPUT DECK

```
@ELT,UL T09R02
PROCESSED BY UNIVAC 1100 SERIES ELT PROCESSOR LEVEL W8 AT 3:39:15 PM ON THURSDAY, JUNE 3, 1976  (CYCLE 1)
      STC INPUT FROM CICM PROGRAM CASE                                              10
      INJECTION PROCESSES PROGRAM TASK IIB M=1 DATA ANALYSIS                        20   1
      TEST 009 CONTRACT NAS 3-11214 NASA CR 72512                                        1
      LAST SUM PERIOD    O/F=5.46 PC(FACE EST)=557 PSIA  1 ZONE ANALYSIS            40   1
        0         1           0          0                                          50
        0         0           0          0                                        5010
      257         6          18         20                                        5020
   .0         40.62       7.         37.825      15.         34.631               5030   1
  20.         32.634      23.469     31.238      29.75       30.612               5040   1
      O2/H2 GAS PROPERTIES FROM CICM INPUT                                        5100   *COR
 .000000     .500000+00  .100000+01 .150000+01  .240000+01  .280000+01            5110   **=1
 .320000+01  .360000+01  .400000+01 .440000+01  .480000+01  .520000+01            5120
 .560000+01  .600000+01  .700000+01 .800000+01  .100000+02  .120000+02            5130
 .970000+02  .973000+03  .183500+04 .261100+04  .380500+04  .426000+04            5210
 .466700+04  .502100+04  .532600+04 .557900+04  .578800+04  .595700+04            5220
 .608900+04  .619000+04  .632300+04 .634400+04  .623300+04  .605300+04            5230
 .215000-05  .103900-04  .181900-04 .255800-04  .380900-04  .433700-04            5310
 .483000-04  .528400-04  .569200-04 .605200-04  .636600-04  .663500-04            5320
 .685800-04  .704000-04  .733700-04 .746400-04  .746200-04  .732700-04            5330
 .140000+01  .138900+01  .135600+01 .131400+01  .126100+01  .123900+01            5410
 .121900+01  .119900+01  .118300+01 .116900+01  .115700+01  .114800+01            5420
 .114200+01  .113600+01  .113000+01 .112800+01  .112900+01  .113200+01            5430
 .201600+01  .302400+01  .403200+01 .504000+01  .685300+01  .765300+01            5510
 .844400+01  .921900+01  .997300+01 .107020+02  .114040+02  .120780+02            5520
 .127210+02  .133330+02  .147260+02 .159370+02  .179300+02  .195140+02            5530
 .225900+04  .585600+04  .701600+04 .756300+04  .794500+04  .800200+04            5610   1
 .802000+04  .800900+04  .797200+04 .791400+04  .784000+04  .775400+04            5620   1
 .765900+04  .755600+04  .728600+04 .702000+04  .655600+04  .618700+04            5630   1
 .000000     .000000     .000000    .000000     .000000     .000000               5710
 .000000     .000000     .000000    .000000     .000000     .000000               5720
 .000000     .000000     .000000    .000000     .000000     .000000               5730
 .000000     .000000     .000000    .000000     .000000     .000000               5740
 .000000     .000000     .000000    .000000     .000000     .000000               5810
 .000000     .000000     .000000    .000000     .000000     .000000               5820
 .000000     .000000     .000000    .000000     .000000     .000000               5830
 .000000     .000000     .000000    .000000     .000000     .000000               5840
 .000000     .000000     .000000    .000000     .000000     .000000               5910
 .000000     .000000     .000000    .000000     .000000     .000000               5920
 .000000     .000000     .000000    .000000     .000000     .000000               5930
 .000000     .000000     .000000    .000000     .000000     .000000               5940
 .200000+03  .265000+03  .275000+03 .285000+03  .300000+03  .340000+03            6010
 .400000+03  .600000+03  .120000+04 .180000+04  .240000+04  .300000+04            6020
 .340000+04  .380000+04  .420000+04 .460000+04  .500000+04  .560000+04            6030
 .600000+04  .640000+04  .000000    .000000     .000000     .000000               6040
 .940000+00  .940000+00  .550000+00 .430000+00  .356000+00  .286000+00            6110
 .257000+00  .226000+00  .245000+00 .260000+00  .269000+00  .276000+00            6120
 .280000+00  .284000+00  .288000+00 .292000+00  .295500+00  .301000+00            6130
 .304000+00  .307000+00  .000000    .000000     .000000     .000000               6140
 .917000-05  .917000-05  .108000-04 .110500-04  .113000-04  .116700-04            6210
 .158900-04  .196600-04  .277600-04 .350000-04  .402800-04  .444400-04            6220
 .458300-04  .458100-04  .472200-04 .463900-04  .450000-04  .380600-04            6230
 .191700-04  .000000     .000000    .000000     .000000     .000000               6240
 .000000     .000000     .000000    .000000     .201600+01  .201600+01            6510
 .102000+03  .203000+03  .413000-01 .266000-01  .320000+02  .320000+02            6520
```

FIGURE C-7. STC INPUT DECK
(Sheet 1 of 2)

55.	.590000+02	.278600+03	.000000	.470000+02			6530
56.	1	3	0	1	25	25	6540
57.	.100000-01	.100000-01					6550
58.	.535331+03	.410000+01					6710
59.	12	1	1	1			6720
60.	.119349+04	.855539+03	.234864+01				7010
61.	.000000	.100000+03	.000000	.792941+02	.503127+03	.821732-02	7011
62.	.792941+02	.474381+03	.103349-01	.792941+02	.444035+03	.133125-01	7012
63.	.792941+02	.415481+03	.167956-01	.792941+02	.387979+03	.206571-01	7013
64.	.792941+02	.362892+03	.243797-01	.792941+02	.361542+03	.228146-01	7014
65.	.792941+02	.369399+03	.190233-01	.792941+02	.370694+03	.154398-01	7015
66.	.396470+02	.357409+03	.131637-01	.396470+02	.318678+03	.113274-01	7016

PAGE 2 OF 2

FIGURE C-7. STC INPUT DECK
(Sheet 2 of 2)

```
@XQT TDK
THERMO
   300.000  1000.000  5000.000
AR                L 5/66AR   100   000   000   0G    300.000   5000.000          1
 0.25000000E 01 0.              0.              0.              0.              2
-0.74537502E 03 0.43660006E 01 0.25000000E 01 0.              0.              3
 0.              0.             -0.74537498F 03 0.43660006E 01                  4
H                 J 9/65H    100   000   000   0G    300.000   5000.000          1
 0.25000000E 01 0.              0.              0.              0.              2
 0.25471627E 05-0.46011763F 00 0.25000000F 01 0.              0.              3
 0.              0.              0.25471627F 05-0.46011762E 00                  4
H2                J 3/61H    20    00    00    0G  . 300.000   5000.000          1
 0.31001901E 01 0.51119464E-03 0.52644210E-07-0.34909973E-10 0.36945345E-14    2
-0.87738042E 03-0.19629421E 01 0.30574451F 01 0.26765200E-02-0.58099162E-05    3
 0.55210391E-08-0.18122739E-11-0.98890474E 03-0.22997056E 01                   4
H2O               J 3/61H    20    100   000   0G    300.000   5000.000          1
.0.27167633E 01 0.29451374E-02-0.80224374E-06 0.10226682E-09-0.48472145E-14    2
 -.29905826E 05 0.66305671E 01 0.40701275E 01-0.11084499E-02 0.41521180E-05    3
 -.29637404E-08 0.80702103E-12-0.30279722F 05-0.32270046E 00                   4
N2                J 9/65N    20    00    00    0G    300.000   5000.000          1
 0.28963194E 01 0.15154866E-02-0.57235277E-06 0.99807393E-10-0.65223555E-14    2
-0.90586184E 03 0.61615148E 01 0.36748261F 01-0.12081500E-02 0.23240102E-05    3
-0.63217559E-09-0.22577253E-12-0.10611588E 04 0.23580424E 01                   4
O                 J 6/62O    100   000   000   0G    300.000   5000.000          1
 0.25420596E 01-0.27550619E-04-0.31028033E-08 0.45510674E-11-0.43680515E-15    2
 0.29230803E 05 0.49203080E 01 0.29464287E 01-0.16381665E-02 0.24210316E-05    3
-0.16028432E-08 0.38906964E-12 0.29147644F 05 0.29639949E 01                   4
OH                J12/70O    1H    10    00    0G    300.000   5000.000          1
 0.29131230E+01 0.95418248E-03-0.19084325E-06 0.12730795E-10 0.24803941E-15    2
 0.39647060E+04 0.54288735E+01 0.38365518E+01-0.10702014E-02 0.94849757E-06    3
 0.20843575E-09-0.23384265E-12 0.36715807F+04 0.49805456E+00                   4
O2                J 9/65O    20    00    00    0G    300.000   5000.000          1
 0.36219535E 01 0.73618264E-03-0.19652228F-06 0.36201558E-10-0.28945627E-14    2
-0.12019825E 04 0.36150960E 01 0.36255985F 01-0.18782184E-02 0.70554544E-05    3
-0.67635137E-08 0.21555993E-11-0.10475226F 04 0.43052778E 01                   4
END
TITLE N=1 ODK DATA TEST 009 INLET CONDS,  PC=517
PROBLEM ODE-ODK-TDK,NZONES=1,
REACTANTS
O 2,                                              99.519   -3027.  L 90.18  O
AR 1,                                              0.437   -2571.  L 90.18  O
N 2,                                               0.044   -2699.  L 90.18  O
H 2,                                             100.      -1837.  L 20.25  F

NAMELISTS
 $ODE
 RKT=.TRUE., PSIA=.TRUE.,
 OF=.TRUE.,
 P=517.,
 OFSKED(1)=5.46,                  NOMINAL TEST  009 O/F
 SUPAR(1)=2.064,
 SUBAR(1)=1.833, ECRAT=1.833,
 EQL=.TRUE., FROZ=.FALSE.,
 PCP(1)=1.01,1.05,1.1,1.2,1.6,2.,5.,10.,20.,
 IPTAB=1, IOFF=0, IPTBL=0,
 $END
REACTIONS
H + H  = H2               ,A=6.4E17, N=1.0, B=0.0,
O + O  =O2                ,A=1.3E17, N=1.0, B=0.34,
H + OH = H2O              ,A=8.4E21, N=2.0, B=0.0,
```

FIGURE C-8. TDK INPUT DECK (Sheet 1 of 2)

```
END TBR REAX
H2 + O  = H   + OH             ,A=1.8E10, N=-1.0, B=8.90,
O2 + H  = OH  + O              ,A=2.2E14, N=0.0, B=16.8,
H2 + OH = H2O + H              ,A=2.20E13, N=0.0, B=5.15,
OH + OH = H2O + O              ,A=6.30E12, N=0.0, B=1.0,
LAST REAX
INERTS N2,AR,END
THIRD BODY REAX RATE RATIOS
SPECIES AR,  1.0,1.0,1.0,
SPECIES H,   25.0,12.5,12.5,
SPECIES H2,  4.0,5.0,5.0,
SPECIES H2O, 20.0,5.0,17.0,
SPECIES N2,  1.5,4.0,3.0,
SPECIES OH,  25.0,12.5,12.5,
SPECIES O,   25.0,12.5,12.5,
SPECIES O2,  1.5,11.0,5.0,
LAST CARD
 $ODK
 RSTAR=15., RWTU=2.132, RWTD=.213, THETAI=11.29, RI=0.0,
 IWALL=1, THETA=29.9,
 EPS=2.064,
 $END
 $TRANS
 XM(1)=1.,
 $END
 $TDK
 $END
```


FIGURE C-8. TDK INPUT DECK (Sheet 2 of 2)

```
@XQT BLIMP
30200623210212        M=1 ANALYSIS TEST 009 CONDS.
 $MISLIS
 NSP=2,  KS=19*1,
 NS=19, KR9=19*2,
 S(1)=.024,
 NETA=12, ETA=0.,.001,.006,.01,.025,.06,.15,.40,.70,1.,1.5,2.5,
 KAPPA=10, CBAR=0.95, KONRFT=1, NPOINT=3, RATLIM=0.5,
 F2FIX=.0,.05,.12,.25,.35,.45,.60,.75,.85,.95,.98,1.,
 GW=-671.,
 RTM=1.25, PTET(1)=35.17, GE(1)=-590.1,
 ELCON=0.4, YAP=-11.8, CLNUM=0.0168, SCT=0.9, PRT=-0.44,
 $END
 $INPUT
 N=81, NTH=27, IP=1,
 NP=2,4,6,10,16,19,22,24,25,26,27,36,44,51,53,54,55,57,60,64,68,72,
 77,81,
 XITAB(  1)=  -.19834+01, YITAB(  1)=   .13539+01, PITAB(  1)=   .93380+00,
 XITAB(  2)=  -.19199+01, YITAB(  2)=   .13412+01, PITAB(  2)=   .93087+00,
 XITAB(  3)=  -.18419+01, YITAB(  3)=   .13256+01, PITAB(  3)=   .92708+00,
 XITAB(  4)=  -.17638+01, YITAB(  4)=   .13101+01, PITAB(  4)=   .92301+00,
 XITAB(  5)=  -.16858+01, YITAB(  5)=   .12945+01, PITAB(  5)=   .91863+00,
 XITAB(  6)=  -.16077+01, YITAB(  6)=   .12789+01, PITAB(  6)=   .91390+00,
 XITAB(  7)=  -.15296+01, YITAB(  7)=   .12633+01, PITAB(  7)=   .90878+00,
 XITAB(  8)=  -.14516+01, YITAB(  8)=   .12477+01, PITAB(  8)=   .90324+00,
 XITAB(  9)=  -.13735+01, YITAB(  9)=   .12321+01, PITAB(  9)=   .89720+00,
 XITAB( 10)=  -.12955+01, YITAB( 10)=   .12166+01, PITAB( 10)=   .89063+00,
 XITAB( 11)=  -.12174+01, YITAB( 11)=   .12010+01, PITAB( 11)=   .88343+00,
 XITAB( 12)=  -.11393+01, YITAB( 12)=   .11854+01, PITAB( 12)=   .87554+00,
 XITAB( 13)=  -.10613+01, YITAB( 13)=   .11698+01, PITAB( 13)=   .86682+00,
 XITAB( 14)=  -.98322+00, YITAB( 14)=   .11542+01, PITAB( 14)=   .85717+00,
 XITAB( 15)=  -.90516+00, YITAB( 15)=   .11386+01, PITAB( 15)=   .84640+00,
 XITAB( 16)=  -.82710+00, YITAB( 16)=   .11231+01, PITAB( 16)=   .83430+00,
 XITAB( 17)=  -.74904+00, YITAB( 17)=   .11075+01, PITAB( 17)=   .82058+00,
 XITAB( 18)=  -.67098+00, YITAB( 18)=   .10919+01, PITAB( 18)=   .80484+00,
 XITAB( 19)=  -.59292+00, YITAB( 19)=   .10763+01, PITAB( 19)=   .78648+00,
 XITAB( 20)=  -.51486+00, YITAB( 20)=   .10607+01, PITAB( 20)=   .76454+00,
 XITAB( 21)=  -.43680+00, YITAB( 21)=   .10451+01, PITAB( 21)=   .73750+00,
 XITAB( 22)=  -.35874+00, YITAB( 22)=   .10304+01, PITAB( 22)=   .70738+00,
 XITAB( 23)=  -.28069+00, YITAB( 23)=   .10186+01, PITAB( 23)=   .67577+00,
 XITAB( 24)=  -.20263+00, YITAB( 24)=   .10097+01, PITAB( 24)=   .64290+00,
 XITAB( 25)=  -.12457+00, YITAB( 25)=   .10036+01, PITAB( 25)=   .60901+00,
 XITAB( 26)=  -.48107-01, YITAB( 26)=   .10005+01, PITAB( 26)=   .57511+00,
 XITAB( 27)=   .00000   , YITAB( 27)=   .10000+01, PITAB( 27)=   .50727+00,
 XITAB( 28)=   .30352-02, YITAB( 28)=   .10000+01, PITAB( 28)=   .48682+00,
 XITAB( 29)=   .62627-02, YITAB( 29)=   .10001+01, PITAB( 29)=   .46829+00,
 XITAB( 30)=   .96349-02, YITAB( 30)=   .10002+01, PITAB( 30)=   .45036+00,
 XITAB( 31)=   .13135-01, YITAB( 31)=   .10004+01, PITAB( 31)=   .43302+00,
 XITAB( 32)=   .16743-01, YITAB( 32)=   .10007+01, PITAB( 32)=   .41599+00,
 XITAB( 33)=   .20449-01, YITAB( 33)=   .10010+01, PITAB( 33)=   .39940+00,
 XITAB( 34)=   .24248-01, YITAB( 34)=   .10014+01, PITAB( 34)=   .38318+00,
 XITAB( 35)=   .28134-01, YITAB( 35)=   .10019+01, PITAB( 35)=   .36729+00,
 XITAB( 36)=   .32102-01, YITAB( 36)=   .10024+01, PITAB( 36)=   .35171+00,
 XITAB( 37)=   .36151-01, YITAB( 37)=   .10031+01, PITAB( 37)=   .33642+00,
 XITAB( 38)=   .40276-01, YITAB( 38)=   .10038+01, PITAB( 38)=   .32141+00,
 XITAB( 39)=   .44476-01, YITAB( 39)=   .10047+01, PITAB( 39)=   .30668+00,
 XITAB( 40)=   .48750-01, YITAB( 40)=   .10057+01, PITAB( 40)=   .29222+00,
 XITAB( 41)=   .53096-01, YITAB( 41)=   .10067+01, PITAB( 41)=   .27803+00,
 XITAB( 42)=   .57513-01, YITAB( 42)=   .10079+01, PITAB( 42)=   .26411+00,
 XITAB( 43)=   .62000-01, YITAB( 43)=   .10092+01, PITAB( 43)=   .25046+00,
```

STAGNATION ENTHALPY OF O/F = 2.5 EDGE GAS

TDK 1 ZONE RESULTS FOR CORE O/F OF 5.46:1

FIGURE C-9. BLIMP INPUT DECK (Sheet 1 of 3)

```
XITAB( 44)=   .66557-01, YITAB( 44)=   .10107+01, PITAB( 44)=   .23709+00,
XITAB( 45)=   .71186-01, YITAB( 45)=   .10122+01, PITAB( 45)=   .22398+00,
XITAB( 46)=   .75884-01, YITAB( 46)=   .10140+01, PITAB( 46)=   .21115+00,
XITAB( 47)=   .80654-01, YITAB( 47)=   .10159+01, PITAB( 47)=   .19859+00,
XITAB( 48)=   .85493-01, YITAB( 48)=   .10179+01, PITAB( 48)=   .18632+00,
XITAB( 49)=   .90404-01, YITAB( 49)=   .10201+01, PITAB( 49)=   .17434+00,
XITAB( 50)=   .95387-01, YITAB( 50)=   .10226+01, PITAB( 50)=   .16265+00,
XITAB( 51)=   .10044+00, YITAB( 51)=   .10252+01, PITAB( 51)=   .15126+00,
XITAB( 52)=   .10557+00, YITAB( 52)=   .10280+01, PITAB( 52)=   .14018+00,
XITAB( 53)=   .11082+00, YITAB( 53)=   .10310+01, PITAB( 53)=   .13871+00,
XITAB( 54)=   .13157+00, YITAB( 54)=   .10430+01, PITAB( 54)=   .13729+00,
XITAB( 55)=   .15227+00, YITAB( 55)=   .10549+01, PITAB( 55)=   .13590+00,
XITAB( 56)=   .17303+00, YITAB( 56)=   .10668+01, PITAB( 56)=   .13445+00,
XITAB( 57)=   .19388+00, YITAB( 57)=   .10788+01, PITAB( 57)=   .13298+00,
XITAB( 58)=   .21485+00, YITAB( 58)=   .10908+01, PITAB( 58)=   .13148+00,
XITAB( 59)=   .23707+00, YITAB( 59)=   .11036+01, PITAB( 59)=   .12979+00,
XITAB( 60)=   .25414+00, YITAB( 60)=   .11134+01, PITAB( 60)=   .12822+00,
XITAB( 61)=   .27919+00, YITAB( 61)=   .11278+01, PITAB( 61)=   .12564+00,
XITAB( 62)=   .29605+00, YITAB( 62)=   .11375+01, PITAB( 62)=   .12367+00,
XITAB( 63)=   .31709+00, YITAB( 63)=   .11496+01, PITAB( 63)=   .12081+00,
XITAB( 64)=   .34457+00, YITAB( 64)=   .11654+01, PITAB( 64)=   .11584+00,
XITAB( 65)=   .37366+00, YITAB( 65)=   .11822+01, PITAB( 65)=   .11303+00,
XITAB( 66)=   .40203+00, YITAB( 66)=   .11985+01, PITAB( 66)=   .10991+00,
XITAB( 67)=   .42870+00, YITAB( 67)=   .12138+01, PITAB( 67)=   .10859+00,
XITAB( 68)=   .45532+00, YITAB( 68)=   .12291+01, PITAB( 68)=   .10739+00,
XITAB( 69)=   .48237+00, YITAB( 69)=   .12447+01, PITAB( 69)=   .10599+00,
XITAB( 70)=   .50989+00, YITAB( 70)=   .12605+01, PITAB( 70)=   .10441+00,
XITAB( 71)=   .53772+00, YITAB( 71)=   .12765+01, PITAB( 71)=   .10279+00,
XITAB( 72)=   .56591+00, YITAB( 72)=   .12927+01, PITAB( 72)=   .10111+00,
XITAB( 73)=   .59442+00, YITAB( 73)=   .13091+01, PITAB( 73)=   .99413-01,
XITAB( 74)=   .62332+00, YITAB( 74)=   .13257+01, PITAB( 74)=   .97680-01,
XITAB( 75)=   .65256+00, YITAB( 75)=   .13425+01, PITAB( 75)=   .95938-01,
XITAB( 76)=   .68218+00, YITAB( 76)=   .13596+01, PITAB( 76)=   .94186-01,
XITAB( 77)=   .71220+00, YITAB( 77)=   .13768+01, PITAB( 77)=   .92420-01,
XITAB( 78)=   .74265+00, YITAB( 78)=   .13943+01, PITAB( 78)=   .90639-01,
XITAB( 79)=   .77346+00, YITAB( 79)=   .14121+01, PITAB( 79)=   .88872-01,
XITAB( 80)=   .80478+00, YITAB( 80)=   .14301+01, PITAB( 80)=   .87083-01,
XITAB( 81)=   .81272+00, YITAB( 81)=   .14346+01, PITAB( 81)=   .86650-01,
$END
 3
H HYDROGEN     1.008  200.         265.                            11100  S
C  CARBON     12.01                127.                            11201  S
O  OXYGEN     16.0     31.          44.                            11202  S
    300.       1000.        5000.                                  11203  S
WALL GAS DUM     MAY 76H 2650  44C 127      S   300.      100.           1
               -1000.                                                     2
                                                                          3
                                             -1000.                       4
EDGE GAS DUM     MAY 76H 2000  31           S   300.      100.           1
                                                                          2
               -1000.                                                     3
                                             -1000.                       4
@ADD,P THERMO/DATA
                                                                 13 LAST
 $STALIS
 TW=5*2560.,2770.,3420.,3640.,11*3830.,
 FLUXJ(2,1,1)=.00232,2*0.0,.00232,2*0.0,.00232,2*0.0,.00232,2*0.0,
```

O/F = 2.5
EDGE GAS

CHEMICAL FORMULA
FOR ABLATIVE WALL PYROLYSIS GAS

FIGURE C-9. BLIMP INPUT DECK (Sheet 2 of 3)

```
,00232,2*0.0,,00271,2*0.0,,00657,2*0.0,,01121,2*0.0
,02127,2*0.0,,02127,2*0.0,,02127,2*0.0,,02127,2*0.0,,02127,2*0.0
,02127,2*0.0,,02127,2*0.0,,02127,2*0.0,,02127,2*0.0,,02127,2*0.0
,02127,2*0.0,
$END
```

LAST S

FIGURE C-9. BLIMP INPUT DECK (Sheet 3 of 3)

APPENDIX D

STATIC PRESSURE PROFILE DATA REDUCTION (REF. 15 PAPER)

An Experimental-Analytical Method to Study Steady Spray Combustion

FREDIANO V. BRACCO*
Guggenheim Laboratories, Princeton University, Princeton, N. J.

Theme

AN experimental-analytical method is presented by which the local combustion gas parameters and flux of liquid fuel drops resulting from the steady burning of a fuel spray in a gaseous oxidizer can be determined. The method does not require any knowledge of the droplet distribution function, drag and vaporization equations. Instead, it requires local static pressure measurements. Results from the application of this method to a liquid oxygen-ethanol rocket combustor are given. They relate mostly to the axial uniformity of the vaporization rate and of the combustion gas variables.

Content

This method is essentially a technique to obtain maximum information out of a set of static pressure measurements based on substituting the measured static pressure values into the conservation equations and in solving them for other unknown quantities. For clarity, the technique is here illustrated using a simplified set of equations which require more assumptions than are necessary. The necessary assumptions are listed after the technique has been introduced. Details about the technique and its extensive application to various configurations of a liquid oxygen-ethanol rocket motor can be found in the thesis referred to in the footnote.

Consider a constant cross-sectional area combustor in which a liquid fuel and a liquid oxidizer are injected. Assume that the oxidizer vaporizes much faster than the fuel and consider that part of the combustor where only gaseous oxidizer, combustion products, and liquid fuel drops exist. Further assume that the combustion is steady, that at the station of interest the flow is one dimensional (uniform through the cross section) and that there is no recirculation. Neglect heat transfer and viscosity effects. Temporarily assume also that all fuel drops have initially the same velocity and radius and that there are no collisions, breakups, or nucleations. The following equations, relating properties at the injector end to properties at any downstream station, can then be written

$$\rho u = -(W_F - W_{0_F}) + W_{0_\phi} \tag{1}$$

$$\rho u^2 = p_0 - p - (W_F u_F - W_{0_F} u_{x_F}) + W_{0_F} u_{x_\phi} \tag{2}$$

$$\rho u[h + (u^2/2)] = -[W_F(\Lambda_F + u^2{}_F/2 + h^0{}_F) - W_{0_F}$$

$$(\Lambda_{0_F} + u^2{}_{0_F}/2 + h^0{}_F) \quad W_{0_\phi}(\Lambda_{0_\phi} + u^2{}_{0_\phi}/2 + h_{0_\phi})] \tag{3}$$

$$T = T(p, \rho, X_i) \tag{4}$$

$$h = h(p, \rho, X_i) \tag{5}$$

$$F_i(p, T, X_{1,2..I}, W_{0_F}, W_{0_\phi}, W_F) = 0 \qquad i = 1, 2 \ldots I$$

$$W_F/r^3 = W_{0_F}/r_0{}^3 \tag{6}$$

$$u_F(du_F/dx) = \tfrac{3}{8} C_D\, \rho |u - u_F|(u - u_F)/r\rho_L \tag{7}$$

$$u_F(dr/dx) = -k[s + g\, R_e{}^q]/8r \tag{8}$$

Where ρ, u, p, T, h are the combustion gas density, velocity, pressure, temperature, and latent enthalpy respectively (p_0 is the value of p at the injector end). W_F (W_ϕ) is the local liquid fuel (oxidizer) flux and W_{0_F} (W_{0_ϕ}) is its value at $x = 0$ (injector end). u_F (u_ϕ) is the liquid fuel (oxidizer) drop velocity, u_{0_F}(u_{0_ϕ}) is the injection velocity and u_{x_F}(u_{x_ϕ}) is its component in the x direction. Λ_F(Λ_ϕ) and $h^0{}_F$($h_\phi{}^0$) are the vaporization energy and the enthalpy of formation respectively. X_i are the number of moles of product i per mole of burned fuel. r is the local drop radius. ρ_L is the specific gravity of the liquid fuel. C_D and R_e are the drag coefficient and the Reynolds number respectively and k, s, g, q are properly selected constants. Equations (1–3) express mass, momentum, and energy conservation, respectively. Equation (4) is the thermal equation of state of the combustion products, and Eq. (5) is the caloric equation of state. F_i stands for a set of I equations which are necessary to relate the amount of vaporized propellants to the variables of the gas (they are as many as the chemical species of which the gas is assumed to be made up.) Equation (6) states the conservation of the drop number. Equations (7) and (8) are possible forms of the drag and vaporization equations for individual drops. If the conditions at the injector end and basic thermodynamic data are known, these $8 + I$ equations contain the following $8 + I$ unknowns: ρ, u, p, T, h, W_F, u_F, r, $X_{1,2..I}$.

It is then observed that the first $5 + I$ equations could be solved if any two of the $7 + I$ unknowns appearing in them were given, in which case the last three equations could be dropped. Notice that the knowledge of two parameters allows the elimination of three equations since Eq. (6) contains the drop radius which appears in the last two equations but not in the first $5 + I$.

Actually, the measurement of just one parameter is sufficient to obtain useful solutions of the first $5 + I$ equations. Indeed the terms containing the liquid drop velocity (u_F) in Eqs. (2) and (3) are small so that the solution of the system is not very sensitive to its value. Accordingly, the ratio $0 < u_F/u \leq 1$ was selected as one of the two parameters.

The selection of the parameter which is to be measured is dictated by the criterion that it must be easy to measure and the solution of the first $5 + I$ equations must be sensitive to its value. The static pressure (actually the loss of static pressure between the injector and any axial location), which meets those requirements, can be selected.

In conclusion, the first $5 + I$ equations can be solved, at various axial locations, for selected values of u_F/u and using static pressure measurements. All the gas variables and the liquid fuel flux are thus determined without any assumption about the droplet drag, and vaporization processes.

Synoptic received October 5, 1972; revision received February 1, 1973. This research, under NASA Grant NGL-31-001-115, was sponsored by the Chemical Rocket Division of NASA Lewis Research Center, M. F. Heidmann, Project Manager. Synoptic based on pp. 57–124 of Bracco, F. V., "The Direct Method as Applied to Liquid Rocket Engine Combustion and Explosion Problems," Ph.D. Thesis, Princeton University, Princeton, N. J., June 1970, available as Report 71-14359 at the University Microfilms, Xerox Company, 300 North Zeeb Road, Ann Arbor, Mich. 48106 ($4 microfilm; $10 hard copy).

Index categories: Combustion in Heterogeneous Media; Liquid Rocket Engines.

*Member of the Research Staff, Guggenheim Laboratories. Associate Member AIAA.

Typical results are presented in Figs. 1 and 2. They were obtained with an oxygen-ethanol rocket motor of constant cross sectional area (7.62 cm ID). The injector was made up of 16 impinging like-on-like doublets with a distance between injector units of 1.5 cm. Chamber pressure, nozzle entrance Mach number and injection mixture ratio (O/F) were 20 atm, 0.15 and 2.33, respectively. The static pressure difference between the injector and various downstream stations was measured accurately and repeatedly by water manometers and is given in Fig. 1 (this technique is feasible only for low chamber pressures and/or small nozzle entrance Mach numbers). The first $5 + I$ equations were then solved for ρ, u, T, h, W_t and the local concentrations of O, H, O_2, H_2, OH, CO, H_2O.

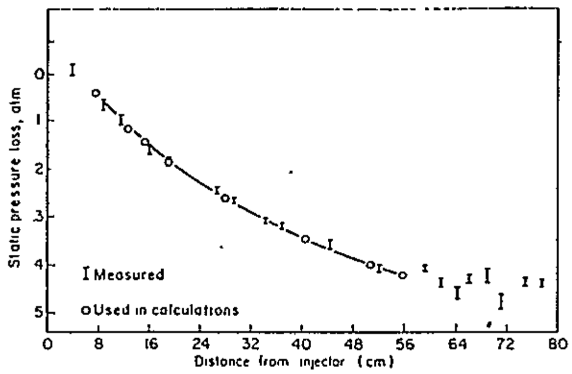

Fig. 1. Measured loss of static pressure vs distance from the inector.

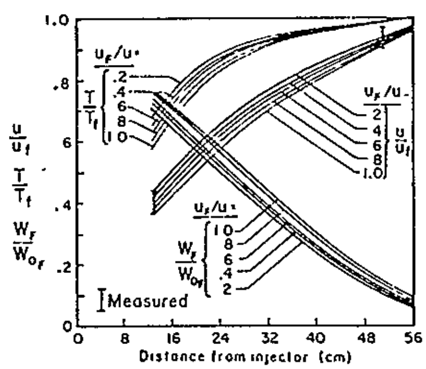

Fig. 2. Calculated dimensionless gas velocity, gas temperature, and liquid fuel flux vs distance from the injector.

and CO_2 ($I = 8$). The calculated local gas velocity, gas temperature, and flux of liquid fuel are given in Fig 2 where u_f and T_f are the complete combustion values and W_0^F is the injection value. The validity of the approach and of the assumptions embodied in the first $5 + I$ equations were further checked by measuring the gas velocity (by streak photography) at two stations (vertical bars in Fig 2) Of particular interest is the calculated dimensionless liquid fuel flux; a parameter which is important for both efficient and stable rocket chamber design.

A re-examination of the assumptions actually needed for the application of this method, leads to the conclusion that only two assumptions influence the results markedly. The first assumption is that of no recirculation at the station of interest (not everywhere between the injector and the station of interest). Near the injector, within distances of the order of the distance between injector units or of the jet break-up length, which ever is longer, recirculation can be expected to be active and the first 5 equations do not apply. Indeed in Fig. 2 no results are given for $x < 13$ cm. The second assumption is that which must be made to write out explicitly the F_i equations. In this study, instantaneous mixing and reaction of the vaporized fuel to equilibrium reaction products was assumed. Notice that the assumption that all fuel drops have initially the same velocity and radius and that there are no collisions, break-ups, or nucleations are not necessary as it is indicated by the relative insensitivity of the solution to the value of the parameter u_i/u.

The objective of this Synoptic has been the explanation of the method. However, the results which were obtained by its extensive application to the liquid oxygen-ethanol system are also of practical importance. They are discussed in the footnote and concern both optimal and steady combustion chamber design and research. The conclusions, which should be valid for liquid oxygen-hydrocarbon systems of practical interest, include: the assumption of chemical equilibrium of the reaction products appears to be a valid one (it simplifies considerably computations), the liquid fuel vaporizes and burns uniformly in the axial direction (see Fig 2, for example) rather than actively near the injector and very slowly far from it (it limits the usefulness of the concentrated combustion models sometimes used in stability studies); the gas parameters are not axially uniform (as exemplified in Fig. 2, it explains why the observed longitudinal instability shock wave frequency is found to be close to the complete combustion acoustic chamber frequency); the energy source is not proportional to the mass source (a consequence of the chemical equilibrium of the reaction products, it complicates considerably stability studies); the initial momenta of the liquids are important in steady state computations (they account, for example, for the observed increase of static pressure near the injector, as shown in Fig 1).

APPENDIX E

NOMENCLATURE

NOMENCLATURE LIST

A	Area
B	Drop size constant
B_A	Drop size constant
C	Constant
C_A	Atomization rate constant
C_D	Drag coefficient
D	Diameter
$\overline{D}$	Mass median drop diameter
J_A	Drop secondary breakup constant
K	Mass transfer coefficient
L'	Chamber length
$\dot{M}$	Flowrate
ODE	One dimensional equilibrium
O/F	Mixture ratio
Pc	Chamber pressure
Re_D	Reynold's number
T	Temperature
U	Velocity
V	Velocity
W_e	Weber number
W_i	Local mass flux
ZOM	Cold flow collection plane distance
Z	Axial distance
Δ	Difference
% C*	Characteristic exhaust velocity efficiency

η_{C*}	Same as % $\dot{C}$*
α	Diffusion correction factor
σ	Surface tension, standard deviation
μ	Viscosity
ρ	Density
ε	Chamber contraction ratio
α	Diffusion correction factor

Subscripts

a,s	Vapor pressure at droplet surface
BL	Boundary layer
C	Chamber
d	drop
D	Drop, diameter
eff	Effective throat stagnation pressure
f	Fuel
g	Gas
HL	Heat loss
HW	Hot wax
j	Jet
Kin	Kinetics
l	Liquid
MIX	Mixing
O	Oxidizer
OPP	Opposite orifice
PRED	Predicted
P	Propellant

Subscripts (cont.)

r	Relative
s	Surface, static pressure
T	Throat, total
TD	Two-Dimensional
Test	Test Value
V	Vapor
VAP	Vaporization

APPENDIX F

REFERENCES

REFERENCES

1. Pieper, J. L., ICRPG Liquid Propellant Thrust Chamber Performance Evaluation Manual, CPIA 178, September 1968

2. Combs, L. P., "Liquid Rocket Performance Computer Model with Distributed Energy Release", Final Report NASA CR-114462, 10 June 1972

3. JANNAF Rocket Engine Performance Prediction and Evaluation Manual, CPIA Publication 246, April 1975

4. Sutton, R. D., et. al., "Operating Manual for Coaxial Injection Combustion Model", NASA CR-129031, Rocketdyne, April 1974

5. JANNAF Two Dimensional Kinetic (TDK) Reference Program, Ultrasystems, Inc. Irvine, Ca., December 1973

6. Combs, L. P., "Liquid Rocket Performance Computer Model with Distributed Energy Release", DER Computer Program Documentation and User's Guide Vol. I, 15 December 1971, Revised Edition, 1 January 1974

7. Bracco, F. V., "Application of Steady-State Spray Equations to Combustion Modeling", AIAA Journal Vol. 12, No. 11, 1974

8. Barsotti, R. J., et. al., Development of Liquid Oxygen/Liquid Hydrogen Thrust Chamber for the M-1 Engine, NASA CR-54813, Contract NAS 3-2555, 15 May 1968

9. Kovach, R. J., et. al., Large Hydrogen-Oxygen Ablative Chamber Test Program, NASA CR 72512, Contract NAS 3-11214, 14 March 1969

10. Evans, R. M., Boundary Layer Integral Matrix Procedure, BLIMP-J User's Manual, Contract NAS8-30930, Aerotherm UM-75-64, July 1975

11. Calhoon, D. F., et. al., Investigation of Gaseous Propellant Combustion and Associated Injector/Chamber Design Guidelines, NASA CR 121234, 31 July 1973

12. JANNAF Rocket Engine Performance Test Data Acquisition and Interpretation Manual, CPIA Publication 245, April 1975

13. Ingebo, R. D., "Maximum Drop Diameters for the Atomization of Liquid Jets Injected Concurrently into Accelerating or Decelerating Gas Streams", NASA TN D-4640, July 1968

14. Ito, J. I., "Development Test Report OMS Injector Subscale Pattern Evaluation", Contract M4J7XMA-483030H, Report No. 6673:207, (PDRD TM05-25), Aerojet Liquid Rocket Co., March 1976

15. Bracco, F. Y., "An Experimental Analytical Method to Study Steady Spray Combustion", Journal of Spacecraft and Rockets, Vol. 10, No. 6, June 1973, pp. 353-354.

16. Ingebo, R. D., "Vaporization Rates and Drag Coefficients for Isoctane Sprays in Turbulent Air Streams", NACA TN 3265, October 1954

17. Priem, R. J. and Heidmann, M. F., "Propellant Vaporization as a Design Criterion for Rocket Engine Combustion Chambers", NASA TR-R-67, 1960

18. Lawver, B. R., High Performance N_2O_4/Amine Elements - "Blowapart", Contract NAS9-14186, Final Report, ALRC, to be published.

19. Falk, A. Y., High Performance N_2O_4/Amine Elements , Final Report, Contract NAS9-14126, Rocketdyne, March 1976

20. Salmon, J. W. and Pieper, J. L., Design Analysis Procedures Using the JANNAF Distributed Energy Release Computer Program, 11th JANNAF Combustion Meeting, 9-13 September 1974

21. Kushida, R., "Application of the Distributed Energy Release (DER) Computer Program to Rocket Engine Performance Analysis II" 10th JANNAF Combustion Meeting, CPIA Publication 243, Volume III, 6-10, August 1973

22. Combs, L. P., "Catalog of Injector Spray Correlations", Contract NAS 7-746, Rocketdyne, 22 June 1972

23. Hines, W. S., et. al., "Extension of a Thrust Chamber Compatibility Model", Final Report AFRPL-TR-72-19, March 1972

24. Dickerson, R. A., et. al., Correlation of Spray Injector Parameters with Rocket Engine Performance, Final Report AFRPL-TR-68-147, Rocketdyne, June 1968

25. Falk, A. Y., et. al., Space Storable Propellant Performance Study, Final Report, NASA CR-72487, Contract NAS 3-11199, Rocketdyne, 24 November 1968

26. Weiss, Malcolm, A., and Worsham, Charles, H., "Atomization in High Velocity Air-Streams", ARS J., Vol. 29, No. 4, April 1959, pp. 252-259

27. Ingebo, R. D., and Foster, H. H., "Drop-Size Distribution for Crosscurrent Breakup of Liquid Jets in Airstreams", NACA TN 4087, 1957

28. Nukiyama, Shiro; and Tanasawa, Yasusi (E. Hope, trans.): Experiments on the Atomization of Liquids in Airstreams, Ref. No. 3, On the Droplet Size Distribution in an Atomized Jet, Defense Res. Board, Dept. Nat. Defense, Ottawa (Canada), Mar. 18, 1950; (Trans from Trans. Soc. Mech. Engr (Japan), Vol. 5, No. 18, Feb. 1939, pp. 62-67)

29. Eisenklam, S. A., et. al., "Evaporation Rates and Drag Resistance on Burning Drops", 11th Symposium on Combustion, 1966, pp. 715-728.

30. El Wakil, M. M., et. al., "Experimental and Calculated Temperature and Mass Histories of Vaporizing Fuel Drops", NACA TN 3490, January 1956

31. Rabin, E., et. al., "Displacement and Shatting of Propellant Droplets", AFOSR-TR-60-75, Rocketdyne, 1960

32. Cramer, F. B., and Baker, P. D., Combustion Processes in a Bipropellant Liquid Rocket Engine, A Critical Review, JPL Report 900-2, 15 Jan. 1967

33. Schuman, M. D., "Distributed Energy Release (DER) Computer Program", Contract F04611-75-C-0055, 2nd Monthly Report, 7 August 1975

34. Breen, B. P., and Beltran, M. R., Steady-State Droplet Combustion with Decomposition: Hydrazine/NTO, presented at AIChE 61st National Meeting, Houston, Texas, February 19-23, 1967

35. Tarifa, C. S. and P. O., del Notario, An Experimental Investigation of The Combustion of Monopropellant Droplets, AFOSR-TN-628, AD 217-813, 1959

36. Sawyer, R. F., The Homogeneous Gas Kinetics of Reaction in the Hydrazine-Nitrogen Tetroxide Propellant System, Princeton Univ. Department of Aerospace and Mechanical Sciences, Tech. Report No. 761, 1965.

37. Webber, W. T., et. al., Plume Contamination Effects Prediction, Final Report, and Program User's Manual, AFRPL-TR-71-109, December 1971

38. Rousar, D. C., Combustion Effects on Film Cooling, Final Report Contract NAS3-17813, Aerojet Liquid Rocket Company, to be published.

39. O'Hara, J. C., et. al., "Analysis of Rocket Combustion Chamber Turbulence Levels from Diffusion Data", Combustion and Flame, Vol. 25, 1975, pp. 161-176.